A review of growth mechanism, structure and crystallinity of anodized TiO_2 nanotubes

D. Regonini[1,2], C. R. Bowen[1], A. Jaroenworaluck[3] and R. Stevens[1]

[1]*Materials Research Centre, Department of Mechanical Engineering, University of Bath, Claverton Down Road, BA2 7AY (UK)*
[2]*Laboratory for High Performance Ceramics, Empa, Swiss Federal Laboratories for Materials Science and Technology, Überlandstrasse 129. CH-8600 Dübendorf, Switzerland*
[3]*National Metal and Materials Technology Center, 114, Thailand Science Park, Paholyothin Road, Klong 1, Klong Luang, Pathumthani 12120, Thailand*

Correspondent Author: D. Regonini
Laboratory for High Performance Ceramics
Empa, Swiss Federal Laboratories for Materials Science and Technology
Überlandstrasse 129, 8600 Dübendorf, Switzerland
Email address: d.regonini@hotmail.com
Tel +41 58 765 4490
Fax +41 58 765 6950

Abstract

This paper reviews the state of the art of anodized titanium dioxide nanotubes (TiO_2 NTs), with an emphasis on the growth mechanism leading to their formation and the effect of heat treatment on their structure and properties. The discussion is primarily focused on TiO_2 NTs grown in fluoride containing electrolytes, although the mechanism of formation of NTs in fluoride free solutions via Rapid Breakdown Anodization (RBA) is briefly covered. After an initial overview of progress made on the synthesis of anodized TiO_2 NTs the review provides an analysis of the factors affecting the anodizing process (fluoride concentration, electrolyte type, applied potential and anodizing time). Details of the current-time transient, the chemistry of the process and the chemical composition of the anodic films are described which provide key information to unveil the nanotube growth mechanism. The main debate is whether NTs growth in fluoride containing solutions occurs via field-assisted plastic flow (i.e. a constant upward displacement of the oxide to form the NTs) combined with field-assisted ejection of the Ti^{4+} ions (i.e. ions are ejected into the electrolyte without oxide formation) or via field-assisted dissolution (i.e. preferential dissolution at the pore base where the field is stronger) or whether both processes play a role. Whenever anodization takes place in organic solutions the experimental evidence supports the plastic flow model, whereas in aqueous media field-assisted (and chemical) dissolution occur. The mechanism of rib formation on the walls of the NTs is also reviewed, and it clearly emerges that the applied potential and water content in the electrolyte are key factors in determining whether the NTs are ribbed or smooth. There also appears to be a relationship between the presence of ribs and the evolution of oxygen bubbles at the anode. The impact of thermal treatment on the properties of the NTs is also described. A variety of crystalline structures are present in the NTs (i.e. anatase or rutile), depending on the heat treatment temperature and atmosphere and the resulting electrical properties can be varied from dielectric to semi-metallic. A heat treatment temperature limit ranging from 500 to 800°C exists, depending on preparation history, above which sintering of nanoscale titania particles occurs leading to collapse of the NTs structure. Future work should aim at using annealing not just to influence the resulting crystalline phase, but also for generating defects to be exploited in specific applications (i.e. photocatalysis, water splitting and photovoltaics).

Keywords: TiO_2, Nanotubes, Anodization, Growth mechanism, Annealing, Grain Growth

1. Introduction

Titanium dioxide (titania, TiO_2) is a versatile material and is used in many different applications, including paints and food [1], biomedicine [2], photocatalysis [3], photo-splitting of water [4], sunscreen protection for cosmetics, light sensitive materials [5], dye sensitized solar cells [6] and gas-sensing [7]. Over the last few years an extensive research effort has been dedicated to the engineering of novel nanomaterials [8], including nanostructured titania [9] prepared via anodization, sol-gel, hydrothermal, and vapour deposition techniques [10]. The ability to grow porous oxide anodic structures has been known for more than a century thanks to the work of Keller and co-workers in 1953 [11], whom described the anodic alumina array as a hexagonally close-packed duplex structure consisting of both a porous and barrier (pore free) layer. A milestone in the field was reached in 1995 when the degree of self-order in Anodized Aluminium Oxide (AAO) was significantly optimized by Masuda and Fukuda [12] using a two-step anodizing approach. The discovery of anodized TiO_2 nanopores and nanotubes (NTs) is more recent, dating back to 1984 [13], although early key contributions to the topic are generally considered to be from Zwilling et al. in 1999 [14, 15] and from Gong et al. in 2001 [16]. In addition to TiO_2 NTs and AAO arrays, the synthesis of anodized porous and tubular structures has also been extended to other valve metals, such as Zr [17, 18], W [19, 20], Nb [21, 22], Ta [23, 24], Hf [25], V [26] as well as several alloys [27] of these metals. Among the non-valve metals, Fe [28], Ga [29] and Co [30] have also been successfully converted into self-organized porous/tubular anodic oxides. This manuscript reviews the state of the art of the growth mechanism leading to the formation of anodized TiO_2 NTs in fluoride containing electrolytes; a section concerning their growth in fluoride free electrolytes is also included. Furthermore, the effect of thermal treatments on the structure, properties and crystallinity [31-34] of the NTs is discussed in detail.

1.1. Barrier and porous/tubular type anodic TiO_2 films

In a similar approach to anodic alumina [35], a first distinction can be made between the barrier (pore free) and porous (or tubular) type anodic TiO_2. The nature of the electrolyte is essential in determining the type of morphology that is eventually formed. Whenever the anodizing solution contains fluoride ions (or perchlorate, chloride or bromide ions), the anodic TiO_2 film will develop a porous/tubular morphology whereas in other electrolyte media the TiO_2 film will be of a barrier type. The pore initiation process [36-38] and the self-assembly of the anodic film remain controversial issues and are discussed in more in detail in **section 4.2**. It should be stated that barrier films arise when the anodic oxide is insoluble in the electrolyte and porous/tubular films are generally formed whenever the oxide is moderately soluble in the electrolyte.

1.1.1. The barrier (pore-free) layer

Anodization of titanium is historically associated with the colouring process, the result of an optical interference effect caused by the thickness of the TiO_2 film and is used commercially for the production of jewellery [39]. During the colouring process, the oxide that is formed is generally a barrier type film. The anodizing ratio, defined as the maximum oxide thickness obtainable per unit volt, is in the range 1-3nm/V [40]. The anodization process is explained in terms of field-assisted oxidation since the oxide grows as a result of the movement of ions under the action of an applied electric field. As the oxide film grows thicker and its overall electrical resistance increases, it acts as a barrier to the flow of ions and electrons. The oxidation process slows down and eventually ceases. The presence of a pore free barrier layer limits the final thickness of the oxide to within a few hundred nanometers. Some of the electrolytes typically leading to barrier type TiO_2 films are aqueous solutions of sulphuric, phosphoric or acetic acid [41], as shown in **Table 1.**

1.1.2 The porous/tubular layer

Nanoporous and tubular titania layers form on passage of an anodization current using fluoride containing electrolytes. The titania layers develop perpendicular to the metal substrate which can be

self-organized under controlled conditions [42]. Recently, bundles of TiO_2 NTs (i.e. not self-organized) have been also prepared by rapid breakdown anodization in perchlorate, chloride or bromide (fluoride free) containing electrolytes [43-54]. NTs have also been obtained in a sulphuric acid electrolyte [55] by tuning the concentration and the anodization potential in order to create a condition for breakdown to occur, although (as stated in **section 1.1.1**) sulphuric acid can generally be considered a TiO_2 barrier layer forming electrolyte [41]. Titanium and titanium dioxide are readily dissolved in fluoride based electrolytes, particularly those containing hydrofluoric acid. In addition to field-assisted oxidation of porous/tubular layers, it is important to define the process of field-assisted dissolution leading to dissolution of the oxide preferentially at the pore/tube base, where the electric field is stronger. This implies that there is a constant dissolution rate of the anodic layer at the base of each pore. In a fluoride containing electrolyte the oxide dissolves leading to the formation of a titanium hexafluoride complex [TiF_6^{2-}], which is stable in water. The applied electric field may also weaken the bond between Ti and O in the oxide, effectively facilitating chemical dissolution of TiO_2 (i.e. dissolution due to the presence of fluoride ions that occurs even in the absence of an electric field) and therefore the formation of [TiF_6^{2-}]. As highlighted in **Table 1**, the anodic structure has a thin barrier inner layer at the metal/oxide interface (M/MO) and a porous outer layer at the oxide/electrolyte (MO/Electrolyte) interface [16].

1.2 Synthesis

This section provides an overview of the synthesis of NTs. For detailed and comprehensive state-of-the-art publications on their applications, ranging from photo-catalysis and dye sensitized solar cells to biomedicine and gas-sensing, the reader should refer to some recent excellent reviews [27, 42, 56-65] and books [66, 67]. The first known manuscript on (ordered) porous anodized titania was reported by Assefpour-Dezfuly et al. [13] in 1984 where Ti metal was firstly etched in an alkaline peroxide and then anodized in chromic acid. In 1999, Zwilling and co-workers reported on the formation of nanoporous anodized titania in a fluoride containing electrolyte [14, 15], prompting the significant body of work undertaken on porous/tubular anodized Ti over the last two decades. Clearly, there has been significant progress made regarding their synthesis, which has led to:

(i) a 1st generation of NTs [16, 34, 68-71] prepared in hydrofluoric acid which were only 0.5μm long,

(ii) a 2nd generation of NTs up to 5 μm long [72-76] grown in water based electrolytes containing fluorine salts

(iii) a 3rd generation of smooth NTs (i.e. no ribs on the tube sides, unlike the 1st and 2nd generations) and longer NTs, up to 100-1000μm grown in organic electrolytes containing fluoride ions [77-84], see **Table 2**.

Macak et al. [85] have also improved the ordering of the NTs to hexagonally close packed arrays using a multi-step approach, in a similar fashion to nanoporous alumina [12]. Similar results have also been achieved by Albu et al. [86] who produced 250μm long NTs with hexagonal self-ordering by working within a critical parameter range of fluoride concentration, anodizing potential and time. In contrast, a regular structure more akin to nanopores was achieved by Shin and Lee [87], using a two-step anodization. These highly ordered anodic TiO_2 nanostructures [85-87] are defined as the 4th generation of anodized TiO_2 NTs and nanopores, as highlighted in **Table 2**. Furthermore it has been shown that the NTs can be generated using an ionic liquid water miscible electrolyte [88, 89] and advanced geometries including bamboo type NTs [90, 91], nanolaces [90], doubled-walled NTs [92] and single walled NTs (i.e. with lower content of carbon and titanium oxy-hydroxide) [93], two size scale NTs on Ti alloys [94], modulated NT stacks [95], multi-layered NTs [96-98], free standing NT membranes [84, 99, 100], extra-wide diameter NTs [101, 102] also with the aid of

UV-Vis irradiation [103], double sided NTs [104], nanocolumns [105], TiO_2/Ta_2O_5 superlattice NTs arrays [106], hierarchically branched NTs [107], nanosponges [108], selectively sculpted NTs by focused ion beam (i.e. open or closed pores/tubes to allow selective modification of their top surface) [109]. This enormous variety of organized nanostructure can be obtained by tuning the growth parameters: applied potential, electrolyte type (organic, aqueous), water content in organic solutions, fluoride concentration, anodizing time, pre-treatment (polishing) of the Ti substrate. It has been recently reported that the growth of the NTs is also influenced by the crystallographic orientation of the titanium substrate grains; for example it appears that NTs preferentially form on Ti (111) sites [110]. Similarly, Su and co-workers have shown that NTs grown from polycrystalline Ti foils exhibit a bimodal pore size distribution, with NTs developing on the Ti (0001) plane showing thinner barrier layer thickness, shorter length, smaller pore size and better crystallinity than NTs grown on other planes [111]. Finally, it should be noted that the growth of NTs is not limited to fluorine based solutions; NTs have also been grown using fluoride free electrolytes containing chloride/perchlorate ions [43-52], bromide ions [47] or nitrates [112]. In most of the cases it is possible to obtain long (several tens of μm) and non-self-organized NTs by adopting a very short anodizing time (seconds/minutes), although the formation of self-ordered NTs in an organic media containing chlorine ions has also been reported [53].

2. Self-ordered anodized TiO_2 nanotubes in fluoride containing electrolytes

In the majority of fluoride free anodization solutions the TiO_2 layer developing at the anode is of a barrier type and the anodizing process stops when the anodic film reaches a critical thickness and prevents the electric field from sustaining ionic migration across the oxide film. The maximum thickness of the oxide is determined by the applied potential and it is quantified by the anodizing ratio. If an optimized concentration of F^- is used, (i.e. typically in the range 0.3-0.5wt.%, below a threshold causing complete dissolution of the oxide formed or electro-polishing of the metallic Ti), then anodization occurs and it is in principle possible to extend the thickness of the anodic film. A schematic summary of the reaction phenomena occurring in fluoride containing media is shown in **Fig. 1a.** The applied electric field drives Ti^{4+} ions from the Ti substrate towards the electrolyte, where they combine with F^- ions to form a stable titanium hexafluoride complex, $[TiF_6]^{2-}$. Anions such as O^{2-} and OH^- originating from the dissociation of water [113] and F^- migrate towards the anode. Hydrogen bubbles are formed at the cathode and, depending on the conditions, a typical side reaction at the anode is oxygen evolution [114, 115]. Additional ions from the electrolyte will also migrate towards or away from the anode depending on their electrostatic charge and can be incorporated within the film, as will be discussed in **section 4.3.1**. The presence of F^- ions, capable of partially dissolving the oxide, is believed to be crucial in forming porosity in the film and possibly act to sustain the porosity during the formation of the NTs, as schematically shown in **Fig 1b**. The synthesis of self-organized TiO_2 NTs in fluoride containing electrolytes is generally performed under potentiostatic conditions, offering overall better control of the morphology and higher growth efficiency than galvanostatic anodization [116, 117].

At this point, an important distinction can be made between aqueous and organic electrolytes: fluoride ions in water based solutions are far more aggressive than in organic media, which is why the growth of the NTs in water is limited to lengths of a few microns [16, 34, 68-76]. Examples of NTs structures formed in aqueous based and organic electrolytes are shown in **Fig. 1c** and **Fig. 1d** respectively. Typical features to observe are the open top (mouth) and the closed scalloped bottom of the NTs. The NTs prepared in water exhibit ripples on the side wall, **Fig. 1c** (side view), whereas those grown in organic solutions can form with ripples or be smooth (**Fig. 1d**). The use of fluoride free solutions enabling the growth of tubular TiO_2 structures via Rapid Anodization Breakdown (RAB) will be discussed separately in **section 6**, whereas the following sections provide a detailed description of the formation of TiO_2 NTs in both fluoride containing aqueous and organic electrolytes.

2.1 TiO_2 NTs in aqueous based electrolytes: a brief history

When TiO_2 NTs are formed in fluoride containing aqueous media the chemical dissolution of Ti and TiO_2 can be significant and needs to be optimized for oxide growth; this is in contrast to the well-known case of Anodized Aluminum Oxide (AAO) [35] where chemical dissolution plays a minor role. Early attempts to use HF containing water media were only able to produce 0.5μm long NTs due to the high chemical dissolution of TiO_2 in the acidic electrolyte [16, 34, 68-71], as shown in **Fig. 2a** [16]. By reducing the electrolyte acidity and using aqueous solutions of fluorine salts rather than HF, the rate of chemical dissolution of TiO_2 was reduced and longer NTs, up to 2-4μm long, could be grown [72-74], see **Fig. 2b** [75]. Macak et al. [75] showed that by using Na_2SO_4/NaF and $(NH_4)_2SO_4/NH_4F$ aqueous solutions it was possible to grow NTs whereas Cs_2SO_4/CsF and K_2SO_4/KF led to a high degree of precipitation and non-uniform TiO_2 dissolution phenomena. These observations provided the first evidence for the importance of selecting an appropriate cation to optimise the growth of the NTs. The earliest proposed titania growth models [16, 68-71] were based on the initial formation of a barrier layer followed by the development of pits and cracks at the surface. Pores/tubes would develop preferentially at such spots (i.e. pits and cracks), since pitting of the oxide allowed the passage of current, effectively creating easy paths for the development of NTs because of (i) the presence of a higher electric field beneath the pores [70] or (ii) localized acidification at the base of the tubes (i.e. a pH gradient between the pore base and mouth), leading to a higher dissolution rate at the pore bottom [73].

The diffusion of ions within the pores appears to be a length limiting factor [42, 118]. The structure does not immediately become self-organized, as demonstrated by Yasuda et al [96] who proposed a change from a random "worm-like" porous structure to a self-ordered nanotubular array as the result of competition between strong pores (i.e. channels where the passage of current and ions is favoured) and weak pores (i.e. channels where the passage of current and ions is more difficult). In AAO, one model suggests that pore self-organization is driven by repulsive forces triggered by the volume expansion during oxidation and the compressive stress [119-121] generated mainly by differential properties at the metal/metal oxide interface. In a similar fashion, volume expansion and compressive stress are believed to trigger the transition from pores to tubes in TiO_2. Alternative models relate the formation of gaps between the NTs either by cationic vacancies generated from Ti dissolution in the electrolyte and their migration towards the outer wall of the NTs [71] or further pitting/etching from fluoride ions between pores followed by deepening of the gaps by means of field-assisted dissolution [68]. Our studies on the early stages of NT growth in aqueous based media indicates that under such conditions cavities of different sizes are evident almost immediately within the anodic film and oxygen evolution at the anode influences the growth process, contributing to the formation of oxide rings which pile up to form the NTs [76, 114]. This implies that in water based electrolytes a transition from pores to tubes, often suggested [68, 70, 73, 96], may not occur. Finally, from **Fig. 1c, Fig. 2a** [16] and **Fig. 2b** [75]**,** it is evident that NTs grown in water media have ripples on the side of the walls and their origin is discussed further in **section 5.2.**

2.2. TiO_2 NTs in organic based electrolytes: a brief history

During anodization in an organic electrolyte, any residual or deliberately added water is generally the source of oxygen [122, 123]. The contribution of oxygen from the organic electrolytes to the anodization process is thought to be rather difficult since the oxygen ion is far more strongly bonded to the carbon either by a single (C-OH) or a double bond (C=O) [124]; nevertheless studies on Al_2O_3 indicate that it is possible [125].

Using specific solvents containing three adjacent hydroxyl group-bonded carbons, C-OH, at a temperature in the range 150-180°C and with a residual amount of water not exceeding 0.1wt% it has been possible to generate "Non-Thickness-Limited" (NTL) and pore free anodic films, with minimal injection of OH^- within the oxide[122]. Li and Young proposed that the NTL mechanism is associated with OH^- injection into the film and the presence of non-stoichiometric (oxygen deficient) regions due to the limited provision of oxygen [126]. Similarly, the formation of NTL

anodic TiO_2 mesosponges has been recently reported [127, 128], although the growth mechanism leading to NTL and the incorporation of organic based oxygen within the anodic film are to date not fully understood.

In the majority of anodizing processes, including the growth of TiO_2 NTs, complete oxidation is generally ensured by adding small amounts of water, or by ageing the electrolyte to allow the absorption of moisture from the environment. According to Raja et al. [129], a minimum amount of water (0.18wt% in their study) is required to sustain the process of NT formation.

By optimizing the anodization process, it has been possible to produce more ordered and longer NTs using organic electrolytes. In early investigations Ruan et al. [77] used a fluorinated dimethyl sulfoxide (DMSO) and ethanol mixture electrolyte to form NTs that were 2.3μm. A breakthrough came with Macak et al. [78] reporting the growth of NTs in a viscous glycerol electrolyte (with 0.5wt% NH_4F) which were 7μm long, smooth and self-organized without ripples on their outer surface, typical of an aqueous process. Further optimization led to significant improvement in NT length, to over 200μm in organic polar electrolytes (DMSO, formamide, ethylene glycol, and *N*-methylformamide) with added fluoride ions and a water level below 5 vol. % to minimise chemical dissolution of the forming oxide [80-82], see **Fig. 2c** [82]. The use of ethylene glycol, with 0.3wt% NH_4F and 2 vol. % water led to improved hexagonal close-packing and faster oxide growth rates compared to previous electrolytes [83], probably associated with a reduced hydroxyl injection into the anodic film. It is known that hydroxyl incorporation negatively affects ion transport through the oxide [126], whereas the incorporation of a small amount of hydroxyl ions and oxygen leads to sub-stoichiometry (oxygen vacancies) of the oxide and enhances ionic transport through the barrier layer [130]. Accurate control of the anodizing parameters in an ethylene glycol/NH_4F/water electrolyte allowed Paulose et al. [84] to prepare TiO_2 NT arrays as self-standing membranes up to 1000μm long. The size and viscosity of the cation of the fluorine salt employed also affected the growth rate and the length of the NTs. Larger and more viscous species such as quaternary ammonium cations were shown to enhance NT formation, possibly as a result of an inhibitory steric effect, maintaining the thickness of the barrier oxide at the tube base below a critical value, thus facilitating ionic migration [131].

A further significant step towards hexagonal self-ordered TiO_2 NTs was reported by Macak et al. [85] using an ethylene glycol/NH_4F electrolyte containing residual water (0.1wt% + adsorbed moisture) and a two-step anodization approach, similar to AAO [12]. Ideal self-ordered structure are also achievable without repeating the anodization process, simply by tuning the anodization potential and the fluorine content below an upper limit which defines the boundaries between the self-ordering anodization and the electro-polishing regimes, **Fig. 2d** [86]. In this case the transition from pores to tubes becomes evident with the TiO_2 film initially growing as a self-organized porous structure and subsequently splitting into individual NTs due to the action of fluoride ions [86]. Shin and Lee [87] combined electro-polishing of Ti with a two-step anodization process and showed it was possible to produce nearly perfect hexagonally self-organized nanostructured TiO_2, more akin to a porous layer rather than typical NTs. It is worth pointing out that due to the limited dissolution in organic solutions, a porous layer covering the top (mouth) of the NTs is generally observed whenever anodizing undertaken in such conditions. This layer is the remnant of the oxide formed at the early stages of the anodization and the NTs develop underneath [96, 132]. Possible approaches to remove this upper porous layer, which can limit the performance of the NTs in photocatalysis and dye sensitized solar cells [133], are for example (i) short etching in dilute hydrofluoric acid solutions [134] and (ii) ultrasonic cleaning in alcohols [80].

The term 'nanograss' [62] or the formation of anodized nanowires [135] is associated with bending and collapse of the NTs leading to the appearance of spikes on the top of the NTs following extended anodization time and partial dissolution of the NT wall. Strategies to prevent the formation (or to remove) of the nanograss have been developed [136, 137]. In a recent report it has also been shown that the addition of lactic acid to the widely used NH_4F/H_2O/Ethylene Glycol electrolyte, allows the application of higher anodization potentials (120-150V) without inducing

electrical breakdown, hence ordered NTs can be grown at an ultrafast rate (i.e. 15μm long layers grown in 45s) [138]. In this case, the chelating effect of the lactic acid is reducing the number of OH groups on the surface of TiO_2. Such sites are known to be preferential electron injection sites when working at high potential (i.e. above 100V), eventually leading to electrical breakdown. By chelating the OH groups breakdown can therefore be inhibited; additionally since the chelating agent is adsorbed on the surface of TiO_2 (in competition with F^- ions) it also reduces dissolution of Ti^{4+} ions by the F^- ions [138].

2.3 Factors affecting the growth of NTs

It is now accepted that growth occurs exclusively at the pore base (i.e. at the metal/oxide interface), whereas oxide dissolution is uniformly distributed over the whole of the NTs, especially in aqueous media. Preferential paths for the electrolyte are possible in organic media and non-uniform dissolution of the oxide can occur. Electrolyte resistance and diffusion processes are generally not considered to be amongst the limiting factors for growth[139]. Clearly the balance between oxide growth and dissolution is important and can be altered by modifying the growth parameters. In addition to the nature of the electrolyte (aqueous or organic) discussed in **sections 2.1 and 2.2** there are several other key factors, such as pH, fluoride content, ageing of the electrolyte, anodizing potential and time, current density and temperature, that need to be taken into account when growing anodized TiO_2 NTs.

2.3.1 Electrolyte pH, fluoride concentration and ageing

The pH of the anodizing solution affects the ability of the electrolyte to dissolve the forming oxide, with higher oxide dissolution rates occurring in an acidic environment, as shown in **Fig. 3** [73]. This is one of the reasons why dissolution of the anodic oxide is at its lowest when fluoride salts are used rather than hydrofluoric acid. Similarly the concentration of fluoride ions has to be kept low to minimise dissolution, but it also has to be at a level sufficient to ensure NT growth. Typical F^- concentrations leading to self-ordered NTs are in the range of 0.3 to 0.5wt.% [140-142] and clearly the fluoride content also affects the pH of the solution.

Another factor to be taken into account, especially when considering growth in organic solutions, is the 'ageing' of the electrolyte [143] which helps to synthesize well defined NTs. It is generally observed that by reusing an organic electrolyte its electrical conductivity increases [66, 83, 144] as a result of (i) a higher TiF_6^{2-} content built-up during previous anodization cycles and (ii) a higher water content, which eventually reaches saturation due to moisture adsorption. A higher TiF_6^{2-} concentration translates into a lower rate of chemical dissolution; hence it is important in establishing the condition required for maximizing oxide growth. Furthermore, the higher conductivity also enhances the growth rate of NTs, as it facilitates the passage of the current required to form the oxide; the effect is well explained in **Fig. 4** [144]. The importance of 'ageing' the anodizing solution is clearly demonstrated by the study from Raja et al. [129], since in anhydrous media the NTs could be only be formed by allowing sufficient uptake of moisture by the electrolyte.

2.3.2 Anodizing potential and current density

As stated in **section 2**, the majority of experiments are performed under potentiostatic conditions, which involves the application of a constant potential and monitoring the anodization current. In contrast, galvanostatic growth has been less investigated; it appears to be more difficult to control the morphology of the anodic NTs under a galvanostatic regime [116]. The applied potential usually ranges from 5 to 30V and 10 to 60V in aqueous and organic electrolytes respectively [42, 145]. The applied potential determines the electric field strength across the oxide, thus affecting the migration of ions and ultimately the nanotube diameter. A linear relationship between the applied potential and the diameter of the NTs is generally observed up to 60V [146, 147], as shown in **Fig. 5** [148]. A

linear dependence relationship also exists between the thickness of the barrier layer at the base of the NTs and the applied potential [149]. However there are also exceptions to this rule. For example, in a recent work, Yin et al. [150] reported an inverse relationship between the potential and NTs diameter at potentials larger than 100V and attributed their findings to the diffusion of water being the rate limiting step under such conditions. Similar observations were also reported by Su and Zhou [151, 152], who found that the pore diameter of porous anodized nanostructures drops when the applied potential exceeds a critical value (generally above 60V), which is determined by the electrolyte and has an influence on the dissociation of water (and on the current density) [113] and therefore on the porosity and the pore size of the anodic film. Clearly the anodizing potential and the modality by which it is applied (i.e. the potential may be established after sweeping or stepping up to a constant value, which is then maintained for the remainder of the anodizing process) have also an influence on the current density. For example, by applying a sweep (ramp) in the range of $100mV/s^{-1}$ to $1V/s^{-1}$ it is possible to obtain a higher current density and longer NTs than by using slower sweep rates [132]. An initial potential sweep also generates porosity in the oxide while the film is still at its minimum thickness (a few nm), hence sustaining the anodizing process [153], as will be discussed in detail in **section 4.1.4**. It is thought that there is a current threshold determining whether a pore being formed will survive and develop into a nanotubes or even cease to grow [132].

2.3.3 Anodizing time

Identification of the optimal anodizing time for a given set of conditions (electrolyte, potential, fluorine concentration, etc.) is required to extend the maximum length of the NTs. When working in aqueous media, the conditions are far too aggressive to allow the NTs to grow any longer than a few μm [72-75]. Such a thickness is usually reached within minutes from the onset of the anodization process, however the anodizing time usually ranges from 30mins to 2hrs in order to allow the structure to rearrange itself and increase the degree of self-order.

In contrast, the growth process in organic electrolytes is much slower and dissolution phenomena are not as significant as in water, although conditions still need to be tuned for optimal growth. As a result, by extending the anodization time from several hrs up to a day, it is generally possible to obtain NTs over 100μm long [84]. One of the issues associated with employing long anodizing times in an organic electrolyte is over-dissolution of the NTs in some areas. As discussed, when using an organic solution it is common to observe a porous layer on top of the NTs, which is a remnant of the initial barrier layer formed during the early stages of anodization [80, 136]. The nanotubular layer develops underneath and it is assumed that there are preferential paths for the organic electrolyte, hence over-dissolution is not homogenous over the entire NT structure [148].

2.3.4 Temperature

The temperature of the electrolyte affects the dissolution rate of the NTs which are normally grown at 20-25ºC (room temperature). Studies performed at low temperature (2ºC) using aqueous solutions suggest the growth of the NTs is inhibited at lower temperatures [154], whereas in organic electrolytes the temperature range most favourable for the growth of NTs is between 0 and 40ºC [79]. It has also been shown that while in aqueous media the diameter on the NTs does not depend on the anodizing temperature, when using an organic electrolyte the diameter of the NTs is larger at a higher anodizing temperature since at a low temperature leads to higher viscosity and reduces both ion migration and especially the dissolution of TiO_2 and Ti by F^- ions) [155].

Having considered the factors influencing the growth of the NTs, the next section of the review discusses the mechanistic regimes associated with the anodization process.

3. Mechanistic regimes associated with anodization

3.1 High-field regime

The anodic growth of barrier type TiO_2 is largely based on a modified version of the high-field regime [40], which applies to a variety of anodic oxides. The main assumptions of this theory are:

i. ions have specific mobility within the anodic layer under the action of the electric field and the oxide can grow both at the metal/oxide and oxide/electrolyte interfaces [156]. Such a condition is not satisfied for porous/tubular films, which are largely growing at the metal/oxide interface only.

ii. the conductivity of the oxide films has an ionic (J_{anions} , $J_{cations}$) and an electronic ($J_{electrons}$) component, hence the current density (J) across the oxide is $J = J_{anions} + J_{cations} + J_{electrons}$

iii. The "rate-determining step" depends on the movement of ions within the oxide. The current density (J) is given by the following expression: $J = J_0 \exp(\beta E)$ where J_0 and β are parameters dependent on temperature and the nature of the metal and E is the electric field strength in the oxide (10^6-10^7V/cm).

iv. The electric field strength (E) is calculated from the potential drop across the oxide and the layer thickness d and is given by $E = \Delta U / d = (U - U_0) / d$, where U is the potential at the electrode and U_0 is the flat band potential.

The high-field regime can also be applied to porous/tubular anodic layers, such as AAO and TiO_2 NTs, However, several considerations need to be taken into account to explain experimental observations and these are now discussed.

3.2 Flow mechanism or field-assisted dissolution?

3.2.1 The case of self-organized Anodized Aluminium Oxide (AAO)

It is useful to consider the case of self-organized AAO [35] to understand how the general view of the formation of anodized porous/tubular structures has changed in recent years. It had been accepted for decades that the development of pores in AAO is based on a field-assisted dissolution process [157, 158]: after the initiation of the pores, the development of the porous anodic layer is ensured by the balance between the formation of a barrier layer oxide at both the metal-oxide and oxide electrolyte interfaces and field-enhanced dissolution at the base of pores, where the electric field is high. Recently, an alternative "field-assisted flow" mechanism has been proposed for AAO by Skeldon et. al [159] and Garcia-Vergara et al. [160] who conducted experiments with W tracers inserted within an Al substrate demonstrating that the development of pores in alumina is driven by oxide displacement from the barrier layer towards the pore walls. During growth, the oxide experiences a stress due to electrostriction [161] and volume expansion [119-121] and this induces a displacement of the oxide (which exhibits a certain plasticity) involving ionic transport under the high electric field to relieve the stress [162-164]. The fact that the anodic film can undergo significant "plastic" deformation is also supported by the expansion of gas bubbles generated at the metal-oxide interface and trapped within the anodic alumina [165, 166]. Furthermore by anodizing a layer of Al on a layer of W results in fingers of tungsten rich oxide penetrating into the alumina layer without any cracking [167]. Oxygen bubbles within the film are an obstacle to ionic transport and this leads to non-uniformity of film thickness and interfacial roughness [168]. The flow or deformation mechanism accounts for the anomalous thickness of the porous alumina anodic films (exceeding an hypothetical 100% growth efficiency) and suggests that the porosity developed is essentially of mechanical origin [119-121] and initiated by instability within the anodic film which occurs when the oxide cannot be formed at the film/electrolyte interface [162].

When using an electrolyte with O^{18} tracers to form a barrier oxide layer and subsequently anodizing the specimen using a "pore forming" electrolyte without tracers (i.e. no O^{18}) it was shown that no loss of O^{18} was registered during the growth of the porous film, an observation which was initially interpreted as an oxide decomposition at the pore base followed by subsequent reincorporation in the anodic structure [169].
However, during the growth of barrier type alumina, the oxygen sublattice is reported to be stationary whilst metallic ions are transported through it (i.e. movement of oxygen ions conserve ionic order) [170]. Hence, by forming an initial barrier layer oxide enriched in O^{18} and then re-anodizing the specimen with an electrolyte without an O^{18} tracer (i.e. so that a new barrier layer is formed), the O^{18} from the first treatment is found to be adjacent to the metal, **Fig. 6a**. In contrast when the second anodization (without O^{18}) forms a porous layer, the O^{18} enriched barrier layer from the first step is situated at the surface of the anodic layer, **Fig. 6b** [159].
The condition for pore initiation in anodic alumina is satisfied when no oxide is formed at the oxide/electrolyte interface, which implies a field-assisted ejection of Al^{3+} ions into the electrolyte [171]. Considering the low chemical dissolution of Al_2O_3 in electrolytes commonly used to produce porosity, the Al^{3+} ions found in the anodizing solution are mostly due to field-assisted ejection; a crucial condition for porosity development because any material forming at the film/electrolyte interface would effectively heal any forming pores [172]. Viscous flow in the AAO system has been modelled recently and validated against experimental observations [173], posing a challenge to the widely accepted field-assisted dissolution theory [157].

3.2.2 The case of self-organized anodized titanium dioxide (TiO_2) NTs

Can a similar plastic flow mechanism be also applied to anodized TiO_2 NTs? This has been the driving force behind the tracer study work on a Ti-W alloy by LeClere et al. [174]. It is worth noting that whenever there are conditions which prevent loss of film species into the electrolyte (i.e. formation of a barrier layer oxide), the relative thickness of material which grows at both the metal/oxide and oxide/electrolyte interfaces is largely determined by the anion and cation transport numbers, which are 0.4 and 0.6 respectively in the case of amorphous barrier layers of TiO_2 and Al_2O_3 [156, 175, 176]. The conclusion from LeClere et al. [174] is that the generation of major pores (tubes) can be ascribed to either a field-assisted flow of film material, with constant displacement of oxide from the barrier layer to the pore walls or to field-assisted dissolution with growth and ionic transport primarily driven by anion migration (i.e. a reduced cation transport number is assumed). A similarity between TiO_2 NTs [174] and a previous study on AAO [159] that supports the flow model is the abnormally large thickness of the oxide that cannot be fully explained by field-assisted dissolution or by the ejection of cations into the electrolyte, which undoubtedly also contributes to release the build-up inner stress due to volume expansion during the anodic growth [71].
Berger et al. established how the anodic oxide and the porosity evolved for NTs grown in an organic electrolyte and monitored the expansion of the oxide film [177, 178]. They describe how:

(i) the film initially evolves as a barrier layer with a volume expansion of 2.4, known as the Pilling-Bedworth Ratio (PBR) [179], in agreement with the value of 2.43 reported for barrier type anodic titania [180],
(ii) at the point of pore initiation the volume expansion decreases to 1.7-1.9,
(iii) the volume expansion then increases to 2.7-3.1 during the development of the nanotubular network.

A comprehensive work recently published by Albu et al. [181] demonstrates how the expansion factor (F_{EXP}) of TiO_2 NTs is affected by the anodization parameters, particularly the water content in the electrolyte, **Fig. 7a**, and applied potential, **Fig. 7b**. An expansion factor ranging from 1.3 to 2.8 was observed [181] and at higher water contents there was a decrease in F_{EXP} due to the higher

dissolution of Ti and TiO_2 and lower growth efficiency. At lower water content F_{EXP} increases due to a higher incorporation of impurities as dissolution is at its minimum, leading to higher growth efficiency. A lower water content and higher applied potential are also likely to induce more defects in the anodic film, leading to a higher F_{EXP}, as the oxide grows at a faster rate under those conditions. Again, such observations cannot solely be explained by a field-assisted dissolution model, whereas they are consistent with the plastic flow model [177]. In contrast, Yang and co-workers [182] reported a volume expansion of 1.0 (i.e. no expansion) in an aqueous electrolyte and 1.8 in glycerol, which would also be compatible with a field-assisted dissolution mechanism. It may be possible that in the case of TiO_2 NTs, the plastic flow model and chemical and field-assisted dissolution at the base of the tubes are both active mechanisms.

Le Clere et al. [174] postulated the need for a reduced cation transport number to explain field assisted dissolution requiring growth and ionic transportation driven by anion migration. A reduced cation transport number for Ti^{4+} ions in the presence of F^- may derive from the high affinity between these two elements which form stable complexes, such as $[TiF_6]^{2-}$. These are indeed found throughout the anodic film, as discussed in **section 4.3.1**. Habazaki et al. [183] report that the rate of F^- migration through the TiO_2 anodic film is twice that of O^{2-} ions and a fluoride rich metal oxide interface therefore exists beneath the oxide film. This fluoride rich layer [183] is thought to be occasionally causing the detachment of the anodic TiO_2 film from the substrate, in a similar manner to anodic tantalum oxide [184, 185]. Detachment of sections of the TiO_2 NTs anodic film have been reported in both aqueous [116] and organic electrolytes [80, 145]. Apart from the enriched interface, the concentration of fluoride ions has generally been reported to be uniform in the anodic film [183, 186], although Sun et al. [187] suggest the presence of a gradient between the pore mouth (13% at.) and the base (8% at.), due to a potential drop occurring at the anode, especially for NTs grown in organic media. Another important point regarding the flow mechanism is its ability to account for the restricted thickness of the fluoride rich layer; if the oxide does not flow upwards to the tube mouth the fluoride rich layer would thicken with time. This mechanism allows incorporation of anions into the oxide with lower transportation numbers (i.e. which are moving slower under the applied electric field and hence are near the oxide/electrolyte interface and would be constantly re-dissolved in the electrolyte if the mechanism would be solely based on field-assisted dissolution) [174].

As an alternative model, an equi-field mechanism is proposed by Su and Zhou [151, 152, 188, 189] with the growth of the porous/tubular oxide occurring not only at the pore/tube base (i.e. downwards, such as in the field-assisted dissolution and plastic flow models), but also on the pore/tube wall (i.e. sideways), with the tube diameter increasing until it makes contact with adjacent pore/tube near neighbours.

4. Key considerations to understand the growth mechanism

In this section the key variables necessary to develop an understanding of the growth mechanism are considered. In addition to the use of tracers and the measurement of the volume expansion associated with the anodizing process (**section 3.2**), important information on the growth mechanism leading to the formation of TiO_2 NTs can be extracted from (i) an analysis of the current-time transients and (ii) chemical analysis of the anodic film. These analyses can help define the chemistry and the efficiency of the process.

4.1 Current-time transient analysis

The current-time transient allows the different stages of anodic film growth to be monitored. For barrier layer type oxides [35] the current density simply decays as the anodic layer thickens, however, for a porous oxide layer three different stages (I, II, III) can be identified as described in **Fig. 8a** [153] and **8b** [145] which illustrate the transients observed for TiO_2 NTs grown in aqueous and organic based electrolytes respectively.

4.1.1 Stage (I)

At stage I the anodizing process begins (i.e. a potential is applied) and the current quickly decreases to a minimum value due to the formation of a high resistance oxide barrier layer, which grows up to 50nm thick at 20-25V [132]. In order to maintain the oxidation process, ions (O^{2-}, OH^{-}, Ti^{4+}, F^{-}) must move through the high resistance barrier layer and at this stage porosity is induced by the presence of F^{-}. A discussion on whether the action of fluorine ions is purely chemical (i.e. dissolution of the oxide) or more complex is provided in **section 4.2**. Despite the induced porosity, the current falls to a minimum because the process is still dominated by the electrical resistance of the barrier oxide.

4.1.2 Stage (II)

The current subsequently rises to a maximum (stage II) as pore nucleation progresses. This is due to a decrease in the resistance of the anodic film as more paths are available for ionic species in the electrolyte. From a flow model perspective, this stage represents the transition from a relatively thin anodic film where upward displacement of the oxide does not occur (i.e. limited mechanical stress) to the beginning of the formation of a porous/tubular structure were the visco-plastic oxide is continually being pushed upwards to minimise stress at the metal/metal oxide interface.

4.1.3 Stage (III)

Finally the current attains a constant value or drops (stage III) when a steady state is reached during the formation of TiO_2 NTs. The classical interpretation of stage III, based on the field-assisted oxidation and dissolution model would be that the steady state is reached because the rate of oxide formation at the metal/oxide interface and the rate of dissolution at the oxide/electrolyte interface are equal, **Fig. 9a** [134]. Hence the NT walls can thicken further by effectively "eating away" the metallic substrate with fluoride ions partially dissolving the oxide, preferentially at the base of pores/tubes where the electric field is stronger. Eventually the process becomes dependent on diffusional effects [42, 78], i.e. the viscosity and temperature of the electrolyte as well as mechanical stirring of the solution [118]. However, in the authors opinion, recent findings [159, 160, 174, 177, 178] (see comprehensive discussion in **sections 3.2.1** and **3.2.2**) supporting the flow model mechanism should not be ignored and it is fair to assume that the growth of the NTs is also "flow assisted", with newly formed oxide being pushed up the wall, as schematically shown in **Fig. 9b** [27]. This flow plays a part in ensuring that the thickness of the barrier layer at the base of the NTs does not exceed a critical value which would prevent ionic conduction and ends the anodization process. The flow assisted interpretation of stage III is compatible with the continuous growth of the NTs over time, considering that in organic media the maximum thickness is reached after several hours of anodization. It is likely that considering the significant level of dissolution in aqueous media, the main process occurring at stage III (constant NT thickness over time) is field-assisted dissolution.

4.1.4 The importance of thinning the thickness of the barrier layer

It is important to sustain the growth of the NTs by ensuring sufficient ionic migration and generation of cavities in the anodic film from the very early stages of growth. It has been found that the larger structured cations (such as quaternary ammonium ions) allow the growth of thicker NTs layers, as well as increasing their rate of formation. This is attributed to the inhibitory effect that restricts the thickness of the interfacial (barrier) oxide layer, enhancing ionic conduction [131]. Similar inhibitory behaviour is observed for ammonium salts in aqueous electrochemical systems due to cation induced structural modification of the solvent [190]. It is also suggested that the high growth rate, up to 15μm/min. [66] observed in certain organic electrolytes, formamide, ethylene glycol, N-methylformamide [80, 81, 83, 131] is due to their high degree of structural organization (i.e. they interact with Ti at the oxide surface). This minimises the injection of hydroxyl ions into the anodic film, effectively introducing non-stoichiometry within the oxide and increasing the ionic

conductivity of the barrier layer [130]. Furthermore, Yoriya et al. [191] investigated the effect of ohmic resistance of the electrolyte, demonstrating that high conductivity solutions improve Ti^{4+} extraction from the metal [131] facilitating ionic transport and the growth of NTs. Improved Ti^{4+} extraction can also be achieved by using an electrolyte with a high dielectric constant, such as formamide or N-methylformamide [66]. A potential ramp prior to reaching a constant potential can also be used to facilitate the formation of pores while the barrier layer that is being formed is still at a minimum thickness, effectively extending stage II of the current transient and thus extending the NTs length from 0.8 to 1.5μm in aqueous media [153].
The next section of the review provides further details on the state of the art of the research aimed at understanding the pore initiation stage leading to the formation of anodized TiO_2 NTs.

4.2 Pore initiation

It is important to establish how porosity is initiated in the film to help understand whether such step is related to chemical dissolution of the oxide or if other factors play a role. For example, in the case of Al_2O_3, Al^{3+} ions in the solution are mainly due to field-assisted ejection into the electrolyte rather than due to chemical dissolution of the oxide (i.e. chemical dissolution is very low in the electrolytes used) and pore initiation is possible when no oxide is formed at the oxide/electrolyte interface [171, 172]. At the early stages of the process a morphological instability develops on the oxide surface, with the appearance of gentle or more pronounced undulations of the film, which eventually leads to self-assembly of the anodic structure [192]. Depending on the applied potential, these perturbations effectively initiate the formation of pores as in **Fig. 10a-d** [37]. It is clear that the undulations are influenced by the metallic substrate underneath, but their origin is still a controversial issue. It has been proposed that the instability is triggered by compositional changes in the oxide and the electrolyte at the interface region [193, 194], with fluoride ions enhancing those changes as they form complexes with the metal cations. Some studies suggest the appearance of such an instability (i.e. pore initiation) occurs only after a critical thickness of a few nm is reached [36], others suggest that instability in the film begins immediately [38]. In the case of TiO_2 it is important to make a distinction between aqueous and organic electrolytes. In an aqueous environment, the pore initiation stage can be attributed to both field-assisted ejection of Ti^{4+} ions into the electrolyte [27] and chemical dissolution of the oxide due to the presence of fluoride ions readily forming cavities within the oxide. In fact, according to our studies in water based electrolytes [114], it appears that pores and cavities are immediately formed once a potential is applied to the cell. However it is interesting to understand how the pore initiation stage occurs when the chemical dissolution is at a minimum, which is the case for organic electrolytes with only small amounts of fluoride ions (0.25-0.5wt%) and water (1-2wt%) present. A comprehensive contribution to the topic has recently been given by Hebert et al. [38] showing that the morphological instability leading to pore initiation and self-order are satisfied only for a narrow range of oxide formation efficiencies (from 0.5 to 0.58 for TiO_2). The efficiency is determined by the fraction of oxidized metal retained in the anodic film; hence the relationship between the conditions for pore initiation and electrochemical dissolution (i.e. Ti ions ejected into the electrolyte at the oxide/electrolyte interface) can be established quantitatively. In their model [38] the plastic flow and the stress associated with volume expansion [195] are not significant at the pore initiation stage and chemical dissolution from the pore walls is also shown to be negligible. Recent experimental work on TiO_2 NTs by Albu et al. [196] is in good agreement with the model proposed by Hebert. However other models have also been recently put forward. Stancheva et al. [197] propose that pore initiation is prompted by a perturbation at the film/electrolyte interface, caused by the presence of zones in the forming film where growth and chemical dissolution occurs and zones where there is electrochemical dissolution (i.e. cation ejection). A similar interpretation [198] for the pore initiation and the self-organization of anodic porous/tubular oxides considers the corrosion at the metal/oxide interface (i.e. oxygen ions interacting with metal ions) coupled with Ti and TiO_2 dissolution at the oxide/solution interface). When referring to organic electrolytes it can be

concluded that Ti ejection into the electrolyte is essential to initiate porosity; however it remains to be established whether the chemical of field assisted dissolution (by F^- ions) of newly formed anodic TiO_2 also plays a role.
The following section describes the chemical composition of the NTs in order to understand the underlying chemistry of NTs formation.

4.3 Chemical composition of the NTs

X-ray Photoelectron Spectroscopy (XPS) is one of the most commonly used techniques to reveal the chemical composition of the NTs and represents a powerful tool to understand the composition of the structure and the chemistry behind the anodizing process.

4.3.1 XPS analysis of the NTs

The chemical composition of the oxide and the incorporation of electrolyte species within the anodic film has been intensively studied in the case of barrier layers [199] and nanoporous Al_2O_3, both in aqueous [200] and organic media [201]. A higher degree of contamination (dependent on electrolyte, electric field, film growth efficiency, charge and concentration of the species) is associated with porous films whereas in barrier layers the incorporation of species from the electrolyte is generally lower [35]. Thompson and Wood [200] reported that porous alumina consisted of an outer layer (i.e. the layer furthest away from the metal) of pure alumina and an inner layer (i.e. the layer closer to the metal) contaminated by electrolyte species, as schematically shown in **Fig. 11**, the relative thickness of the two being dependent on the electrolyte. The subject of anodic TiO_2 NTs is a rather new field of research compared with porous alumina and electrolyte contamination has yet to be investigated as intensively. Nevertheless useful information is available in the literature [32, 42, 66, 77]. The main contaminants in the anodic NTs are generally fluoride ions and carbon. As an example, using Rutherford backscattering spectroscopy and nuclear reaction analysis, Valota et al. [117] have determined a film composition of $TiO_2.0.15TiF_4.0.09(C_3H_8O_3)$ in a glycerol electrolyte containing fluoride. In a similar way to the barrier layer type titania [202], sulphate and phosphate ions have also been reported to be present to a few atomic % within the NTs [62].

Ti and F XPS peaks

Peaks obtained from XPS analysis of anodized TiO_2 NTs [134] are shown in **Fig. 12a-d**, with the typical signal of titanium dioxide at 459.1eV and 464.8eV, **Fig. 12a**, due to Ti 2p (3/2) and Ti 2p (1/2) respectively. A shoulder on the peak at 459.1eV is due to the highly electronegative hexafluorotitanate complex $[TiF_6]^{2-}$ in the anodic film and it is also confirmed by the fluorine (F 1s) peak at 684.9eV, **Fig. 12b**, which is characteristic of $[TiF_6]^{2-}$ [203]. In contrast "free" fluoride ions give rise to a characteristic signal at a slightly lower energy (683-684eV) [204]. Clearly fluoride ions from the electrolyte are incorporated in the anodic film; the as-prepared film contains an amount of fluorine of the order of 4at% in aqueous media and 8at% in organic media**.** Furthermore it is well established that fluorine content can be sensibly reduced (i.e. to 1.0 - 0.3at%) by annealing at 300-400°C [32].

O peak

Important information on the chemical composition of the anodic film are also provided by the depth profiling (etching time of 180s) of the oxygen O 1s peak at 530.4eV, reported in **Fig. 12c** and **Fig. 12d** for aqueous and organic electrolytes respectively. Such a peak is indeed characteristic of Ti and O in TiO_2 [205, 206]. The O 1s peak prior to any etching of the surface, are shown in the inset in **Fig. 12c** for aqueous media and **Fig. 12d** for organic electrolyte. Clearly, before etching (**Fig. 12c inset**) along with the O 1s at 530.6eV typical for TiO_2 (O_{OXIDE}), there are two additional components (interpreted using a Shirley background [207]) attributed to the hydration of the oxide

($O_{OH\,/\,ORGANIC}$) at 531.4-531-6eV[208] and organic species at 533-534eV ($O_{ORGANIC}$) absorbed within the anodic film. It is generally not possible to completely separate these contributions, however, by etching away a few atomic layers it can be seen that the $O_{ORGANIC}$ component is effectively eliminated and represents predominately a surface contamination. In the case of water based electrolytes, organic species are either adsorbed from the atmosphere (or post-cleaning treatment using organic solvents) and 10-20at% contamination is common for TiO_2 surfaces [209]. Furthermore, when using an organic solution, the carbon uptake is increased due to chemi-adsorption of electrolytes species which strongly bond to the oxide and do not migrate within the anodic film [134]. Again, the carbon content is greatly reduced by annealing the structure at 400°C. By comparing the depth profiling peaks of F 1s and O1s, **Fig. 13a-b** [134, 148], it is clear that whereas carbon contaminants are mainly incorporated on the surface and are etched away with time, the fluorine is incorporated into the film and the fluorine concentration remains constant with surface etching. This is made evident by the disappearance of the C shoulder and an increase in the O1s signal as etching time increases, **Fig. 13b**. The fluorine concentration, **Fig. 13a**, does not seem to diminish within the anodic film.

The presence of a carbon rich layer as a double-walled structure on the NTs, where the inner wall is carbon rich, has been observed in ethylene glycol/HF electrolytes [92] and has been associated with an electric field induced decomposition of the electrolyte[210].

Although fluorine is present throughout the entire film (**Fig. 13a**), it is well known from transmission electron microscopy (TEM) analysis that it is not homogeneously distributed on the nanoscale [33]. Some interesting findings indicate that fluoride ions migrate at twice the rate of oxygen ions [183] and as a consequence a fluoride rich layer is present at the metal/oxide interface [92]. In a recent publication, Berger et al. [211] provide convincing High Resolution Scanning Auger Electron Spectroscopy (AES) evidence for the presence of a fluoride rich layer between the NT walls (i.e. at triple points of the hexagonally structured array), which is useful to elucidate the growth mechanism, as will be discussed in **section 5**.

4.4 Chemistry of the anodizing process

The current-time transient and the X-ray Photospectroscopy studies (XPS) allow development of a chemical model for the growth process. The following discussion applies to both aqueous and organic based electrolytes, considering that it has been shown that the presence of water is necessary for the anodic process and formation of the nanotubes [129]. When operating in aqueous media, it is well established that the outer (i.e. exposed to the electrolyte) anodic layer has an excess of hydroxyl ions compared to the inner layer, as confirmed by XPS studies [32, 132]. This hydrated layer is considered to be $Ti(OH)_4$ whereas the de-hydroxylated inner layer of the film (water release) is represented as TiO_2. In reality, there is likely to be a concentration gradient across the film, which can be written as $TiO_2 \cdot xH_2O$, to represent the inner (anhydrous) and outer (hydrated) anodic oxide. The degree of hydration and the hydration gradient across the film are also influenced by the potential sweep rate applied during the anodization, being larger for faster sweep rates because under such conditions more water is incorporated in the anodic film and the subsequent dehydration process cannot catch up with the continuous formation of hydrated oxide [212].

It is likely that the anodic oxide is also hydrated when grown in organic electrolytes [148]. The reactions occurring at the anode are oxidation of the metal, which releases Ti^{4+} ions and electrons *(Eqn. 1)*:

$$Ti \rightarrow Ti^{4+} + 4e^{-} \qquad \textit{(Equation 1)}$$

together with recombination of Ti^{4+} ions with OH^- and O^{2-} species provided by the water. The dissociation of water is also field-assisted (i.e. the high electric field facilitates the heterolytic

scission of water molecules) [113]. This results in the formation of hydrated oxide, which occurs over several steps and it is summarized for simplicity as a single process in *(Eqn. 2)*, and in the formation of the oxide *(Eqn. 2b)*. Further oxide is subsequently produced when the hydrated anodic layer releases water by a condensation reaction *(Eqn. 3)*:

$$Ti^{4+} + 4OH^{-} \rightarrow Ti(OH)_4 \qquad \textit{(Equation 2)}$$

$$Ti^{4+} + 2O^{2-} \rightarrow TiO_2 \qquad \textit{(Equation 2b)}$$

$$Ti(OH)_4 \rightarrow TiO_2 + 2H_2O \qquad \textit{(Equation 3)}$$

These reactions *(Eqn.s 1-3)* represent the possible field-assisted oxidation processes, since the applied potential controls the rate of ion migration within the metal/metal oxide interface. At the cathode, there is hydrogen evolution, *(Eqn. 4)*:

$$4H^{+} + 4e^{-} \rightarrow 2H_2 \qquad \textit{(Equation 4)}$$

On summing the reactions above *(Eqn.s 1-4)*, the overall process of oxide formation is represented as:

$$Ti + 2H_2O \rightarrow TiO_2 + 2H_2 \qquad \textit{(Equation 5)}$$

In addition, the fluoride ions present in the electrolyte can chemically dissolve both the hydrated layer and the oxide (*Eqn.s 6-7)*, or react with Ti^{4+} *(Eqn. 8)*, the ions being mobile in the anodic layer under the applied electric field [40]. It may also be possible that the combined action of fluoride ions (chemical dissolution) and the electric field weakens the bond between adjacent Ti and O (field-assisted dissolution). Certainly, the presence of fluoride ions in the electrolyte leads to the formation of fluoro-complexes. The most stable is TiF_6^{2-}, which has a large negative Gibb's free energy of formation ($\Delta G^0_{298} = -2118.4 kJ/mol$) [213]. For comparison, the Gibb's free energy of formation TiO_2 is $\Delta G^0_{298} = -821.3 kJ/mol$ [213]. The formation of fluoro-complexes is also aided by the applied potential, which drives fluoride ions (F^-) toward the metal along with Ti^{4+} toward the electrolyte. These processes are best described by the following chemical equations:

$$TiO_2 + 6F^{-} + 4H^{+} \rightarrow TiF_6^{2-} + H_2O \qquad \textit{(Equation 6)}$$

$$Ti(OH)_4 + 6F^{-} \rightarrow TiF_6^{2-} + 4OH^{-} \qquad \textit{(Equation 7)}$$

$$Ti^{4+} + 6F^{-} \rightarrow TiF_6^{2-} \qquad \textit{(Equation 8)}$$

It is believed the competition between the formation of the oxide *(Eqn.s 2-3)* and its dissolution (*Eqn.s 6-8*), is a key factor in determining the anodic titanium oxide structure produced. An aspect which has been largely overlooked is the evolution of oxygen at the anode *(Eqn.s 9)*, a side reaction which occurs during anodization of titanium [41, 214] and that may be a factor affecting the morphology of the anodic layer, as discussed later.

$$2H_2O \rightarrow O_2 + 4e^{-} + 4H^{+} \qquad \textit{(Equation 9)}$$

Oxygen evolution is generally more significant in aqueous media [114, 115], nevertheless it has also been observed in organic media containing relatively small amounts (up to 5vol.%) of water and is among the processes which affect the growth efficiency of the NTs, the topic of the next section.

4.5 Film growth efficiency

The growth efficiency, defined as the fraction of oxidized metal atoms retained in the anodic film, can be determined from the ratio between the Ti loss to the electrolyte and the total Ti consumed during anodization [38]. The growth efficiency can also be calculated using the total charge passed over a certain anodizing time, t. Assuming that all the anodization charge at a time t is used to form the anodic structure, it is possible to define an ideal thickness, $T_{id.}$ whereas the true experimental thickness, T_{real}, can be measured using scanning electron microscopy (SEM) analysis. From Faraday's law:

$$T_{id.} = \frac{QM_w}{AencN_A\rho} \cdot 10^7 \qquad \textit{(Equation 10)}$$

where $T_{id.}$ is expressed in nm, Q is the electric charge (A sec), M_w the molecular weight of TiO_2 (79.9 g mol^{-1}), A is the surface area (cm^2), e is the charge on an electron ($1.602 \cdot 10^{-19}$ A sec), n is the number of electrons involved per Ti atom (4, assuming complete oxidation), c is the number of Ti atom per TiO_2 molecule (1), N_A is Avogadro's constant (mol^{-1}) and ρ is the density of amorphous TiO_2 (3.1g cm^{-3}). The ratio $T_{real}/T_{id.}$ provides a measure of the growth efficiency (ε_{NTs}) of the process. However, if it is assumed that the growth mechanism occurs mainly by the 'plastic flow' mechanism rather than field-assisted dissolution, the porosity of the film, P, should be taken into account since $T_{id.}$ is calculated for a non-porous film (i.e. for a set of given conditions a porous film is thicker than a non-porous one). For a 'plastic flow' model the effect of dissolution is considered secondary in the formation of porosity since NTs are generated in response to a mechanical stress induced by volume expansion and electrostriction. Experimental evidence has shown that the NTs grow much larger than expected for a purely field-assisted dissolution mechanism, with an expansion factor (as a result of the metal converting into an oxide) up to 3, whereas the expansion factor (Pilling-Bedworth ratio) of amorphous TiO_2 is ~2.43 [27]. The revised efficiency taking account of the presence of porosity is therefore given by:

$$\varepsilon_{NTs} = \frac{T_{real}}{T_{id.}} \cdot (1 - P) \qquad \textit{(Equation 11)}$$

For TiO_2 NTs the growth processes of field-assisted and chemical dissolution of the oxide and field-assisted ejection of Ti ions into the electrolyte will lower the growth efficiency. Furthermore the growth efficiency can be affected by oxygen evolution at the anode, which is typical in the case of anodic TiO_2 [215-217]. Indeed the generation of oxygen bubbles at the anode has been reported for fluoride containing water and organic based electrolytes (containing small amount of water, i.e. 2vol.%) during the formation of TiO_2 NTs and have also been suggested to play a role in the formation of the nanotubular structure [76, 114, 145, 218]. In an aqueous electrolyte the significant evolution of oxygen affects the formation of the NTs, which are best described as being formed by a stack of oxide rings [76, 114]. However, in organic media oxygen evolution may or may not occur depending on the amount of water contained in the electrolyte, as well as on the applied potential. In the authors opinion, whenever it occurs, oxygen evolution affects the morphology of the NTs and is responsible for the appearance of oxide rings and ribs on the wall of the NTs, which otherwise grow smooth [148].

It has been found that potentiostatic conditions lead to higher efficiency than galvanostatic conditions, with Valota et al. [117] reporting efficiencies of ~48% at constant potential and <40% at constant current density (over the range 0.1-0.5 $mA \cdot cm^2$) when anodizing in a fluoride containing glycerol based electrolyte (it is assumed that the water content was kept to a minimum, i.e. 1-2 vol.

%). Efficiencies as high as ~90% were instead reported by Macak et al. [141] for a fluoride containing glycerol electrolyte with 50 vol. % of added water. According to these reports oxygen evolution can be ignored [117, 141]. No significant improvement were observed by increasing the electrolyte temperature from 20 to 40°C [79]. Interestingly, in another study conducted with a similar electrolyte (fluoride containing and glycerol based), Valota et al. [219] report oxygen evolution to affect the NTs growth efficiency whenever the water content is above 10 vol. %. Furthermore, Berger et al. [220], who used a fluoride containing ethylene glycol electrolyte, report oxygen evolution as a side reaction and a reduced growth efficiency for a water content above 2.5 vol. %, with a maximum efficiency (25%) observed for a water content of 1 vol. % and a minimum (10%) for water content of 25 vol. %. We reached similar conclusions using a glycerol electrolyte containing 2wt% of water, with efficiency dropping from 70% to ~50% and finally 14% on increasing the applied potential from 10V (no oxygen bubbles) to 20-40V (oxygen bubbles observed) [148]. Similar efficiencies (50-60%) have also been reported in ethylene glycol containing 1.5 to 5wt% of water [38]. Efficiencies are lower in aqueous based media, in the range 3-10%, especially for acidic solutions [42]; this is to be expected considering that in water based electrolytes both dissolution and oxygen evolution phenomena are enhanced.

5. Formation of anodized TiO_2 NTs: mechanistic aspects

This section reviews the state-of-the-art of mechanistic aspects related to the formation of anodized TiO_2 NTs. Among the topics to be considered are:

(i) the transition from pores to NTs,
(ii) the role of oxygen bubbles generated at the anode during the formation of TiO_2 NTs,
(iii) the factors determining whether the NTs are smooth or ribbed.

5.1 Transition from pores to tubes

An aspect requiring clarification regarding the growth of anodized TiO_2 NTs is why the structure develops as a nanotubular structure rather than nanoporous, as in the well-known case of AAO. We discuss recent findings suggesting that the situation between TiO_2 NTs and AAO is not so different. As pointed out by Roy et al. [27], the distinction between nanopores and nanotubes is mechanistically not justified (i.e. both are the result of a flow assisted anodic process), however it is interesting to try to understand when and why the pores to NTs transition occurs. In the authors view it is also necessary to stress that according to the currently available data, the structure varies depending on whether an aqueous or an organic electrolyte is used.

5.1.1 No transition observed in aqueous media

In aqueous electrolytes chemical dissolution due to fluoride ions is significant and assuming the existence of a minimum potential to sustain the anodizing process (>5V) [16, 72], a transition from pores to tubes does not occur. The freshly formed structure already has a nanotubular morphology and the presence of oxide rings, the building blocks of the NTs (stack of oxide rings), is evident from the very early stages of the process [76, 114], as also reported in **Fig. 14a-b**.

5.1.2 Transition observed in organic media

A different process occurs when anodizing in organic electrolytes, to which are usually added small amounts of water to ensure sufficient provision of oxygen for the anodic process. For fluoride containing organic electrolytes, whenever the anodization is performed outside a dry glove box, the formation of TiO_2 NTs take place; in contrast nanoporous TiO_2 is obtained under a controlled atmosphere [221]. Hence the water content in the electrolyte plays a decisive role in determining whether a porous or tubular structure is formed, as clearly shown by **Fig. 15a-d**, where TiO_2 NTs were obtained for a water content $\geq$0.7vol. % [221]. Some important considerations can be also

drawn on the basis of experiments conducted on Ti alloys and other valve metals. Bayoumi and Ateya [222] reported the formation of anodized TiO_2 NTs on a Ti-Al alloy, which consisted of a de-alloying process (removal of Al, passivation of Ti) to obtain a nanoporous structure and subsequent anodization with the formation of the nanotubular structure of titania. This is to be expected considering the behaviour observed for Al and Ti which, if anodized under suitable conditions, leads to the formation of nanoporous Al_2O_3 and TiO_2 NTs. Furthermore, Berger et al. [223] investigated the growth of self-ordered structures on pure Ti and Al, as well as on different Ti-Al alloys, demonstrating that a morphological change occurs depending on alloy composition and applied potential. When the Al content in the alloy was the major component the final structure was porous, whereas an increase in the Ti content led to a transition to the formation of NTs and the higher the Ti % in the alloy the lower the potential needed to trigger the transition to NTs. The explanation accounts for the increased stress with increasing Ti content in the alloy, as the Pilling Bedworth Ratio for Ti/TiO_2 (2.43) is larger than Al/Al_2O_3 (1.38) [223]. Similarly, by anodizing a Nb/Ti alloy in a fluoride containing media, Ghicov et al. [224] demonstrated it was possible to produce a mixture of Nb_2O_5-TiO_2 NTs whereas anodization of Nb under identical conditions would lead to generation of nanoporous Nb_2O_5, since niobia is less prone than TiO_2 to attack by fluoride ions. Berger et al. [225] also showed it was possible to generate nanoporous ZrO_2, rather than ZrO_2 NTs, by controlling the water content (1vol.%) in fluoride containing glycerol electrolyte whereas Muratore et al. [226] demonstrated the conversion from ZrO_2 nanopores to ZrO_2 NTs by ageing the anodic film in the electrolyte so that chemical dissolution could take place. Similar conclusions with regards to the transition from nanopores to nanotubes also applies to anodic HfO_2 [227].
The transition from pores to tubes is also favoured by an increase of the fluoride concentration; it occurs because of the higher chemical solubility of the cell boundary (triple point) where a fluoride rich layer accumulates [27], as recently confirmed by a High Resolution Scanning Auger Electron Spectroscopy investigation [211]. This supported the hypothesis that the transition from pores to tubes is triggered by a higher chemical dissolution occurring in the fluoride rich layers. The pore-tube transition due to a fluoride rich layer is schematically shown in **Fig. 16a** [211]. It has also been shown that viscous electrolytes contribute to the suppression of fluoride rich boundaries favouring the formation of TiO_2 nanopores [228]. An alternative mechanism is proposed by Su and Zhou [188]; according to this study the pore to tube transition is driven by dehydration of a $TiO_2 \cdot xH_2O$ complex present on the outer wall of the NTs. Their TEM observations are in good agreement with other reports on the presence of a hydrated outer layer in anodized TiO_2 films and it is known that the anodic structure can harden and shrink following ejection of this excess water [76, 114, 208]. Similar suggestions on the role of dehydration causing the pore to tube transition have been also put forward by Chen et al. [229]. However, despite the fact that such dehydration processes cannot be neglected, based on the evidence available to date, the authors' believe the most plausible reason behind the transition pores to tubes remains the formation of a fluoride rich layer at the NTs cell boundary.

5.1.3 Pore to pore (or NT to NT) spacing and self-ordering

The pore (tube) spacing and the self-ordering established during anodization is strongly related to the pore (tube) nucleation and initial growth processes and the transition from pores to tubes. Again, a useful analogy with AAO exists. Ono et al. [230, 231] provided evidence that a key factor in enhancing the ordering of the AAO array is the electric field, with the most ordered structure obtained at a high current density and applied potential. Chu et al. [232], by adopting a high field anodizing method, reported a change in the junction strength of the alumina cells in the anodic film: at a high potential the junction strength was lower at the boundaries than in the cell walls, hence it was possible to separate alumina cells with increasing electric field and obtain alumina NTs. This was explained in terms of interacting repulsive forces produced from a volume expansion [233]. In the case of TiO_2 NTs the real situation is probably rather more complex and dissolution at the cell boundaries, discussed in **section 5.1.2**, may not be able to explain all the observed morphologies.

For example, Yoriya et al. [191, 234] suggest that the degree of self-order and the formation of either nanopores or NTs are also affected by the conductivity of the electrolyte. **Fig. 16b** [234] shows three different cases of pore spacing, ideally porous TiO_2 (case 1), close packed TiO_2 NTs (case 2) and separated NTs (case 3). While the pore size is determined by the applied potential [147], enhancing the conductivity of the electrolyte causes sufficient ionic mobility (to eliminate competition between pores) [235] and both oxide growth and dissolution is enhanced, leading to a larger pore size and larger pore spacing [234].

5.2 Formation of ribs on the wall of the NTs

Another fascinating aspect of TiO_2 NTs is the presence of ribs along the tubes walls, typical in the case of the 1st and 2nd generations of NTs formed in aqueous solutions; they can also be observed in organic based electrolytes whenever the anodizing conditions are favourable, see **Table II**. It should be noted that in the case of organic electrolytes the ability to discriminate between smooth (rib free) and ribbed NTs could be exploited to tune the surface area and more generally the properties of TiO_2 NTs for specific applications. Several reasons have been put forward to provide a mechanistic explanation for the presence of ribs and major contributions to the field are now discussed.

5.2.1 Studies in aqueous systems

Ribs are always observed in anodized TiO_2 NTs grown in water. An early model proposed by Macak et al. [78] associated rib in water media with regular current oscillations recorded in the current-time transient, associated with pH bursts at the base of the tubes as the anodization progressed. It was possible to suppress the formation of ribs using a highly viscous electrolyte such as glycerol; clearly the water content in the glycerol, although unspecified, must have been below a critical threshold, as discussed in **section 5.2.2**. According to our studies [76, 114], when working with aqueous based electrolytes oxygen evolution is a side reaction that should be taken into account and has an influence on the formation of irregular NTs and on the presence of oxide rings, which pile up to form the NTs. One cannot ignore oxygen evolution when anodizing Ti in water at a potential of typically 20-30V. In water based media oxygen evolution in Ti occurs at potentials as low as 10V and its evolution is recorded as the presence of bubbles within the barrier anodic film [216].

In the case of anodic alumina the pressure inside the bubbles, which varies according to the bubble diameter, is reported to be of the order of 8000, 800, 160 MPa for bubbles of diameter 1nm, 10nm and 50nm respectively [165] and similar pressures (80MPa for 100nm diameter) are reported for barrier layer anodic TiO_2 [236]. The evolution of oxygen occurs whenever there is a significant component of electronic current and it is believed to be triggered by the development of crystalline regions within the anodic film [215]. In the case of anodic TiO_2 NTs, oxygen bubbles are not easily trapped within the oxide as the presence of fluoride ions and the high pressure within the bubbles offer a means of escape for the gas; on the other hand such bubbles can be observed evolving from the anode and reaching the surface of the electrolyte.

5.2.2 Studies in organic systems

When using organic electrolytes, Raja et al. [129] indicate that a minimum concentration of water of 0.5wt. % is a threshold between smooth NTs and the existence of ripples of the NTs. Undoubtedly, the role of water is a key factor in determining the presence or absence of ripples as confirmed by several additional studies [148, 219, 220].

It has been suggested that the ridges represent the growth front of the anodization process and since the NTs are interconnected by these ridges, the passage of the electrolyte is restricted and the electrolyte does not participate in the formation of gaps between the NTs [237]. Similarly, Su et al. [189] reported the ribs to be the remains of two-dimensional sheets supporting the NTs and demonstrated it is also possible to separate such porous layers from the NTs. Valota et al. [219]

associated the formation of ribs with increasing water content, the result of penetration of the electrolyte between the NTs, with subsequent partial chemical dissolution of a fluoride rich boundary present on the outer walls of the NTs. The presence of a fluoride rich layer at the boundaries between cells has indeed been confirmed [33, 211]. To date a clear mechanism fully elucidating the formation process of ribbed NTs is not available. We have recently suggested [148] that given a critical amount of water and a sufficient anodizing potential, an outer layer characterized by oxide rings will form and partial dissolution will then convert such rings into ribs bridging the NTs (eventually a smooth top and a ribbed bottom is obtained for an extended anodizing time and dissolution). Considering that such the ribs could be associated with the anodizing front, it may be possible that they form as a result of partial dissolution of a sequence of anodic layers developing while the NTs are also growing. We believe oxygen evolution is also responsible for the formation of the ribbed NTs, considering that ribs are triggered by the presence of water [145]. Similarly to the formation of oxide rings building up to form the NTs [76, 114], a layer by layer growth model (i.e. breakdown occuring for each single oxide layer eventually leading to a tubular structure) has been recently suggested by Cao et al. based on their observations on a fluoride containing glycerol/water electrolyte [238-240].

Other groups have also considered the influence of oxygen on the anodization of Ti. Valota et al. [146] observed a change in the growth mechanism at 40V in a fluoride containing glycerol electrolyte (again with sufficient water to assist anodization) with oxygen evolution becoming relevant and affecting the regularity of the NTs. Indeed the applied potential is another key factor in determining whether the NTs are smooth or ribbed, because it determines the formation or absence of oxygen bubbles at the anode. Oxygen bubbles lead to the formation of oxide rings and after sufficient time partial dissolution of the rings generates ribs [148]. Similar suggestions on the role of oxygen affecting the morphology of the anodic film have also been put forward by Lee et al. [241, 242] and Schwirn et al. [243] for hard anodized AAO, following the observation of voids/gaps along the cell boundaries and periodic variations in the external pores diameter.

If the ribs are formed as a result of water in the organic electrolyte partially dissolving the oxide, then one would expect the NTs grown in water based electrolytes to be free of ribs, which is clearly not the case. A possible explanation is that ribs and oxide rings are never totally dissolved when anodizing in an aqueous system as the oxide hardens by ejecting excess water and in the process becomes more resistant to attack by fluoride ions. In other words the anodizing process is reasonably fast in water based electrolytes and the denser rings of oxide restructure together to form an irregular tube (i.e. ripples) whereas in organic electrolytes the oxidation process and the dissolution rate are slower, allowing more time for the NTs to equilibrate and become smoother, as confirmed by the observation of partially smooth and partially ribbed NTs [145]. What can be appreciated is that water content, applied potential, evolution of oxygen bubbles and (partial) dissolution phenomena play an important role in the formation of ripples on the wall of the NTs, with a mechanism which is likely to be similar in both water and organic systems.

5.3 Does oxygen evolution have a role on the growth of anodized TiO_2 NTs?

While it has been suggested that oxygen evolution does not represent a significant side reaction during the formation of anodized TiO_2 NTs [139], other reports indicate oxygen evolution at the anode should be taken into account in aqueous media [76, 114] and, depending on applied potential and water content, also in organic electrolytes [145, 146, 148, 219, 220]. It remains to be established whether oxygen bubbles at the anode have a key role in the formation of anodized TiO_2 NTs. The fact that oxygen evolution influences the morphology of anodic porous/tubular structures has been put forward for many other anodized and self-organized structures [244-256]. A theoretical model accounting for the ionic and electronic currents during anodization and supporting the role of oxygen in the growth of the NTs (termed the ‘oxygen bubble mould’ effect) has been recently developed [257].

There are strong arguments in favour of a flow model to account for the formation of anodized TiO_2 NTs [174] as well as other self-organized anodic nanostructures [160], and major progress has been made over the last decade to progress the development of growth models [16, 68-71] proposed in the early stages of the research on anodic TiO_2 NTs. It should be noted that evidence for the "plastic flow" model has been provided for TiO_2 NTs grown in organic electrolytes, whereas it is difficult to collect such evidence in aqueous media, considering anodizing conditions are much more aggressive. From the data available, it is clear that oxygen bubbles are not essential for generating porosity in the anodic structure, and this can be confirmed, for example, by growing TiO_2 NTs in organic electrolytes at a sufficiently low potential such that oxygen evolution does not occur [148]. However, when oxygen gas evolves at the anode it greatly affects the morphology of the NTs.

In aqueous media oxygen bubbles generated within the oxide may line up under the action of the electric field and eventually escape to the surface, aided by the action of fluoride ions breaching through the oxide and partially dissolving it, as shown in **Fig. 17** [76]. As previously discussed, oxygen bubbles would also account for the formation of ribbed TiO_2 NTs in aqueous media. It is interesting to observe that Shin et al. [244] reported the growth of anodic porous tin oxide, a process disrupted by oxygen evolution leading to a structure of the type shown in **Fig. 18a** (top view) and **Fig. 18b** (cross-section). The similarity of the tin oxide NTs to the TiO_2 NTs structure grown in an aqueous electrolyte [114], **Fig.18c-d**, is rather striking. Finally we make note that in the case of self-ordered anodized HfO_2 structure, the presence of oxygen bubbles has been related to the formation of regular dimples on the metallic substrate and it has been suggested that bubbles are key in initiating the growth of the NTs [255].

6. Growth of TiO_2 NTs in fluoride free electrolytes

Nearly all the work undertaken in fluoride free solutions has been performed in electrolytes containing perchlorate, chloride or bromide ions [43-54], leading to the formation of bundles of non self-organized NTs. It has also been demonstrated that NTs bundles can be grown in sulphuric acid by properly tuning the conditions (i.e. electrolyte concentration and applied potential) [55]. The process proceeds at a much faster rate compared to fluoride containing media and long (several μm) NTs are obtained within a few minutes. Clearly the mechanism behind the development of the NTs is different from the plastic flow mechanism observed in fluoride solutions [174]; instead both the lack of self-organization and the faster speed of the process are due to the presence of ions (perchlorate, chloride, bromide) capable of inducing rapid breakdown anodization. By stepping the potential (instead of sweeping) up to several tens of volts, conditions for the passivity breakdown are established (i.e. pitting corrosion [258]); in specific areas the surface is activated and a high current density and rapid growth of the bundles of NTs are observed [43]. Whereas in fluoride solutions the diameter of the NTs is proportional to the applied potential (at least in the range 10 to 60V), when rapid breakdown growth occurs, the NTs exhibit a diameter which does not depend on the applied potential [43-47, 51].

A change in the applied potential does not affect the NTs morphology whereas it affects the number of nucleation sites and therefore the growth rate [47]. Furthermore, since the process is very rapid, the tubes are of significantly smaller diameters (~ 20nm) and a high amount of electrolyte species can be incorporated in the anodic film, for example over 20at% of carbon when operating in organic solutions. This can be exploited to enhance the overlap between the NTs' absorption spectrum and the solar spectrum [44]. Richter et al. [45] studied the anodizing process using chlorinated organic compounds and suggested that the role of carbon is to act as a reducing agent in the complex chlorine-based chemistry leading to the formation of NTs. An interaction between the chloride ions and carbon is hypothesised, based on the fact that the carbon content in the anodic film increased when using a compound with a higher number of chlorine atoms. The same group [46] argue that the high reactivity (i.e. faster rate of formation of NTs) is not simply due to chloride ions breaking

down the barrier layer formed at the metal/metal oxide interface; a sufficiently high potential is also needed to ensure competition between the chlorine (formation of pits, oxidation to chlorine gas) and the oxygen chemistry (i.e. oxidation leading to oxide growth), effectively keeping the barrier layer thickness to a minimum. A thin barrier layer combined with a high potential leads to high reactivity. It is important to highlight that owing to the faster rate of formation, NTs grown by Rapid Breakdown Anodization (RBA) often detach from the metallic substrate and are released in bundles in the electrolyte; this technique may well be exploited as a means for significant production of relatively cheap TiO_2 NT powders [52]. It has also been demonstrated that under specific conditions a change in mechanism from RBA to a plastic flow mechanism leading to self-organized growth of the NTs can be achieved in an organic electrolyte containing chloride ions [53]. Hence ordered structures can be prepared in fluoride free solutions, although those systems are more sensitive to changes and the processing window (applied potential, water content, chloride concentration) within which self-organization occurs is narrower [49, 53]. Interestingly, when the reaction rate is slowed down and the mechanism shifted from RBA to plastic flow, the diameter of the NTs is again observed to be dependent on applied potential [53].

6.1 A comparison between electrolytes with and without fluorine addition

Table 3 lists all the different regimes to be considered for the growth of anodic TiO_2 NTs. In the case of fluoride containing aqueous solutions the process is determined by the competition between field-assisted oxidation and chemical and field-enhanced dissolution. The presence of fluoride ions ensures there is a high density of nucleation sites for the reactions. However in aqueous media chemical dissolution is difficult to control and only short NTs can be grown, whereas chemical dissolution is suppressed in fluoride containing organic electrolytes, growth by plastic flow is prevalent and NTs several tens of μm long can be obtained.

In contrast, what becomes clear observing the nanostructures grown by RBA using the fluoride free approaches [43, 47-49, 52], **Fig. 19a-c**, is that the NTs appear to be interconnected by many TiO_2 nanoparticles, reported to be either amorphous [52] or crystalline [48]. This implies that there are fewer than desired growth points (and concentrated where pitting occurs) and the process is consequently developing much faster than in fluoride containing solutions. The high rate of the growth process also makes self-organization more difficult to achieve. Even in the presence of $ClO_4^-/Cl^-/Br^-$, RBA is poorly sustained by purely organic electrolytes [47] and the best results are observed either in mixed (organic/aqueous) or aqueous electrolytes.

The remaining part of the review discusses the crystallinity (or lack of) in as-prepared anodized TiO_2 NTs and on the effect that heat treatment has on the structure, properties and crystallinity of the NTs.

7. Effect of heat treatments on the structure, properties and crystallinity of anodized TiO_2 NTs

7.1 Crystallography of TiO_2

TiO_2 is known to crystallize in three different polymorphs: rutile (tetragonal), anatase (tetragonal) and brookite (orthorhombic) [259], respectively shown in **Fig. 20a-c** [260]**.**

Rutile has the lowest free energy and it is the most common natural form of titania [261], the most studied and well known of the three polymorphs. Anatase, which is rare in comparison to rutile, is of great interest particularly for its key role in the injection and transport of electrons in photovoltaic devices [262]. Brookite is the rarest form of the mineral, and is not easily obtained synthetically [263]. Brookite and anatase are metastable polymorphs and transform exothermally into rutile; the transformation is irreversible and occurs over a range of temperatures (400 to

1200°C) depending on several factors such as the presence of impurities, the size of the particles and whether the oxide is supported over another material [264, 265]. As can be seen from **Fig. 20a-c,** all three crystal structures are made up of distorted octahedra, each one representing a TiO_6 unit, where each Ti^{4+} is at the centre of the unit and coordinates six O^{2-} ions. The manner in which the octahedra assemble to form a TiO_6 based chain is different and characteristic of each polymorph**.** **Table 4** lists some of the key properties [261, 263] of the three predominant titania polymorphs. Rutile is the most dense phase and has the highest refractive index, while anatase is characterized by the widest band-gap (~3.2eV) [263]. The properties (density, band-gap and refractive index) of brookite fall between those of rutile and anatase.

7.2 As-prepared barrier type anodic TiO_2

Most of the studies on the development of crystallinity during the anodic process have been performed on barrier layer type anodic TiO_2 films and are briefly summarized here. Crystallization takes place gradually over the course of the anodization [266] and is usually associated with breakdown (which for TiO_2 can occur at low potentials [267]) and with compressive stress at the oxide-metal interface [268]. According to Vanhumbeeck et al. [269, 270] the crystallization of anodic TiO_2 contributes to a stress relaxation mechanism which is triggered when reaching a maximum compressive stress (quantified as 4GPa at 12V). A transition from amorphous to crystalline implies a change in the efficiency of the anodic growth, since oxygen evolution (i.e. due to electronic conduction) is aided by the crystallinity. However change in the growth efficiency and oxygen evolution can also be induced by a phase transition from anatase to rutile [271]. Rutile has a narrower band gap (3.05eV) than anatase (3.2eV) [272] thus can better sustain electronic conduction. This implies that oxygen evolution during anodization of barrier type TiO_2 is not homogenous but it depends on the grain orientation of the Ti substrate as well as on the TiO_2 polymorph [236].

7.3 As-prepared anodic TiO_2 NTs

Regarding TiO_2 NTs and more generally porous/tubular anodic oxides, it appears that a necessary condition for porosity is that cations migrating away from the anode are ejected into the electrolyte[159, 160, 174] and therefore the oxide forms mainly at the oxide-metal interface. Hence one may think that, analogous to barrier layer titania, the presence of crystalline regions within the NTs can be expected. However, what it is generally observed is that the as-prepared NTs are amorphous, although nanocrystalline regions may also be present. There are a series of challenges associated with the surface characterization of TiO_2 NTs [273]. It is known for example that crystallization of TiO_2 can be induced by a sufficiently high electron beam and time exposure [274], hence interpretation of results is not always straightforward. However there is convincing evidence suggesting that the presence of crystalline regions within the NTs is not an artifact. Using Raman Spectroscopy, Zhao et al. [70] reported the presence of anatase crystals in TiO_2 NTs anodized in aqueous electrolytes, associating their presence with dielectric breakdown [266]. Our studies revealed the presence of very finely divided crystallized phase (within an overall amorphous structure) possibly due to localized heating associated with the Precision Ion Polishing System (PIPS) used to thin the samples [76]. However, further work [114] without the use of PIPS confirmed the presence of crystalline regions within the as-prepared NTs (grown in an aqueous media), due to crystallization of the hydrated gel ($TiO_2 \cdot xH_2O$) triggered by random differences in concentration, temperature or anode interface morphology during the anodization. Similar findings have also been reported by Low et al. for aqueous media [275] and it appears that slightly heated electrolytes (50°C) also trigger the formation of anatase [276]. Glancing Angle X-Ray Diffraction (GAXRD) work by Yoriya et al. [235] show that partial crystallinity can also be induced in as-prepared NTs anodized in organic electrolytes, specifically at 80V in diethylene glycol (DEG) with

2% of water. Similar results were obtained by Macak et al.[141] for an anodizing potential of 40V and by Cao et al. [240] with crystallinity increasing with increase in water content and anodizing time.

Considering the importance of developing fully crystalline TiO_2 NTs at a sufficiently low temperature to use them with flexible polymeric substrates for photovoltaic applications (although temperature resistant flexible substrates are also available[277]) and in conjunction with temperature sensitive devices, efforts have been made to enhance crystallization without annealing the NTs. Allam et al. [278] demonstrated that the growth of anatase crystals can be improved by adopting a two-step low-temperature (80°C) synthesis process where the Ti substrate is firstly treated with an oxidizing agent and then anodized in a fluorine containing electrolyte. In another work Allam et al. [279] generated partially crystalline NTs using a polyol electrolyte, as a high viscosity was considered beneficial to induce crystal nucleation and formation. Their performance as a photo-anode material for water splitting was investigated and it was concluded a thermal treatment was still necessary to boost their potential; nevertheless, full crystallinity was reached at a relatively low temperature, 300°C, suggesting an enhanced nucleation rate was triggered by pre-existing crystals formed during anodization. In contrast, an amorphous to anatase conversion without thermal treatment to generate highly photoactive NTs has been recently achieved using a simple technique involving the soaking of as-prepared anodized NTs in water [280]. Similarly a post-growth hydrothermal treatment (hot water at ~90°C) is also reported to induce crystallinity in the anodic NTs [281]. However, Liu et al. [282] compared the photoactivities of NTs crystallized at low temperatures treatment and of NTs crystallized by a classic thermal annealing, concluding that the latter remains to date the most reliable approach to induce full crystallinity and a better performing material. Interestingly, a fluoride induced formation of rutile crystals on as-prepared TiO_2 can also be achieved, as shown by Kunze et al. [283], although the mechanism underlying this process is currently not clear.

7.4 Annealed anodic TiO_2 NTs

In a recent review, Paramasivam et al. [64] highlight the need to establish a more quantitative analysis on the influence of tube morphology and composition and the need to investigate approaches to modify the electronic, optical and chemical properties in order to maximize the outcome on the applied research on anodized TiO_2 NTs. While the morphology and composition can be varied by operating either in aqueous or organic electrolytes [284, 285], a straightforward way to modify and enhance the electronic and optical properties of the NTs is certainly represented by post-growth annealing treatments. The annealing and the resulting crystal phase(s) have a significant impact on the electrochemical properties of the NTs [286].

Generally the amorphous nature of most mesoporous materials (such as as-prepared TiO_2 NTs discussed in **section 7.3**) translates into poor thermal and mechanical stability and limits their applications; a crystallized structure not only provides better thermal and mechanical properties, but also enhanced electric, optical and catalytic properties [287]. Indeed several applications are envisaged for films of fully crystalline NTs, including Dye Sensitized Solar Cells (DSSCs) [288], photochemical applications and more generally, redox processes [61, 289, 290]. For such applications the phase, its purity and even the particle/grain size influence the band-gap and the efficiency of a material [263]. Therefore parameters such as crystal structure, degree of crystallinity of anodized TiO_2 NTs as well as their chemical, morphological changes and thermal stability at higher temperatures need to be carefully considered. For example anatase is usually the phase of choice in photovoltaics and photocatalysis as it ensures a better percolation of electrons [262, 291], although it is also known that a mixture of rutile and anatase can be acting as an efficient photocatalysts due to enhanced charge separation [292]. Rutile is instead preferred as a dielectric and in gas-sensing devices [293].

7.4.1 Thermal stability and collapse of the NTs

The first comprehensive work shedding light on the effect of annealing on anodized TiO_2 NTs was reported by Varghese et al. in 2003 [34] who demonstrated that the NTs were stable up to 580°C and did not suffer any major shrinkage when annealed in an oxygen atmosphere. Similar stability temperatures (600-700°C) have been also reported elsewhere [294, 295]. Glancing Angle X-Ray Diffraction (GAXRD) analysis on annealed NTs, **Fig. 21**, shows the presence of anatase (A) crystals in specimens annealed at 280-430°C, whereas rutile (R) crystals begin to appear at 480°C so that a mixture of A and R crystals is detected. As the temperature is further increased only rutile is observed and eventually the NTs collapse as described in **Fig. 22.** Rutile formation on Ti due to thermal oxidation and eventually protrusions emerging from the metal at 550-580°C are considered to be the principal cause of collapse of the NTs [34].

The presence of rutile above 450°C was also reported by Lai et al. who observed a corresponding reduction of the photocatalytic activity of the NTs, although the authors did not clarify whether the rutile was present within the NTs or solely on the Ti support [296]. Further studies confirmed that the NTs collapse above 550-600°C [33, 153, 297-300], with the structure becoming more angular and dense as a result of a sintering process which is aided by the high surface area of the nanoparticles, by an amorphous layer on the outer wall of the tubes and by the residual presence of fluoride ions (i.e. these ions are mostly expelled during the annealing process, but a residual amount remains incorporated within the NTs) [33]. This non-uniform concentration of fluoride ions across the film which is still present in the outer amorphous layer [92] may be an important component in a liquid phase sintering mechanism [301], reducing the temperature of formation of an eutectic mixed oxide fluoride liquid.

Collapse at higher temperatures (800-900°C) is associated with double walled NTs [92] and free standing NTs membranes [302], however degradation of the NTs and the sintering process is evident from TEM observations at temperatures similar to those previously reported with anatase crystals appearing at 300°C. It has also been shown that in N-doped NTs the damage induced by ion bombardment, leading to lower photo-conversion response, can be healed with a thermal treatment [303]. As an alternative to classic annealing treatments performed in furnaces, flame annealing has been also investigated as a technique capable of producing crystalline NTs within seconds and providing good control over the anatase/rutile ratio produced by monitoring the time of the flame treatment [304].

7.4.2 Anatase to rutile transformation

As discussed in the previous section, the phase and crystallinity of TiO_2 NTs are dependent on the calcination temperature. For very small crystallite sizes (i.e. few nm), HRTEM is the best method to determine the phase and such investigations has been covered by several works [33, 152, 189, 305, 306]. As previously highlighted, care needs to be taken in making definitive conclusions since the TiO_2 can undergo phase "premature" transformation in the TEM particularly when the electron beam is condensed to a small spot, giving a high energy density and heating of the specimen. Indeed, crystallization and shrinkage of a structure may be induced by TEM [274]. Nevertheless, HRTEM represents a powerful instrument to investigate nanostructured materials, including TiO_2.

According to Varghese et al. [34], considering the size constraints imposed by the NTs wall and the reported stability of 10-15nm anatase nanocrystals [307, 308] it is likely that the crystal within the NTs walls may not undergo any transition and can remain as anatase up to 500-600°C. The eventual transition to rutile coincides with the collapse of the NTs. Jaroenworaluck et al. [33] discussed the crystallinity of the NTs over a range of temperatures, combining evidence from HRTEM characterization [33] with Raman [153], XRD [218] and XPS [32, 134] analysis. Whereas at room temperature the samples consisted of very fine grains within an overall amorphous matrix [114], the presence of anatase is clearly shown at temperatures as low as 200°C, although Raman and XRD cannot easily detect it, as the particle size is very small and an amorphous matrix persists. According to HRTEM, crystallization of the NTs to anatase can be considered completed at a

temperature as low as 300°C, as shown in **Fig. 23a-b** [33]. The NTs were annealed without the presence of the Ti substrate, and rutile was not detected (i.e. rutile crystals were detected only at 500°C or above), consolidating Varghese's model on the formation of rutile crystals taking place mainly at the Ti/TiO_2 interface. Factors contributing to a reduction of the crystallization temperature (i.e. 300°C from TEM whereas it can be assumed at around 400°C according to XRD studies) are the very high surface area of the small crystallites, the strain energy due to presence of defects as well as impurity effects [33].

However from HRTEM analysis performed by Su et al. on NTs calcined at 300°C [305], **Fig. 24a-d**, both anatase (**Fig. 24 c**) and rutile crystals (**Fig. 24b** and **24d**) can be observed at the tube bottom and on the outer tube wall. It is evident that the crystallization process also depends on the sample preparation and history. For example our samples for TEM [33] were grown in aqueous media whereas the analysis of Su et al. [305] were carried out on NTs obtained in ethylene glycol (with only minor water content). Generally, it can be concluded rutile becomes dominant above 500-600°C (depending on sample preparation and history) and nucleate preferentially at the interface between the NTs and the Ti substrate. However the phase transition from anatase to rutile can also begin at a lower temperature, especially when the anodization is carried out in an organic media. Considering the higher carbon content in as prepared NTs grown in organic electrolytes (as discussed in **section 4.3.1**), in our view it is likely that during the calcination step a higher amount of oxygen vacancies is induced in the anodic NTs. It is known that oxygen vacancies are generally better accommodated by rutile rather than anatase [309].

Indeed it has been suggested in other studies that the formation of rutile at the metal/metal oxide interface observed for NTs on the Ti support is associated with oxygen vacancies generated at the interface due to a reaction between Ti and TiO_2 at the base of the tubes [302]. Oxygen deficiency at the metal/metal oxide interface is also common for TiO_2 anodized in NaCl [208] and it is interesting that differences in the oxygen and titanium concentrations between the NTs wall and the barrier layer at the bottom of the NTs have been found by Nguyen et al. [237], with the barrier layer exhibiting higher oxygen vacancy density following heat treatments at 400°C. Macak et al. reported similar results for smooth tubes prepared in viscous electrolytes, obtaining anatase crystals at 450°C, also showing that fluorine ions are mostly expelled from the anodic film during the thermal treatment [310]. The presence of cracks (or possibly so called 'ghost boundaries') within the NTs walls when annealing above 450°C [31] suggests a lower temperature of 350°C to be the most suitable for thermal treatment of NTs.

The anatase-rutile transition in the NTs occurs at lower temperatures in Ar [34, 311], allowing rutile crystals to form within the NTs wall without the structure collapsing, although pore shrinkage and thinning of the NTs wall is observed [34]. The temperature utilized (>500°C) and the Ar atmosphere are capable of inducing partial reduction of bulk TiO_2 into Ti_nO_{2n-1}, known as Magnéli phases[312, 313], which presents crystallographic shear planes to accommodate the oxygen loss[314, 315]. These shear planes derive from the initial presence of the rutile structure, the formation of which is therefore facilitated in Ar. Recent studies performed on TiO_2 nanoparticles and NT_s confirms that whenever annealing is performed in a depleted oxygen atmosphere, reduction of Ti^{4+} to Ti^{3+} occurs and the anatase to rutile transformation is promoted [316-318]. Ti_nO_{2n-1} phases have a higher density than TiO_2 [313] and also contribute to the shrinkage of the structure. It is worth noting that semi-metallic NTs containing such Magnéli phases have been successfully prepared by adopting a carbo-thermal treatment (i.e. high thermal treatment in acetylene). Hence not only can the crystalline phase be controlled through annealing, but the conductivity of the material can be shifted from semi-conductor to semi-metallic [319, 320]. The possibility of ranging the conductivity of the NTs within several order of magnitude is appealing not only in photo-voltaic technology, but also in sensing [321, 322], electrocatalysis [323] and more generally in electrochemical applications where good conductivity and chemical resistance are both required [324, 325].

7.4.3 Crystal size-effects

Recently Bauer et al. [326] reported on an unusual "size-effect" dependent anatase/rutile stabilisation for TiO_2 NTs; their results are in line with previous studies[33, 34] showing that to induce rutile formation the aid of a Ti support is necessary. However, whereas nanocrystalline TiO_2 anatase is generally favoured within small crystals (10-30nm) [307, 308], rutile is the stable phase within the NTs walls for NT diameters <30nm and anatase is stabilized in the larger diameter NTs [326]. Further studies on the crystal size and phases present in the NTs should be carried out, considering the importance of TiO_2 in photocatalysis: it is expected that the crystallite size and phase can modify the internal reflection of light and ultimately the phonon absorption, hence affecting the efficiency of a photocatalytic process. Finally, another aspect that should be considered in future investigations is also the impact of defects (such as oxygen vacancies) on the properties of TiO_2 NTs. For example, very little is known on the effect of oxidation state of TiO_2 NTs on their photocatalytic activity [327], although there is a raising awareness that defect chemistry can be exploited for the processing of structures with tailorable properties [328].

8. Conclusions

The review has presented a comprehensive analysis of the state of the art of the growth mechanism behind the formation of anodized TiO_2 NTs and on post-growth treatments to induce full crystallinity in the NTs. A number of key points emerge:

i. Major breakthroughs have been made over the last decade, progressing from a 1^{st} generation of short and poorly organized NT arrays to a 3^{rd} and 4^{th} generations of long (hundreds of μm) and highly organized arrays of anodized TiO_2 NTs.
ii. The mechanism behind the growth of the NTs is a fascinating topic and the understanding of the process has been recently greatly improved. A modified high field regime (i.e. the NTs growth occurs only at the metal/metal oxide interface) can be assumed. The TiO_2 NTs are then growing principally by plastic flow model when organic electrolytes containing fluoride ions are used. In organic media the TiO_2 film initially develops as a porous film, then due to the presence of fluoride ions accumulating at triple points, the pores separate each other into well-defined NTs.
iii. The situation is more complex in aqueous electrolytes (1^{st} and 2^{nd} generations) where chemical dissolution cannot be ignored. A transition from a porous to tubular nanostructure is not observed and NTs are found to be present from the early stages of the process.
iv. The ejection of Ti^{4+} ions into the electrolyte is essential to initiate porosity in the anodic film. Chemical dissolution can also help initiate and sustain porosity during the anodization
v. Whenever oxygen bubbles form at the anode, they influence the morphology of the NTs. There is possibly a link between oxygen evolution and the presence of ribs on their outer wall (i.e. smooth NTs are formed when oxygen evolution does not occur).
vi. The NTs can also be grown in fluoride free electrolytes by Rapid Breakdown Anodization (RBA), although self-organization is difficult to achieve by RBA due to the fast growth of the anodic film under such conditions.
vii. Depending on the heat treatment temperature and atmosphere different crystalline structures are induced in the NTs (i.e. anatase or rutile) and the electrical properties change from semi-conductor to semi-metallic. A temperature limit exists (500 to 800°C depending on preparation history) above which sintering of particles and collapse of the NTs structure occurs and any benefits associated with an ordered nanostructure are lost. There is also the need to develop ways to control not only the crystalline phase, but also the defects generated during the annealing and to investigate how these defects can be exploited in specific applications (i.e. photocatalysis, water splitting, photovoltaics).

Acknowledgements

The authors wish to acknowledge the support of the National Metal and Materials Technology Center (MTEC) under project No. MT-B-48-CER-07-190-I. D. Regonini would also like to thank the Royal Academy of Engineers (RAEng) and The Worshipful Company of Armourers and Brasiers. C.R. Bowen acknowledges funding from the European Research Council under the European Union's Seventh Framework Programme (FP/2007-2013) / ERC Grant Agreement no. 320963 on Novel Energy Materials, Engineering Science and Integrated Systems (NEMESIS).

References

[1] G. Pfaff, P. Reynders, Chem. Rev. 99 (1999) 1963-1982.
[2] R. Van Noort, J. Mater. Sci. 22 (1987) 3801-3811.
[3] M.A. Fox, M. Dulay, Chem. Rev. 93 (1993) 341-357.
[4] A. Fujishima, K. Honda, Nature 238 (1972) 37-38.
[5] M. Zayat, P. Garcia-Parejo, D. Levy, Chem. Soc. Rev. 36 (2007) 1270-1281.
[6] B. O'Regan, M. Gratzel, Nature 353 (1991) 737-740.
[7] K. G, Mater. Sci. Eng. B 139 (2007) 1-23.
[8] H. Chik, J.M. Xu, Mater. Sci. Eng. R 43 (2004) 103-138.
[9] P.V. Kamat, J. Phys. Chem. C 116 (2012) 11849-11851.
[10] X. Chen, S.S. Mao, Chem. Rev. 107 (2007) 2891-2959.
[11] F. Keller, M.S. Hunter, D.L. Robinson, J. Electrochem. Soc. 110 (1953) 411-419.
[12] H. Masuda, K. Fukuda, Science 268 (1995) 1466-1468.
[13] M. Assefpour-Dezfuly, C. Vlachos, E.H. Andrews, J. Mater. Sci. 19 (1984) 3626-3639.
[14] V. Zwilling, E. Darque-Ceretti, A. Boutry-Forveille, D. David, M.Y. Perrin, M. Aucouturier, Surf. Int. Analysis 27 (1999) 629-637.
[15] V. Zwilling, M. Aucouturier, E. Darque-Ceretti, Electrochim. Acta 45 (1999) 921-929.
[16] D. Gong, C.G. Grimes, O.K. Varghese, W. Hu, R.S. Singh, Z. Chen, E.C. Dickey, J. Mater. Res. 16 (2001) 3331-3334.
[17] H. Tsuchiya, P. Schmuki, Electrochem. Comm. 6 (2004) 1131-1134.
[18] W.-J. Lee, W.H. Smyrl, Electrochem. Solid-State Lett. 8 (2005) B7-B9.
[19] H. Tsuchiya, J.M. Macak, I. Sieber, L. Taveira, A. Ghicov, K. Sirotna, P. Schmuki, Electrochem. Comm. 7 (2005) 295-298.
[20] N.R. de Tacconi, C.R. Chenthamarakshan, G. Yogeeswaran, A. Watcharenwong, R.S. de Zoysa, N.A. Basit, K. Rajeshwar, J. Phys. Chem. B 110 (2006) 25347-25355.
[21] I. Sieber, H. Hildebrand, A. Friedrich, P. Schmuki, Electrochem. Comm. 7 (2005) 97-100.
[22] K. Robert L, Electrochem. Comm. 7 (2005) 1190-1194.
[23] I. Sieber, B. Kannan, P. Schmuki, Electrochem. Solid-State Lett. 8 (2005) J10-J12.
[24] H. El-Sayed, S. Singh, M.T. Greiner, P. Kruse, Nano Lett. 6 (2006) 2995-2999.
[25] H. Tsuchiya, P. Schmuki, Electrochem. Comm. 7 (2005) 49-52.
[26] Y. Yang, S.P. Albu, D. Kim, P. Schmuki, Angew. Chem. Int. Ed. Engl. 50 (2011) 9071-9075.
[27] P. Roy, S. Berger, P. Schmuki, Angew. Chem. Int. Ed. Engl. 50 (2011) 2904-2939.
[28] S.P. Albu, A. Ghicov, P. Schmuki, Phys. Status Solidi RRL 3 (2009) 64-66.
[29] B. Pandey, P.S. Thapa, D.A. Higgins, T. Ito, Langmuir 28 (2012) 13705-13711.
[30] C.-Y. Lee, K. Lee, P. Schmuki, Angew. Chem. Int. Ed. Engl. 52 (2013) 2077-2081.
[31] S.P. Albu, H. Tsuchiya, S. Fujimoto, P. Schmuki, Eur. J. Inorg. Chem. 2010 (2010) 4351-4356.
[32] D. Regonini, A. Jaroenworaluck, R. Stevens, C.R. Bowen, Surf. Int. Analysis 42 (2010) 139-144.
[33] A. Jaroenworaluck, D. Regonini, C.R. Bowen, R. Stevens, Appl. Surf. Sci. 256 (2010) 2672-2679.
[34] O.K. Varghese, D. Gong, M. Paulose, C.G. Grimes, E.C. Dickey, J. Mater. Res. 18 (2003) 156-165.
[35] J.W. Diggle, T.C. Downie, C.W. Goulding, Chem. Rev. 69 (1969) 365-405.
[36] Q. Van Overmeere, B. Nysten, J. Proost, Appl. Phys. Lett. 94 (2009) 074103.
[37] A. Baron-Wiecheć, J.J. Ganem, S.J. Garcia-Vergara, P. Skeldon, G.E. Thompson, I.C. Vickridge, J. Electrochem. Soc. 157 (2010) C399.
[38] K.R. Hebert, S.P. Albu, I. Paramasivam, P. Schmuki, Nat. Mater. 11 (2012) 162-166.
[39] J.B. Ward, The colouring and working of the refractory metals Titanium, Niobium and Tantalum for jewellery and allied applications The Worshipful Company of Goldsmiths, Design and Technology Committee, London, 1982.
[40] M.M. Lohrengel, Mater. Sci. Eng. R 11 (1993) 243-294.
[41] Y. Sul, C.B. Johansson, Y. Jeong, T. Albrektsson, Med. Eng. Phys. 23 (2001) 329-346.
[42] J.M. Macak, H. Tsuchiya, A. Ghicov, K. Yasuda, R. Hahn, S. Bauer, P. Schmuki, Curr. Opin. Solid Stat. Mater. Sci. 11 (2007) 3-18.
[43] R. Hahn, J.M. Macak, P. Schmuki, Electrochem. Comm. 9 (2007) 947-952.
[44] C. Richter, Z. Wu, E. Panaitescu, R.J. Willey, L. Menon, Adv. Mater. 19 (2007) 946-948.
[45] C. Richter, E. Panaitescu, R. Willey, L. Menon, J. Mater. Res. 22 (2007) 1624-1631.
[46] E. Panaitescu, C. Richter, L. Menon, J. Electrochem. Soc. 155 (2008) E7-E13.
[47] Q.A. Nguyen, Y.V. Bhargava, T.M. Devine, Electrochem. Comm. 10 (2008) 471-475.
[48] R.P. Antony, T. Mathews, A. Dasgupta, S. Dash, A.K. Tyagi, B. Raj, J. Solid State Chem. 184 (2011) 624-632.
[49] N.K. Allam, C.G. Grimes, J. Phys. Chem. C 111 (2007) 13028-13032.
[50] K.-I. Ishibashi, R.-T. Yamaguchi, Y. Kimura, M. Niwano, J. Electrochem. Soc. 155 (2008) K10-K14.

[51] K. Nakayama, T. Kubo, Y. Nishikitani, Electrochem. Solid-State Lett. 11 (2008) C23-C26.
[52] N.F. Fahim, T. Sekino, Chem. Mater. 21 (2009) 1967-1979.
[53] R. Hahn, K. Lee, D. Kim, S. Narayanan, S. Berger, P. Schmuki, ECS Trans. 16 (2008) 369-373.
[54] H. Jha, R. Hahn, P. Schmuki, Electrochim. Acta 55 (2010) 8883-8887.
[55] N.F. Fahim, T. Sekino, M.F. Morks, T. Kusunose, J. Nanosci. Nanotech. 9 (2009) 1803-1818.
[56] G.K. Mor, O.K. Varghese, M. Paulose, K. Shankar, C.A. Grimes, Sol. Energy Mater. Sol. Cells 90 (2006) 2011-2075.
[57] C.A. Grimes, J. Mater. Chem. 17 (2007) 1451-1457.
[58] A. Ghicov, P. Schmuki, Chem. Comm. (2009) 2791-2808.
[59] P. Roy, D. Kim, K. Lee, E. Spiecker, P. Schmuki, Nanoscale 2 (2010) 45-59.
[60] Y.C. Nah, I. Paramasivam, P. Schmuki, Chem. Phys. Chem. 11 (2010) 2698-2713.
[61] S. Rani, S.C. Roy, M. Paulose, O.K. Varghese, G.K. Mor, S. Kim, S. Yoriya, T.J. Latempa, C.A. Grimes, Phys. Chem. Chem. Phys. 12 (2010) 2780-2800.
[62] S. Berger, R. Hahn, P. Roy, P. Schmuki, Phys. Status Solidi B 247 (2010) 2424-2435.
[63] Y. Jun, J.H. Park, M.G. Kang, Chem. Comm. 48 (2012) 6456-6471.
[64] I. Paramasivam, H. Jha, N. Liu, P. Schmuki, Small 8 (2012) 3073-3103.
[65] P. Szymanski, M. El-Sayed, Theor. Chem. Acc. 131 (2012) 1-12.
[66] C.A. Grimes, G.K. Mor, TiO2 Nanotube Arrays: Synthesis, Properties, and Applications, 1st Edition, Springer, 2009.
[67] D.V. Bavykin, F.C. Walsh, Titanate and Titania Nanotubes: Synthesis, Properties and Applications, 1st Edition, Royal Society of Chemistry, Cambridge, 2009.
[68] J.K. Mor, O.K. Varghese, M. Paulose, N. Mukherjee, C.G. Grimes, J. Mater. Res. 18 (2003) 2588-2593.
[69] R. Beranek, H. Hildebrand, P. Schmuki, Electrochem. Solid-State Lett. 6 (2003) B12-B14.
[70] J. Zhao, X. Wang, R. Chen, L. Li, Solid State Comm. 134 (2005) 705-710.
[71] K. Raja, M. Misra, K. Paramguru, Electrochim. Acta 51 (2005) 154-165.
[72] Q. Cai, M. Paulose, O.K. Varghese, C.A. Grimes, J. Mater. Res. 20 (2005) 230-236.
[73] J.M. Macak, H. Tsuchiya, P. Schmuki, Angew. Chem. Int. Ed. Engl. 44 (2005) 2100-2102.
[74] J. Macak, K. Sirotna, P. Schmuki, Electrochim. Acta, 50 (2005) 3679-3684.
[75] J.M. Macak, L.V. Taveira, H. Tsuchiya, K. Sirotna, J. Macak, P. Schmuki, J. Electroceram. 16 (2006) 29-34.
[76] A. Jaroenworaluck, D. Regonini, C.R. Bowen, R. Stevens, D. Allsopp, J. Mater. Sci. 42 (2007) 6729-6734.
[77] C. Ruan, M. Paulose, O.K. Varghese, G.K. Mor, C.G. Grimes, J. Phys. Chem. B 109 (2005) 15754-15759.
[78] J.M. Macak, H. Tsuchiya, L. Taveira, S. Aldabergerova, P. Schmuki, Angew. Chem. Int. Ed. Engl. 44 (2005) 7463-7465.
[79] J. Macak, P. Schmuki, Electrochim. Acta, 52 (2006) 1258-1264.
[80] M. Paulose, K. Shankar, S. Yoriya, H.E. Prakasam, O.K. Varghese, G.K. Mor, T.A. Latempa, A. Fitzgerald, C.G. Grimes, J. Phys. Chem. B, 110 (2006) 16179-16184.
[81] S. Yoriya, H.E. Prakasam, O.K. Varghese, K. Shankar, M. Paulose, G.K. Mor, T.A. Latempa, C.A. Grimes, Sensor Lett. 4 (2006) 334-339.
[82] K. Shankar, G.K. Mor, H.E. Prakasam, S. Yoriya, M. Paulose, O.K. Varghese, C.A. Grimes, Nanotechnology 18 (2007) 065707.
[83] H.E. Prakasam, K. Shankar, M. Paulose, O.K. Varghese, C.G. Grimes, J. Phys. Chem. C 111 (2007) 7235-7241.
[84] M. Paulose, H.E. Prakasam, O.K. Varghese, L. Peng, K.C. Popat., G.K. Mor, T.A. Desai, C.G. Grimes, J. Phys. Chem. C 111 (2007) 14992-14997.
[85] J.M. Macak, S.P. Albu, P. Schmuki, Phys. Status Solidi RRL 1 (2007) 181-183.
[86] S.P. Albu, A. Ghicov, J.M. Macak , P. Schmuki, Physica Status Solid RRL 1 (2007) R65-R67.
[87] Y. Shin, S. Lee, Nano Lett., 8 (2008) 3171-3173.
[88] I. Paramasivam, J.M. Macak, T. Selvam, P. Schmuki, Electrochim. Acta, 54 (2008) 643-648.
[89] H. Wender, A.F. Feil, L.B. Diaz, C.S. Ribeiro, G.J. Machado, P. Migowski, D.E. Weibel, J. Dupont, S.R. Teixeira, ACS Appl. Mater. Interfaces 3 (2011) 1359-1365.
[90] S.P. Albu, D. Kim, P. Schmuki, Angew. Chem. Int. Ed. Engl. 47 (2008) 1916-1919.
[91] Y. Ji, K.-C. Lin, H. Zheng, J.-J. Zhu, A.C.S. Samia, Electrochem. Comm. 13 (2011) 1013-1015.
[92] S.P. Albu, A. Ghicov, S. Aldabergenova, P. Drechsel, D. LeClere, G.E. Thompson, J.M. Macak, P. Schmuki, Adv. Mater. 20 (2008) 4135-4139.
[93] H. Mirabolghasemi, N. Liu, K. Lee, P. Schmuki, Chem. Comm. 49 (2013) 2067-2069.
[94] H. Tsuchiya, J.M. Macak, A. Ghicov, P. Schmuki, Small 2 (2006) 888-891.
[95] Y.-Y. Song, P. Schmuki, Electrochem. Comm., 12 (2010) 579-582.
[96] K. Yasuda, J.M. Macak, S. Berger, A. Ghicov, P. Schmuki, J. Electrochem. Soc. 154 (2007) C472-C478.
[97] J.M. Macak, S. Albu, D.H. Kim, I. Paramasivam, S. Aldabergerova, P. Schmuki, Electrochem. Solid-State Lett. 10 (2007) K28-K31.
[98] H. Li, J. Wang, K. Huang, G. Sun, M. Zhou, Mater. Lett. 65 (2011) 1188-1190.
[99] S. Albu, A. Ghicov, J.M. Macak , S.H. Han, P. Schmuki, Nano Lett. 7 (2007) 1286-1289.
[100] J. Wang, Z. Lin, Chem. Mater. 20 (2008) 1257-1261.
[101] S. Yoriya, C.G. Grimes, Langmuir 26 (2010) 417-420.
[102] S.P. Albu, P. Schmuki, Phys. Status Solidi RRL 4 (2010) 215-217.
[103] Y.R. Smith, B. Sarma, S.K. Mohanty, M. Misra, ACS Appl. Mater. Interfaces 4 (2012) 5883-5890.
[104] L. Sun, S. Zhang, X.W. Sun, X. Wang, Y. Cai, Langmuir 26 (2010) 18424-18429.
[105] T. Ruff, R. Hahn, P. Schmuki, Appl. Surf. Sci. 257 (2011) 8177-8181.
[106] W. Wei, H. Jha, G. Yang, R. Hahn, I. Paramasivam, S. Berger, E. Spiecker, P. Schmuki, Adv. Mater. 22 (2010) 4770-4774.
[107] B. Chen, K. Lu, Langmuir 28 (2012) 2937-2943.
[108] R. Sánchez-Tovar, K. Lee, J. García-Antón, P. Schmuki, Electrochem. Comm. 26 (2013) 1-4.
[109] B. Chen, K. Lu, Physical Chemistry Chemical Physics, 15 (2013) 1854-1862.
[110] S. Leonardi, A. Li Bassi, V. Russo, F. Di Fonzo, O. Paschos, T.M. Murray, H. Efstathiadis, J. Kunze, J. Phys. Chem. C 116 (2012) 384-392.

[111] Z. Su, L. Zhang, F. Jiang, W. Zhou, Z. Deng, Y. Cao, M. Hong, Electrochem. Comm. 31 (2013) 67-70.
[112] W. Wei, R. Kirchgeorg, K. Lee, S. So, P. Schmuki, Phys. Status Solidi RRL 5 (2011) 394-396.
[113] Z. Su, M. Buhl, W. Zhou, J. Am. Chem. Soc. 131 (2009) 8697-8702.
[114] A. Jaroenworaluck, D. Regonini, C.R. Bowen, R. Stevens, J. Mater. Res. 23 (2008) 2116-2124.
[115] A. Mazzarolo, M. Curioni, A. Vicenzo, P. Skeldon, G.E. Thompson, Electrochim. Acta, 75 (2012) 288-295.
[116] L.V. Taveira, J.M. Macak, K. Sirotna, L.F.P. Dick, P. Schmuki, J. Electrochem. Soc. 153 (2006) B137-B143.
[117] A. Valota, D.J. Leclere, T. Hashimoto, P. Skeldon, G.E. Thompson, S. Berger, J. Kunze, P. Schmuki, Nanotechology 19 (2008) 355701-355707.
[118] K. Yasuda, P. Schmuki, Electrochim. Acta 52 (2007) 4053-4061.
[119] O. Jessensky, F. Müller, U. Gösele, Appl. Phys. Lett.72 (1998) 1173-1175.
[120] O. Jessensky, F. Muller, U. Gosele, J. Electrochem.Soc. 145 (1998) 3735-3740.
[121] A.P. Li, F. Müller, A. Birner, K. Nielsch, U. Gösele, J. Appl. Phys. 84 (1998) 6023-6026.
[122] B. Melody, T. Kinard, P. Lessner, Electrochem. Solid-State Lett. 1 (1998) 126-129.
[123] G.M. Krembs, J. Electrochem. Soc. 110 (1963) 938-940.
[124] R.G. Kelly, P.J. Moran, J. Kruger, J. Electrochem. Soc. 136 (1989) 3262-3269.
[125] M. Ue, H. Asahina, S. Mori, J. Electrochem. Soc. 142 (1995) 2266-2271.
[126] Y.M. Li, L. Young, J. Electrochem. Soc.148 (2001) B337-B342.
[127] D. Kim, K. Lee, P. Roy, B.I. Birajdar, E. Spiecker, P. Schmuki, Angew. Chem. Int. Ed. Engl. 48 (2009) 9326-9329.
[128] K. Lee, D. Kim, P. Roy, I. Paramasivam, B.I. Birajdar, E. Spiecker, P. Schmuki, J. Am. Chem. Soc. 132 (2010) 1478-1479.
[129] K.S. Raja, T. Gandhi, M. Misra, Electrochem. Comm. 9 (2007) 1069-1076.
[130] Q. Lu, T. Hashimoto, P. Skeldon, G.E. Thompson, H. Habazaki, K. Shimizu, Electrochem. Solid-State Lett. 8 (2005) B17-B20.
[131] K. Shankar, G.K. Mor, A. Fitzgerald, C.G. Grimes, J. Phys. Chem. C Lett. 111 (2007) 21-26.
[132] L.V. Taveira, J.M. Macák, H. Tsuchiya, L.F.P. Dick, P. Schmuki, J. Electrochem. Soc. 152 (2005) B405.
[133] K. Zhu, N.R. Neale, A. Miedaner, A.J. Frank, Nano Lett. 7 (2006) 69-74.
[134] D. Regonini, Anodised TiO_2 nanotubes: synthesis, growth mechanism and thermal stability, PhD Thesis, University of Bath, 2008.
[135] J.H. Lim, J. Choi, Small, 3 (2007) 1504-1507.
[136] D. Kim, A. Ghicov, P. Schmuki, Electrochem. Comm. 10 (2008) 1835-1838.
[137] S.P. Albu, P. Schmuki, Phys. Status Solidi RRL 4 (2010) 151-153.
[138] S. So, K. Lee, P. Schmuki, J. Am. Chem. Soc. 134 (2012) 11316-11318.
[139] F. Thébault, B. Vuillemin, R. Oltra, J. Kunze, A. Seyeux, P. Schmuki, Electrochem. Solid-State Lett. 12 (2009) C5-C9.
[140] A. Kaczmarek, T. Klekiel, E. Krasicka-Cydzik, Surf. Int. Analysis 42 (2010) 510-514.
[141] J.M. Macak, H. Hildebrand, U. Marten-Jahns, P. Schmuki, J. Electroanalytical Chem. 621 (2008) 254-266.
[142] C.-C. Chen, S.-J. Hsieh, J. Electrochem. Soc. 157 (2010) K125-K130.
[143] S. Li, G. Zhang, D. Guo, L. Yu, W. Zhang, J. Phys. Chem. C 113 (2009) 12759-12765.
[144] K. Lee, J. Kim, H. Kim, Y. Lee, D. Kim, P. Schmuki, Y. Tak, J. Korean Phys. Soc. 54 (2009) 1027-1031.
[145] D. Regonini, A. Satka, D. Allsopp, A. Jaroenworaluck, R. Stevens, C.R. Bowen, J. Nanosci. Nanotech. 9 (2009) 4410-4416.
[146] A. Valota, M. Curioni, D.J. Leclere, P. Skeldon, P. Falaras, G.E. Thompson, J. Electrochem. Soc. 157 (2010) K243-K247.
[147] S. Yoriya, M. Paulose, O.K. Varghese, G.K. Mor, C.A. Grimes, J. Phys. Chem. C 111 (2007) 13770-13776.
[148] D. Regonini, A. Satka, A. Jaroenworaluck, D.W.E. Allsopp, C.R. Bowen, R. Stevens, Electrochim. Acta, 74 (2012) 244-253.
[149] S.A. Ali Yahia, L. Hamadou, A. Kadri, N. Benbrahim, E.M.M. Sutter, J. Electrochem. Soc. 159 (2012) K83-K92.
[150] L. Yin, S. Ji, G. Liu, G. Xu, C. Ye, Electrochem. Comm. 13 (2011) 454-457.
[151] Z. Su, W. Zhou, J. Mater. Chem. 21 (2011) 357-362.
[152] Z. Su, W. Zhou, J. Mater. Chem. 21 (2011) 8955-8970.
[153] D. Regonini, C.R. Bowen, R. Stevens, D. Allsopp, A. Jaroenworaluck, Phys. Status Solidi A 204 (2007) 1814-1819.
[154] V.M. Prida, E. Manova, V. Vega, M. Hernandez-Velez, P. Aranda, K.R. Pirota, M. Vázquez, E. Ruiz-Hitzky, J. Magnetism and Magnetic Mater. 316 (2007) 110-113.
[155] J. Wang, Z. Lin, J. Phys. Chem. C 113 (2009) 4026-4030.
[156] N. Khalil, J.S. Leach, Electrochim. Acta 31 (1986) 1279-1285.
[157] T.P. Hoar, N.F. Mott, J. Phys. Chem. Solids 9 (1959) 97-99.
[158] J.P. O'Sullivan, G.C. Wood, Proceedings of the Royal Society A: Math. Phys. Eng. Sci. 317 (1970) 511-543.
[159] P. Skeldon, G.E. Thompson, S.J. Garcia-Vergara, L. Iglesias-Rubianes, C.E. Blanco-Pinzon, Electrochem. Solid-State Lett. 9 (2006) B47-B51.
[160] S. Garcia-Vergara, P. Skeldon, G. Thompson, H. Habazaki, Electrochim. Acta 52 (2006) 681-687.
[161] N. Sato, Electrochim. Acta, 16 (1971) 1683-1692.
[162] P. Campestrini, G.E. Thompson, P. Skeldon, C.E. Blanco-Pinzon, L. Iglesias-Rubianes, S.J. Garcia-Vergara, Proceedings of the Royal Society A: Math. Phys. Eng. Sci. 462 (2006) 2345-2358.
[163] J.P.S. Pringle, Electrochim. Acta 25 (1980) 1423 -1437.
[164] J.S.L. Leach, P. Neufeld, Corr. Sci. 9 (1969) 225-244.
[165] A.C. Crossland, H. Habazaki, K. Shimizu, P. Skeldon, G.E. Thompson, G.C. Wood, X. Zhou, C.J.E. Smith, Corr. Sci. 41 (1999) 1945-1954.
[166] X. Zhou, H. Habazaki, K. Shimizu, P. Skeldon, G.E. Thompson, G.C. Wood, Proceedings of the Royal Society A: Math. Phys. Eng. Sci. 455 (1999) 385-399.
[167] L. Iglesias-Rubianes, P. Skeldon, G.E. Thompson, H. Habazaki, K. Shimizu, J. Electrochem. Soc. 149 (2002) B23-B26.
[168] X. Zhou, G.E. Thompson, H. Habazaki, M.A. Paez, K. Shimizu, P. Skeldon, G.C. Wood, J. Electrochem. Soc. 147 (2000) 1747-1750.
[169] J. Siejka, C. Ortega, J. Electrochem. Soc. 124 (1977) 883-891.
[170] G. Amsel, D. Samuel, J. Phys. Chem. Solids 23 (1962) 1707-1718.
[171] G.E. Thompson, Y. Xu, P. Skeldon, K. Shimizu, S.H. Han, G.C. Wood, Phil. Mag. B 55 (1987) 651-667.

[172] G.E. Thompson, Thin Solid Films 297 (1997) 192-201.
[173] J.E. Houser, K.R. Hebert, Nat. Mater. 8 (2009) 415-429.
[174] D.J. LeClere, A. Velota, P. Skeldon, G.E. Thompson, S. Berger, J. Kunze, P. Schmuki, H. Habazaki, S. Nagata, J. Electrochem. Soc. 155 (2008) C487-C494.
[175] H. Habazaki, K. Shimizu, S. Nagata, P. Skeldon, G.E. Thompson, G.C. Wood, Corr. Sci. 44 (2002) 1047-1055.
[176] F. Brown, W.D. Mackintosh, J. Electrochem. Soc. 120 (1973) 1096-1102.
[177] S. Berger, J. Kunze, P. Schmuki, D. LeClere, A.T. Valota, P. Skeldon, G.E. Thompson, Electrochim. Acta, 54 (2009) 5942-5948.
[178] S. Berger, J.M. Macak, J. Kunze, P. Schmuki, Electrochem. Solid-State Lett. 11 (2008) C37-C40.
[179] N.B. Pilling, R.E. Bedworth, J. Inst. Met. 29 (1923) 529-591.
[180] H. Habazaki, M. Uozumi, H. Konno, K. Shimizu, S. Nagata, K. Takayama, Y. Oda, P. Skeldon, G.E. Thompson, J. Electrochem. Soc. 152 (2005) B263-B270.
[181] S.P. Albu, P. Schmuki, Electrochim. Acta, 91 (2013) 90-95.
[182] D.-J. Yang, H.-G. Kim, S.-J. Cho, W.-Y. Choi, Materials Letters, 62 (2008) 775-779.
[183] H. Habazaki, K. Fushimi, K. Shimizu, P. Skeldon, G.E. Thompson, Electrochem. Comm. 9 (2007) 1222-1227.
[184] K. Shimizu, K. Kobayashi, G.E. Thompson, P. Skeldon, G.C. Wood, J. Electrochem. Soc.144 (1997) 418-423.
[185] K. Shimizu, K. Kobayashi, G. Thompson, P. Skeldon, G.C. Wood, Phil. Mag. B. 73 (1996) 461-485.
[186] R.E. Pawel, G.P. Pemsler, C.A. Evans Jr., J. Electrochem. Soc. 119 (1972) 24-29.
[187] L. Sun, S. Zhang, X.W. Sun, X. He, J. Electroanalytical Chem. 637 (2009) 6-12.
[188] Z. Su, W. Zhou, Adv. Mater., 20 (2008) 3663-3667.
[189] Z. Su, W. Zhou, J. Mater. Chem. 19 (2009) 2301–2309.
[190] I.B. Shirobokov, M.A. Pletnev, T.A. Povolyako, S.M. Reshetnikov, Protect. Met. 31 (1995) 516-519.
[191] S. Yoriya, C.A. Grimes, J. Mater. Chem. 21 (2011) 102-108.
[192] L. Stanton, A. Golovin, Phys. Rev. B 79 (2009) 035414-035420.
[193] Q.A.S. Nguyen, Y.V. Bhargava, T.M. Devine, J. Electrochem. Soc. 156 (2009) E55-E61.
[194] Y.V. Bhargava, Q.A.S. Nguyen, T.M. Devine, J. Electrochem. Soc. 156 (2009) E62-E68.
[195] Q. Van Overmeere, F. Blaffart, J. Proost, Electrochem. Comm. 12 (2010) 1174-1176.
[196] S.P. Albu, N. Taccardi, I. Paramasivam, K.R. Hebert, P. Schmuki, J. Electrochem. Soc. 159 (2012) H697-H703.
[197] M. Stancheva, M. Bojinov, Electrochim. Acta 78 (2012) 65-74.
[198] F.D.A.A. Reis, J.P. Badiali, D. di Caprio, Langmuir 28 (2012) 13034-13041.
[199] G.C. Wood, P. Skeldon, G. Thompson, K. Shimizu, J. Electrochem. Soc. 143 (1996) 74-83.
[200] G.E. Thompson, G.C. Wood, Nature 290 (1981) 230-232.
[201] K. Shimizu, G.E. Thompson, G.C. Wood, Thin Solid Films 85 (1981) 53-59.
[202] C. Jaeggi, P. Kern, J. Michler, J. Patscheider, J. Tharian, F. Munnik, Surf. Int. Analysis, 38 (2006) 182-185.
[203] D. Briggs, Handbook of X-Ray and Ultraviolet Photoelectron Spectroscopy, Heyden & Son Ltd., 1977.
[204] V.I. Nefedov, Y.V. Salyin, G. Leonhardt, R. R. Scheibe, J. Electron Spectroscopy Rel. Phen. 10 (1977) 121-124.
[205] S.O. Saied, J.L. Sullivan, T. Choudhury, C.G. Pearce, Vacuum 38 (1988) 917-922
[206] D. Gonbeau, C. Guimon., G. Pfister-Guillouzo, A. Levasseur, G. Meunier, R. R. Dormoy, Surf. Sci. 254 (1991) 81-89.
[207] A.F. Carley, P.R. Chalker, J.C. Riviere, M.W. Roberts, Faraday Transactions 1: Phys. Chem. Cond. Phases 83 (1987) 351-370.
[208] Y. Huang, D. Blackwood, Electrochim. Acta 51 (2005) 1099-1107.
[209] M. Textor, C. Sittig, V. Frauchiger, S. Tosatti, D.M. Brunette, Properties and Biological Significance of Natural Oxide Films on Titanium and Its Alloys, in: Titanium in Medicine: Material Science, Surface Science, Engineering, Biological Responses and Medical Applications, Springer Verlag, Heidelberg and Berlin 2001, 171-230.
[210] Y.Y. Song, P. Roy, I. Paramasivam, P. Schmuki, Angew. Chem. Int. Ed. Engl. 49 (2010) 351-354.
[211] S. Berger, S.P. Albu, F. Schmidt-Stein, H. Hildebrand, P. Schmuki, J.S. Hammond, D.F. Paul, S. Reichlmaier, Surf. Sci. 605 (2011) L57-L60.
[212] T. Ohtsuka, T. Otsuki, Corr. Sci. 45 (2003) 1793-1801.
[213] A.J. Bard, R. Parsons, J. Jordan, Standard Potentials in Aqueous Solution, New York, 1985.
[214] M.A.A. Rahim, J. Appl. Electrochem. 25 (1995) 881-885.
[215] C.K. Dyer, J.S.L. Leach, J. Electrochem. Soc. 125 (1978) 1032-1038.
[216] H. Habazaki, M. Uozumi, H. Konno, K. Shimizu, P. Skeldon, G.E. Thompson, Corr. Sci. 45 (2003) 2063-2073.
[217] A. Aladjem, J. Mater. Sci. 8 (1973) 688-704.
[218] R. Stevens, D. Regonini, C.R. Bowen, A. Jaroenworaluck, Adv. Mater. Res. 55-57 (2008) 23-26.
[219] A. Valota, D.J. LeClere, P. Skeldon, M. Curioni, T. Hashimoto, S. Berger, J. Kunze, P. Schmuki, G.E. Thompson, Electrochim. Acta 54 (2009) 4321-4327.
[220] S. Berger, J. Kunze, P. Schmuki, A.T. Valota, D.J. LeClere, P. Skeldon, G.E. Thompson, J. Electrochem. Soc. 157 (2010) C18-C23.
[221] W. Wei, S. Berger, C. Hauser, K. Meyer, M. Yang, P. Schmuki, Electrochem. Comm. 12 (2010) 1184-1186.
[222] F.M. Bayoumi, B.G. Ateya, Electrochem. Comm. 8 (2006) 38-44.
[223] S. Berger, H. Tsuchiya, P. Schmuki, Chem. Mater. 20 (2008) 3245-3247.
[224] A. Ghicov, S. Aldabergenova, H. Tsuchyia, P. Schmuki, Angew. Chem. Int. Ed. Engl. 45 (2006) 6993-6996.
[225] S. Berger, F. Jakubka, P. Schmuki, Electrochem. Comm. 10 (2008) 1916-1919.
[226] F. Muratore, T. Hashimoto, P. Skeldon, G.E. Thompson, Corr. Sci. 53 (2011) 2299-2305.
[227] S. Berger, F. Jakubka, P. Schmuki, Electrochem. Solid-State Lett. 12 (2009) K45-K48.
[228] G. Ali, C. Chen, S.H. Yoo, J.M. Kum, S.O. Cho, Nanoscale Res. Lett. 6 (2011) 332-341.
[229] B. Chen, J. Hou, K. Lu, Langmuir 29 (2013) 5911-5919.
[230] S. Ono, M. Saito, M. Ishiguro, H. Asoh, J. Electrochem. Soc. 151 (2004) B473-B478.
[231] S. Ono, M. Saito, H. Asoh, Electrochem. Solid-State Lett. 7 (2004) B21-B24.
[232] S.Z. Chu, K. Wada, S. Inoue, M. Isogai, A. Yasumori, Adv. Mater. 17 (2005) 2115-2119.

[233] D.J. Arrowsmith, A.W. Clifford, D.A. Moth, J. Mater. Sci. Lett. 5 (1986) 921-922.
[234] S. Yoriya, N. Bao, C.A. Grimes, J. Mater. Chem. 21 (2011) 13909-13912.
[235] S. Yoriya, G.K. Mor, S. Sharma, C.A. Grimes, J. Mater. Chem. 18 (2008) 3332-3336.
[236] E. Matykina, R. Arrabal, P. Skeldon, G. Thompson, H. Habazaki, Thin Solid Films 516 (2008) 2296-2305.
[237] Q.A.S. Nguyen, Y.V. Bhargava, V.R. Radmilovic, T.M. Devine, Electrochim. Acta 54 (2009) 4340-4344.
[238] C. Cao, G. Zhang, X. Song, Z. Sun, J. Electrochem.Soc. 158 (2011) E8-E11.
[239] C. Cao, J. Li, X. Wang, X. Song, Z. Sun, J. Mater. Res. 26 (2011) 437-442.
[240] C. Cao, G. Zhang, X. Song, Z. Sun, Nanoscale Res. Lett. 6 (2011) 64-68.
[241] W. Lee, R. Ji, U. Gosele, K. Nielsch, Nat. Mat. 5 (2006) 741-747.
[242] W. Lee, K. Schwirn, M. Steinhart, E. Pippel, R. Scholz, U. Gosele, Nat. Nanotechnol. 3 (2008) 234-239.
[243] K. Schwirn, W. Lee, R. Hillebrand, M. Steinhart, K. Nielsch, U. Gösele, ACS Nano 2 (2008) 302-310.
[244] H.-C. Shin, J. Dong, M. Liu, Adv. Mater. 16 (2004) 237-240.
[245] X.F. Zhu, D.D. Li, Y. Song, Y.H. Xiao, Mater. Lett. 59 (2005) 3160-3163.
[246] X. Zhu, L. Liu, Y. Song, H. Jia, H. Yu, X. Xiao, X. Yang, Chem. Monthly 139 (2008) 999-1003.
[247] X. Zhu, L. Liu, Y. Song, H. Jia, H. Yu, X. Xiao, X. Yang, Mater. Lett. 62 (2008) 4038-4040.
[248] X.F. Zhu, Y. Song, L. Liu, C.Y. Wang, J. Zheng, H.B. Jia, X.L. Wang, Nanotechnology 20 (2009) 475303-475309.
[249] D. Li, C. Jiang, J. Jiang, J.G. Lu, Chem. Mater. 21 (2008) 253-258.
[250] V.C. Chu, H. Li, H. Kim, J.M. Seo, J. Korean Phys. Soc. 54 (2009) 2415-2419.
[251] L. Yi, L. Zhiyuan, H. Xing, L. Yisen, C. Yi, Chem. Comm. 47 (2011) 2173-2175.
[252] A. Suleiman, T. Hashimoto, P. Skeldon, G.E. Thompson, F. Echeverria, M.J. Graham, G.I. Sproule, S. Moisa, H. Habazaki, P. Bailey, T.C.Q. Noakes, Corr. Sci. 50 (2008) 1353-1359.
[253] M. Abkarian, A. Subramaniam, S.-H. Kim, R. Larsen, S.-M. Yang, H. Stone, Phys. Rev. Lett. 99 (2007) 188301-1-4.
[254] E. Dressaire, R. Bee, D.C. Bell, A. Lips, H.A. Stone, Science 320 (2008) 1198-1201.
[255] X. Qiu, J.Y. Howe, M.B. Cardoso, O. Polat, W.T. Heller, M. Parans Paranthaman, Nanotechnology, 20 (2009) 455601-455609.
[256] W.-H. Chen, M.-Y. Lai, K.-T. Tsai, C.-Y. Liu, Y.-L. Wang, J. Phys. Chem. C 115 (2011) 18406-18411.
[257] Y. Ruiquan, J. Longfei, Z. Xufei, S. Ye, Y. Dongliang, H. Aijun, RSC Advances 2 (2012) 12474-12481.
[258] P. Schmuki, J.Solid State Electrochem. 6 (2002) 145-164.
[259] S. Sankar, K.G. Gopchandran, P. Kuppusami, S. Murugesan, Ceram. Int. 37 (2011) 3307-3315.
[260] http://ruby.colorado.edu/~smyth/min/tio2.html (website courtesy of J. R. Smith), last accessed on 9th of July 2013
[261] S.-D. Mo, W.Y. Ching, Phys. Rev. B 51 (1995) 13023-13032.
[262] H. Tang, K. Prasad, R. Sanjinès, P.E. Schmid, F. Lévy, J. Appl. Phys. 75 (1994) 2042-2047.
[263] J.-G. Li, T. Ishigaki, X. Sun, J. Phys. Chem. C 111 (2007) 4969-4976.
[264] K.-N.P. Kumar, K. Keizer, A.J. Burggraaf, J. Mater. Chem. 3 (1993) 1141-1149.
[265] K.-N.P. Kumar, K. Keizer, A.J. Burggraaf, T. Okubo, H. Nagamoto, J. Mater. Chem. 3 (1993) 1151-1159.
[266] L.D. Arsov, C. Kormann, W. Plieth, J. Electrochem. Soc. 138 (1991) 2964-2970.
[267] J. Yahalom, J. Zahavi, Electrochim. Acta 15 (1970) 1429-1435.
[268] J.S.L. Leach, B.R. Pearson, Corr. Sci. 28 (1988) 43-56.
[269] J.F. Vanhumbeeck, J. Proost, J. Electrochem. Soc. 155 (2008) C506-C514.
[270] J.-F. Vanhumbeeck, H. Tian, D. Schryvers, J. Proost, Corr. Sci. 53 (2011) 1269-1277.
[271] J.F. Vanhumbeeck, L. Ryelandt, J. Proost, Electrochim. Acta 54 (2009) 3330-3338.
[272] M. Santamaria, F. Di Quarto, H. Habazaki, Corr. Sci. 50 (2008) 2012-2020.
[273] J. Kunze, A. Ghicov, H. Hildebrand, J.M. Macak, L. Traveira, P. Schmuki, Zeitschrift für Physikalische Chemie 219 (2005) 1561-1582.
[274] A. Aladjem, D.G. Brandon, J. Yahalom, J. Zahavi, Electrochim. Acta 15 (1970) 663-671.
[275] C.T.J. Low, M.D. Corral, F.C. Walsh, Trans. Inst. Metal Finishing 89 (2011) 44-50.
[276] X. Xiao, K. Ouyang, R. Liu, J. Liang, Appl. Surf. Sci. 255 (2009) 3659-3663.
[277] V. Galstyan, A. Vomiero, I. Concina, A. Braga, M. Brisotto, E. Bontempi, G. Faglia, G. Sberveglieri, Small 7 (2011) 2437-2442.
[278] N.K. Allam, K. Shankar, C.A. Grimes, Adv. Mater. 20 (2008) 3942-3946.
[279] N.K. Allam, C.A. Grimes, Langmuir 25 (2009) 7234-7240.
[280] D. Wang, L. Liu, F. Zhang, K. Tao, E. Pippel, K. Domen, Nano Letters 11 (2011) 3649-3655.
[281] Y. Liao, W. Que, P. Zhong, J. Zhang, Y. He, ACS Appl. Mater. Interfaces 3 (2011) 2800-2804.
[282] N. Liu, S.P. Albu, K. Lee, S. So, P. Schmuki, Electrochim. Acta 82 (2012) 98-102.
[283] J. Kunze, A. Seyeux, P. Schmuki, Electrochem. Solid-State Lett. 11 (2008) K11-K13.
[284] R.P. Lynch, A. Ghicov, P. Schmuki, J. Electrochem. Soc. 157 (2010) G76-G84.
[285] P. Acevedo-Pena, I. Gonzalez, J. Electrochem. Soc. 160 (2013) H452-H458.
[286] G. Du, B. Wan, Z. Guo, J. Shen, Y. Li, H. Liu, Adv. Sci. Lett. 4 (2011) 469-473.
[287] J.N. Kondo, K. Domen, Chem. Mater. 20 (2007) 835-847.
[288] K. Zhu, A.J. Frank, MRS Bulletin 36 (2011) 446-452.
[289] K. Shankar, J.I. Basham, N.K. Allam, O.K. Varghese, G.K. Mor, X. Feng, M. Paulose, J.A. Seabold, K.-S. Choi, C.A. Grimes, J. Phys. Chem. C 113 (2009) 6327-6359.
[290] S.C. Roy, O.K. Varghese, M. Paulose, C.A. Grimes, ACS Nano 4 (2010) 1259-1278.
[291] N.G. Park, J. van de Lagemaat, A.J. Frank, J. Phys. Chem. B 104 (2000) 8989-8994.
[292] D.C. Hurum, A.G. Agrios, K.A. Gray, T. Rajh, M.C. Thurnauer, J. Phys. Chem. B 107 (2003) 4545-4549.
[293] U. Diebold, Surf. Sci. Rep. 48 (2003) 53-229.
[294] G. Li, Z.-Q. Liu, J. Lu, L. Wang, Z. Zhang, Appl. Surf.Sci. 255 (2009) 7323-7328.
[295] J. Yu, B. Wang, Appl. Catal. B: Environmental 94 (2010) 295-302.
[296] Y. Lai, L. Sun, Y. Chen, H. Zhuang, C. Lin, J.W. Chin, J. Electrochem. Soc. 153 (2006) D123-D127.
[297] H. Tsuchiya, J.M. Macak, A. Ghicov, L. Taveira, P. Schmuki, Corr. Sci. 47 (2005) 3324-3335.

[298] J. Zhao, X. Wang, T. Sun, L. Li, J. Alloys Comp. 434-435 (2007) 792-795.
[299] J. Zhao, X. Wang, T. Sun, L. Li, Nanotechnology 16 (2005) 2450-2454.
[300] B. Yang, C.K. Ng, M.K. Fung, C.C. Ling, A.B. Djurišić, S. Fung, Mater. Chem.Phys. 130 (2011) 1227-1231.
[301] I. Bennett, R. Stevens, Br. Ceram. Trans. 97 (1998) 117-125.
[302] D. Fang, Z. Luo, K. Huang, D.C. Lagoudas, Appl. Surf. Sci. 257 (2011) 6451-6461.
[303] A. Ghicov, J.M. Macak, H. Tsuchiya, J. Kunze, V. Haeublein, L. Frey, P. Schmuki, Nano Lett. 6 (2006) 1080-1082.
[304] A. Mazare, I. Paramasivam, F. Schmidt-Stein, K. Lee, I. Demetrescu, P. Schmuki, Electrochim. Acta 66 (2012) 12-21.
[305] Z. Su, W. Zhou, F. Jiang, M. Hong, J. Mater. Chem. 22 (2012) 535-544.
[306] A. Wisnet, M. Thomann, J. Weickert, L. Schmidt-Mende, C. Scheu, J. Mater. Sci. 47 (2012) 6459-6466.
[307] H. Zhang, J.F. Banfield, J.Mater. Res. 15 (2000) 437-448.
[308] H. Zhang, J.F. Banfield, J. Phys. Chem. B 104 (2000) 3481-3487.
[309] D.A.H. Hanaor, C.C. Sorrell, J. Mater. Sci. 46 (2010) 855-874.
[310] J.M. Macak, S. Aldabergerova, A. Ghicov, P. Schmuki, Phys. Status Solidi A 203 (2006) R67-R69.
[311] A. Ghicov, H. Tsuchiya, J.M. Macak, P. Schmuki, Physica Status Solidi A 203 (2006) R28-R30.
[312] S. Andersson, A. Magneli, Naturwissenschaften, 43 (1956) 495-496.
[313] P.C. Hayfield, Development of a New Material - Monolithic Ti_4O_7 Ebonex Ceramic, Royal Society of Chemistry, Cambridge, 2002.
[314] S. Harada, K. Tanaka, H. Inui, J.Appl. Phys. 108 (2010) 0837031-0837036.
[315] L. Liborio, N. Harrison, Phys. Rev. B , 77 (2008) 104101-104110.
[316] M. Salari, K. Konstantinov, H.K. Liu, J. Mater. Chem. 21 (2011) 5128-5133.
[317] M. Salari, S.H. Aboutalebi, A.T. Chidembo, I.P. Nevirkovets, K. Konstantinov, H.K. Liu, Phys. Chem. Chem. Phys. 14 (2012) 4770-4779.
[318] R. Chandana, P. Mohanty, A.C. Pandey, N.C. Mishra, J. Phys. D: Appl. Phys. 42 (2009) 205101-205106.
[319] R. Hahn, F. Schmidt-Stein, J. Salonen, S. Thiemann, Y. Song, J. Kunze, V.P. Lehto, P. Schmuki, Angew. Chem. Int. Ed. Engl. 48 (2009) 7236-7239.
[320] F. Schmidt-Stein, S. Thiemann, S. Berger, R. Hahn, P. Schmuki, Acta Mater. 58 (2010) 6317-6323.
[321] D. Regonini, A.C.E. Dent, C.R. Bowen, S.R. Pennock, J. Taylor, Mater. Lett.65 (2011) 3590-3592.
[322] D. Regonini, V. Adamaki, C.R. Bowen, S.R. Pennock, J. Taylor, A.C.E. Dent, Solid State Ionics 229 (2012) 38-44.
[323] A. Tighineanu, T. Ruff, S. Albu, R. Hahn, P. Schmuki, Chem. Phys. Lett. 494 (2010) 260-263.
[324] J.R. Smith, F.C. Walsh, R.L. Clarke, J. Appl. Electrochem. 28 (1998) 1021-1033.
[325] F.C. Walsh, R.G.A. Wills, Electrochim. Acta 55 (2010) 6342-6351.
[326] S. Bauer, A. Pittrof, H. Tsuchiya, P. Schmuki, Electrochem. Comm.13 (2011) 538-541.
[327] N. Liu, I. Paramasivam, M. Yang, P. Schmuki, J. Solid State Electrochem. 16 (2012) 3499-3504.
[328] T. Bak, J. Nowotny, N.J. Sucher, E.D. Wachsman, Adv. Appl. Ceram. 111 (2012) 4-15.

Tables, Figures and Captures

Table 1. The different morphologies of titanium oxide obtained by anodization.

	Barrier type	**Nanoporous and nanotubular type**
Structure	Thin (few hundreds of nm) and compact	i. Inner layer at the M/MO interface: thin (≤ 50nm), barrier type ii. Outer layer at the MO/electrolyte interface: porous/tubular form (up to >1000μm)[84]
Electrolyte	Solutions of sulphuric, phosphoric, acetic acid [41]	i. Aqueous and organic solutions containing fluoride ions [42] ii. aqueous and organic solution containing perchlorate, chloride, bromide ions [43-54]

Table 2. Evolution of TiO_2 NTs from 1st to 4th generation.

TiO_2 NTs	***Electrolyte***	***Features***	***Refs.***
1st generation	HF aqueous solutions	i. 0.5μm long ii. poorly self-organized iii. ribbed	[16, 34, 68-71]
2nd generation	Aqueous solutions of fluoride salts (0.1-0.5wt%)	i. up to 5 μm long ii. self-organized iii. ribbed	[72-76]
3rd generation	Organic solutions containing fluoride salts (0.1-0.5wt%) and small amount of water (0.1-5wt.%)	i. up to 100-1000 μm long ii. self-organized iii. smooth (ribbed if water content is above a critical threshold)	[77-84]
4th generation	Organic solutions containing fluoride salts (0.1-0.5wt%) and small amount of water (usually 0.1-5wt.%)	i. up to 100-1000 μm long ii. highly self-organized iii. smooth (ribbed if water content is above a critical threshold) iv. fine tuning of anodizing conditions or multi-step approach	[85-87]

Table 3. Different regimes for anodized TiO_2 NTs growth. In aqueous electrolytes containing fluoride ions field-assisted and chemical dissolution processes are significant and only short tubes form. In organic media containing fluoride ions chemical dissolution is reduced and growth of long NTs by plastic flow is possible. The mechanism in fluoride free solutions is believed to be of a Rapid Breakdown Anodization (RBA) type.

	Formation of TiO_2 NTs	Refs.
F^- in aqueous electrolytes	i. NTs are formed, but of limited length (0.5μm) ii. High density of nucleation sites. Pore nucleation due to F^- ions (and presence of water) iii. Growth process determined by chemical dissolution and field-enhanced dissolution/oxidation iv. Difficult to control chemical dissolution	[16, 68, 69, 74, 114]
F^- in organic electrolytes	i. Long NTs are formed. A small % of water is generally required as an oxygen source and to assist ionic migration and dissolution ii. High density of nucleation sites due to F^- ions (and small water content). Pore nucleation due to field-enhanced dissolution (i.e. chemical dissolution becomes relevant only for water content above a few wt. %) iii. Growth process by 'plastic flow'	[38, 117, 129, 146, 177, 219, 220]
ClO_4^-/Cl^-/Br^- in aqueous electrolytes	i. Long NTs are formed, but are not self-organized ii. High density of nucleation sites due to water and presence of ClO_4^-/Cl^-/Br^- ions. High rate of formation. The process is initiated by localized anodic breakdown iii. Growth process by Rapid Breakdown Anodization (RBA)	[43, 47-49, 52]
ClO_4^-/Cl^-/Br^- in organic electrolytes	i. NTs are formed, but are not self-organized ii. Sufficient density of nucleation sites provided by ClO_4^-/Cl^-/Br^- ions. The process is initiated by localized anodic breakdown iii. RBA is poorly sustained by the electrolyte (current density too low) and the process soon stops iv. By increasing water content it is possible to form longer tubes v. Self-organization is possible, particularly in mixed (aqueous/organic) solution, where the current density is sufficiently high. The mechanism behind self-organization is likely to be of a “plastic flow” type	[44, 47, 50]

Table 4. Different TiO_2 polymorphs and some physical properties.

	Crystal System	**Density (g/cm^3)** [261, 263]	**Optical Band-gap (eV)** [263]	**Refractive Index** [263]
Rutile	Tetragonal	4.13 - 4.26	3.0	2.72
Brookite	Orthorhombic	3.99 - 4.11	3.11	2.63
Anatase	Tetragonal	3.79 - 3.84	3.19	2.52

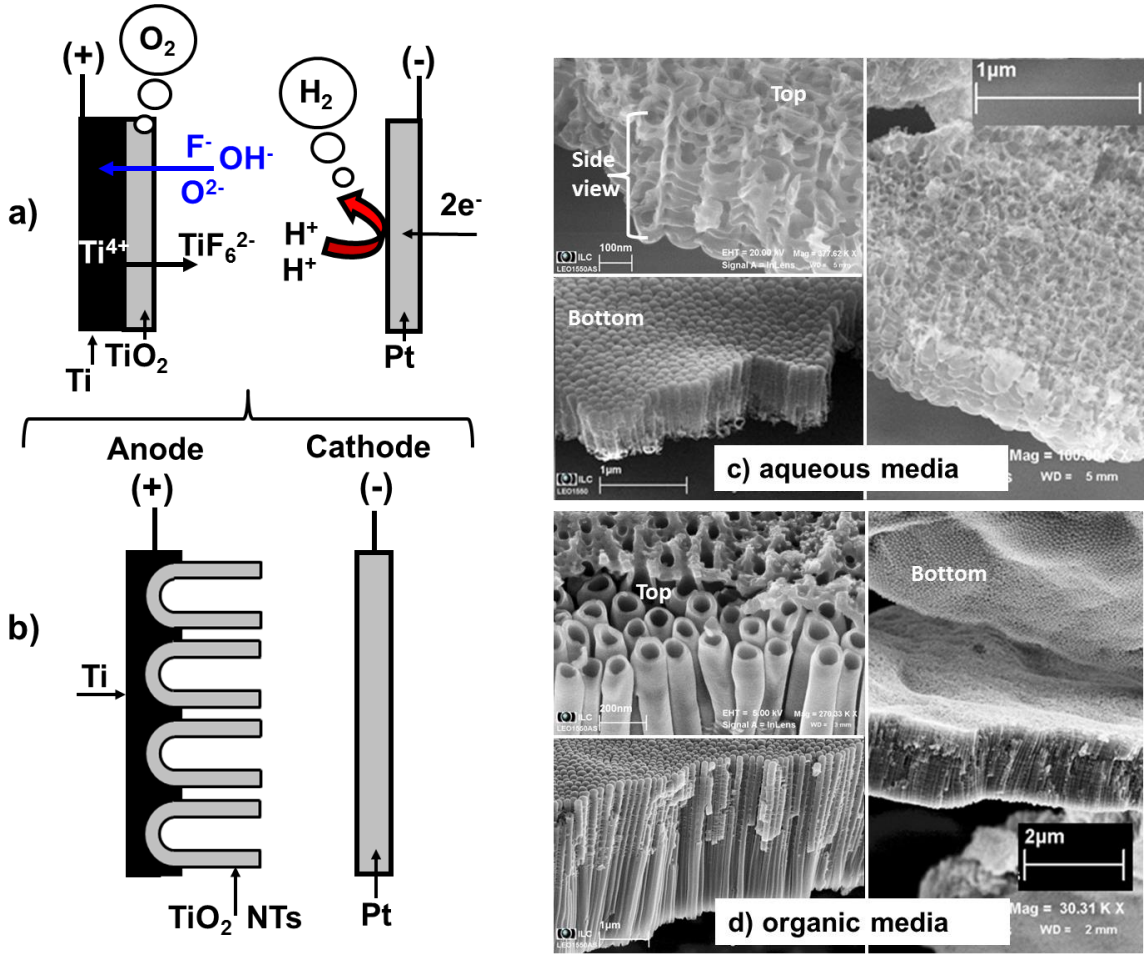

Figure 1. Schematic of the processes occurring during the anodization of Ti in fluoride containing electrolytes **(a)** and formation of TiO_2 NTs **(b)**. Examples of NTs obtained in fluoride containing aqueous **(c)** and organic **(d)** electrolytes illustrate the morphology of the NTs which reveal a closed scalloped bottom, an open top (mouth) and side walls with ripples (in water media) or smooth/partially smooth and partially rippled (in organic media, depending on water content).

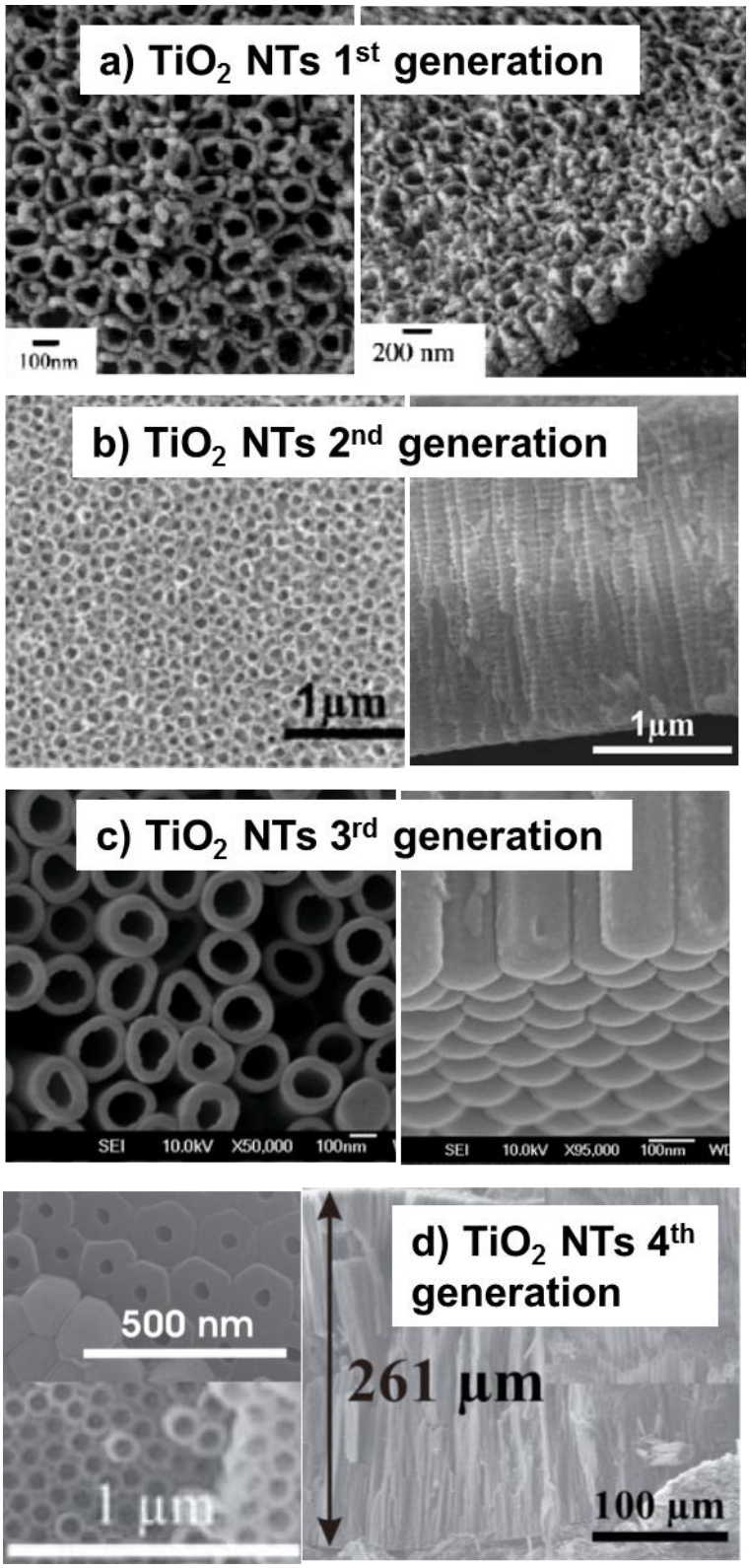

Figure 2. Evolution of the self-organization (and length) of anodized TiO_2 NTs: **(a)** 1st generation grown in HF containing aqueous electrolytes, reprinted and adapted from ref. [16] with permission from Materials Research Society **(b)** 2nd generation grown in water electrolytes containing fluoride salts rather than HF, reprinted and adapted from ref. [75] with permission from Springer **(c)** 3rd generation grown in fluoride containing organic electrolytes, reprinted and adapted from ref. [82] with permission from Institute of Physics Publishing, **(d)** 4th generation grown in fluoride containing electrolytes with careful control of anodizing parameters, particularly time, applied

potential and fluoride ions concentration, reprinted and adapted from ref. [86] with permission from Wiley-VCH.

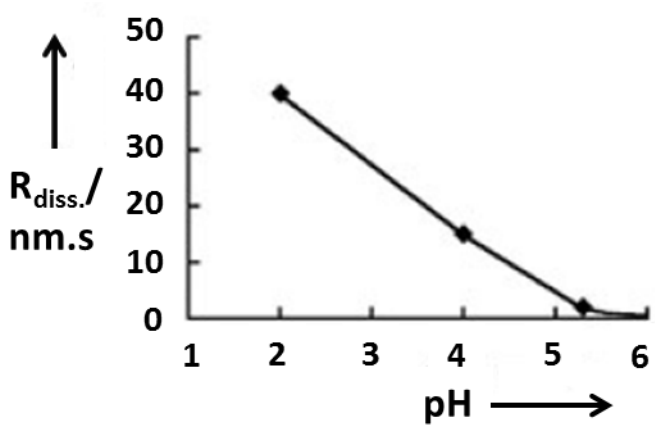

Figure 3. The solubility of TiO_2 depends on the pH of the electrolyte and is greater for acidic pH levels. Reprinted and adapted from Ref. [73] with permission from Wiley-VCH

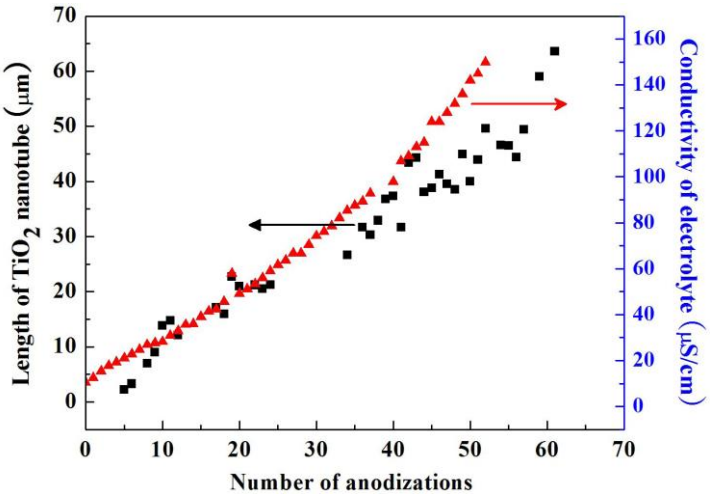

Figure 4. Ageing of the electrolyte leading to an increase of electrical conductivity and formation of longer NTs. Reprinted from ref. [144] with permission from the Korean Physical Society.

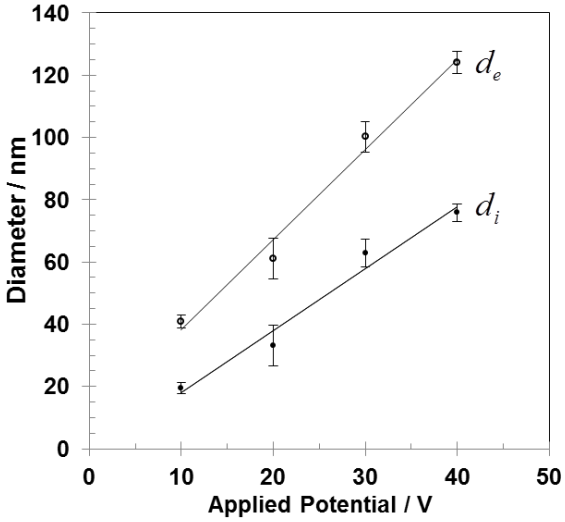

Figure 5. Linear relationship between the applied potential and the internal (d_i) and external (d_e) diameter of TiO_2 NTs. Reprinted from ref. [148] with permission from Elsevier.

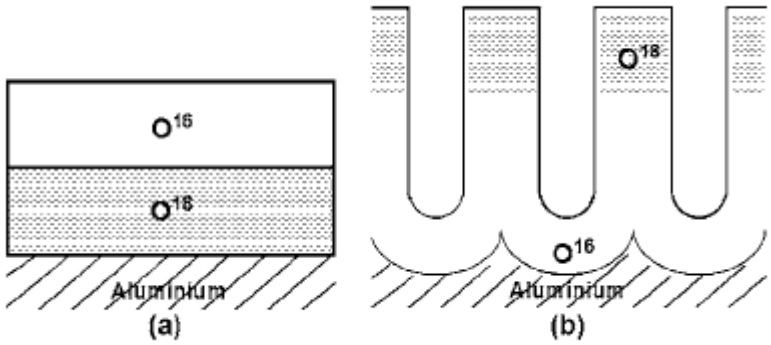

Figure 6. Schematic illustration using an O^{18} tracer in the case of barrier (a) and porous (b) anodic films. Anodization was firstly carried out in an O^{18} enriched electrolyte followed by a second oxidation in a tracer free electrolyte. Reprinted from Ref. [159] with permission from The Electrochemical Society.

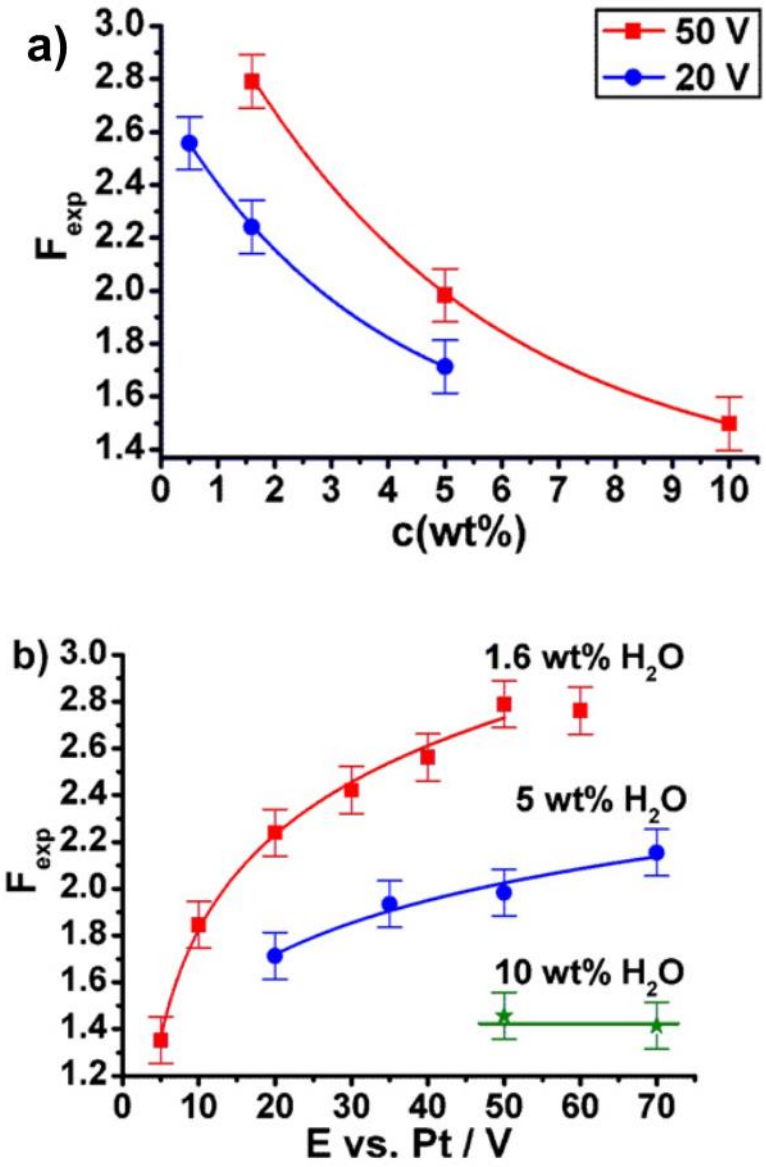

Figure 7. Influence of the water content on the expansion factor of TiO_2 calculated at 20 and 50V **(a)** and influence of applied potential on the expansion factor of TiO_2 calculated for different water content in an organic electrolyte **(b)**. Reprinted from ref. [181] with permission from Elsevier.

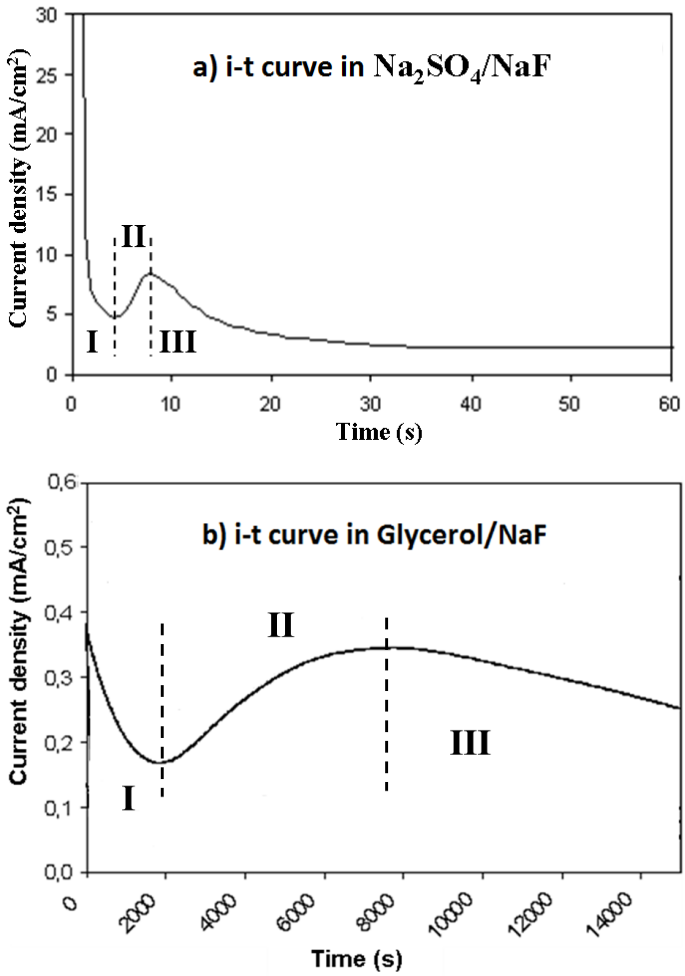

Figure 8. Current-time transient registered for a sample anodized in a NaF/H_2O electrolyte at 20V **(a)** [153] and during the anodization of titanium at different potentials in glycerol/NaF **(b)** [145]. Reprinted and adapted from ref. [153] and [145] with permission from Wiley-VCH and American Scientific Publishers, respectively.

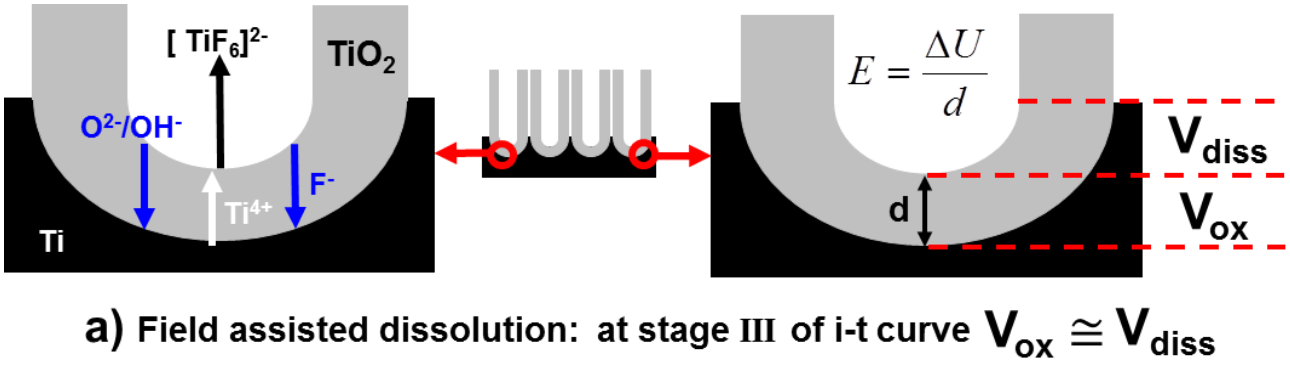

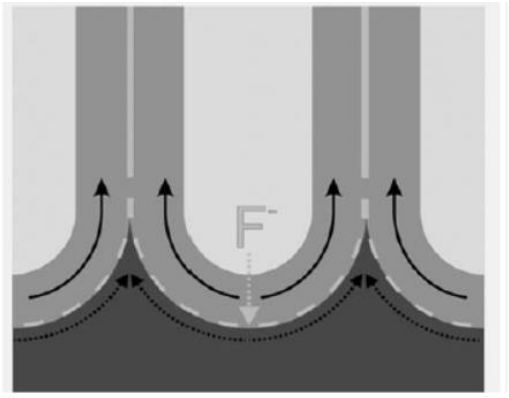

b) Flow model mechanism: forming oxide being pushed upwards

Figure 9. Schematic of the growth of TiO_2 NTs by field-assisted dissolution **(a)** and by plastic flow with the forming oxide being constantly pushed upwards **(b)**. Fig. 9b is reprinted from ref. [27] with permission from Wiley-VCH.

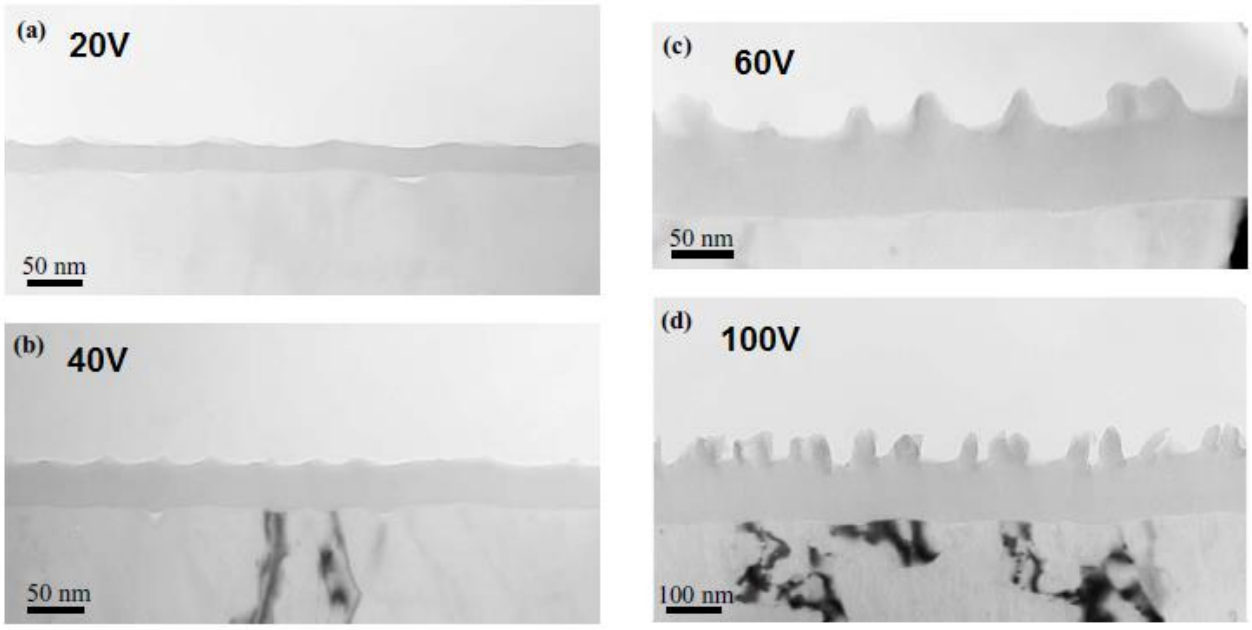

Figure 10. Morphological instabilities (undulations) generated in anodized alumina grown at different potentials. Reprinted from ref. [37] with permission from The Electrochemical Society.

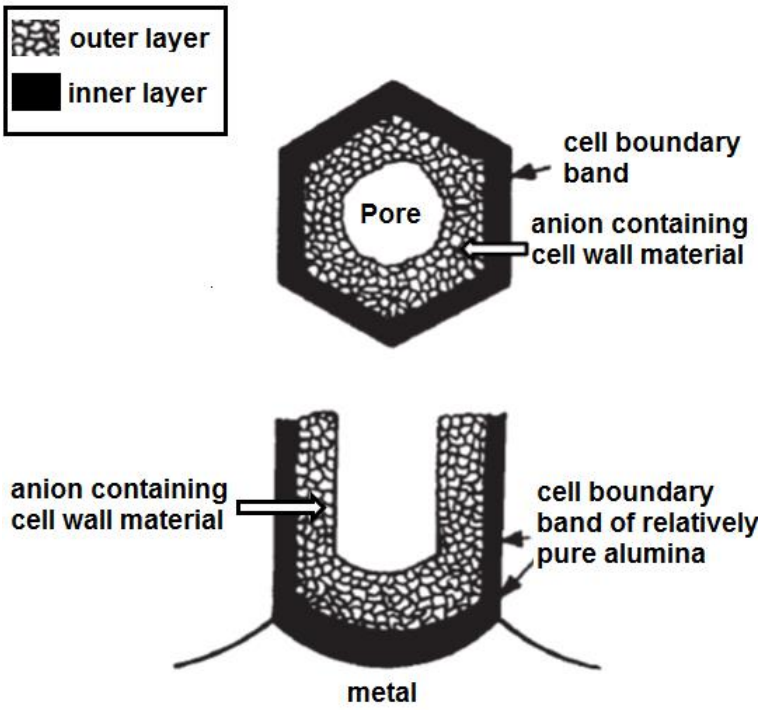

Figure 11. Schematic of a pure inner layer of anodized alumina and an outer layer contaminated by anions from the electrolyte. Reprinted and adapted from ref. [200] with permission from Nature Publishing Group.

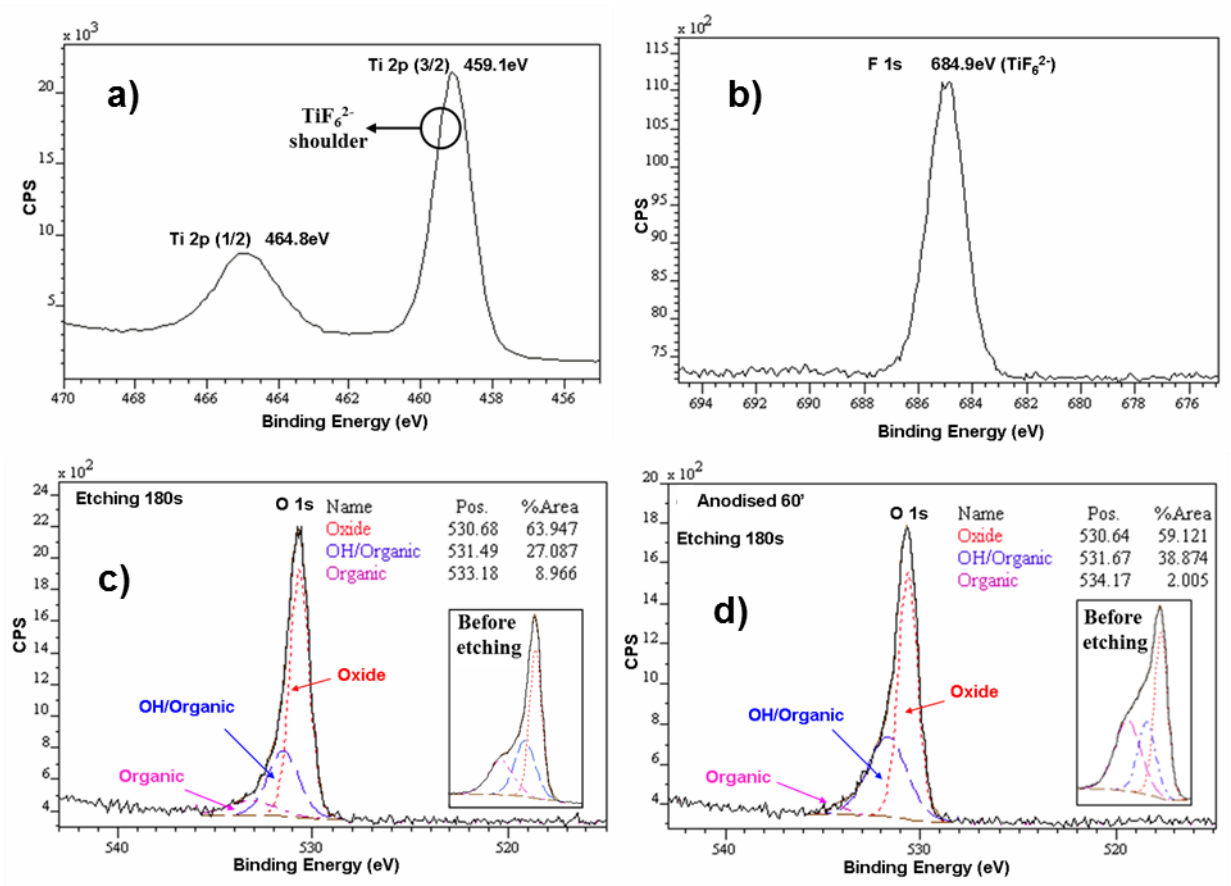

Figure 12. Typical XPS peaks for Ti **(a)** and fluorine as TiF_6^{2-}, **(b)** in the anodic TiO_2 NTs. The peak relative to oxygen reveals the presence of three different components both in aqueous **(c)** and organic **(d)** electrolytes: O due to the oxide, O due to the hydration of the oxide and O due to organic C contaminants originating from the atmosphere and from post-growth cleaning with an organic solvent in case **(c)** and mainly from the organic electrolyte in case **(d)**. Figs. 12a,b, c are reprinted from ref. [134]; Fig. 12d is reprinted and adapted from ref. [148] with permission from Elsevier.

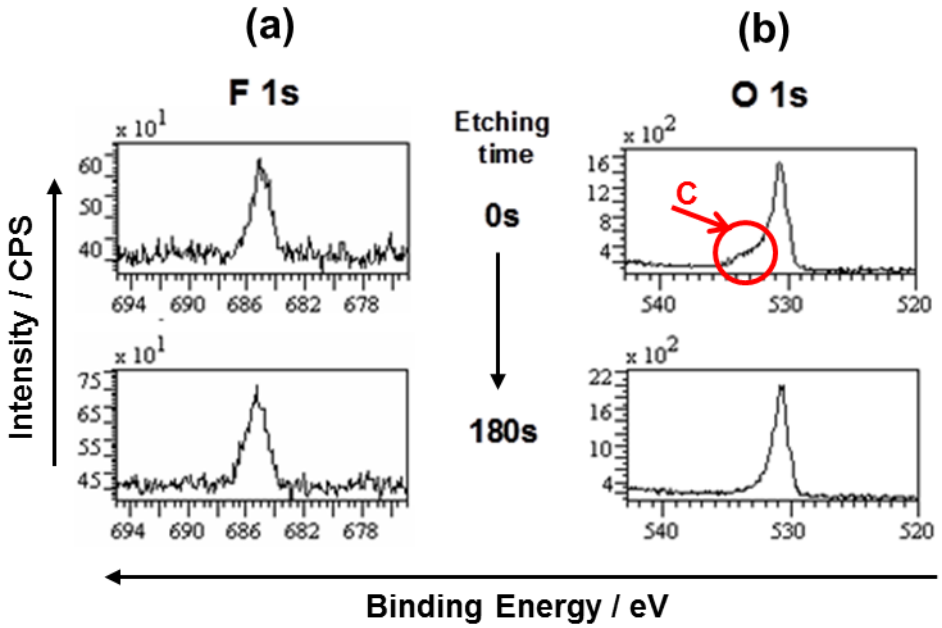

Figure 13. XPS depth profiling analysis of the fluorine **(a)** and oxygen **(b)** content in an as-prepared TiO_2 film anodized in aqueous NaF/Na_2SO_4. Intensities of oxygen and fluorine increase after the removal of the organic contaminants from the surface of the film [134, 148]. Fig. 13a is reprinted from ref. [148] with permission from Elsevier.

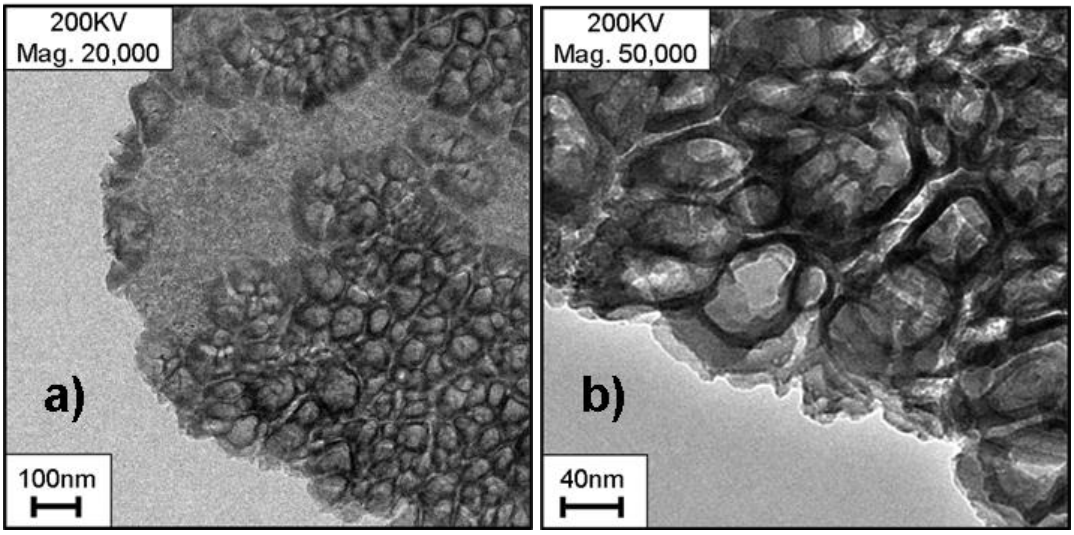

Figure 14. TEM micrographs of the TiO_2 anodic film grown in aqueous NaF/Na_2SO_4 after 200s. It is evident that oxide rings (building blocks of the NTs) have already formed **(a)**, with higher magnification image providing further details of the 3D TiO_2 network making up the structure **(b).** Reprinted from ref. [114] with permission from Materials Research Society.

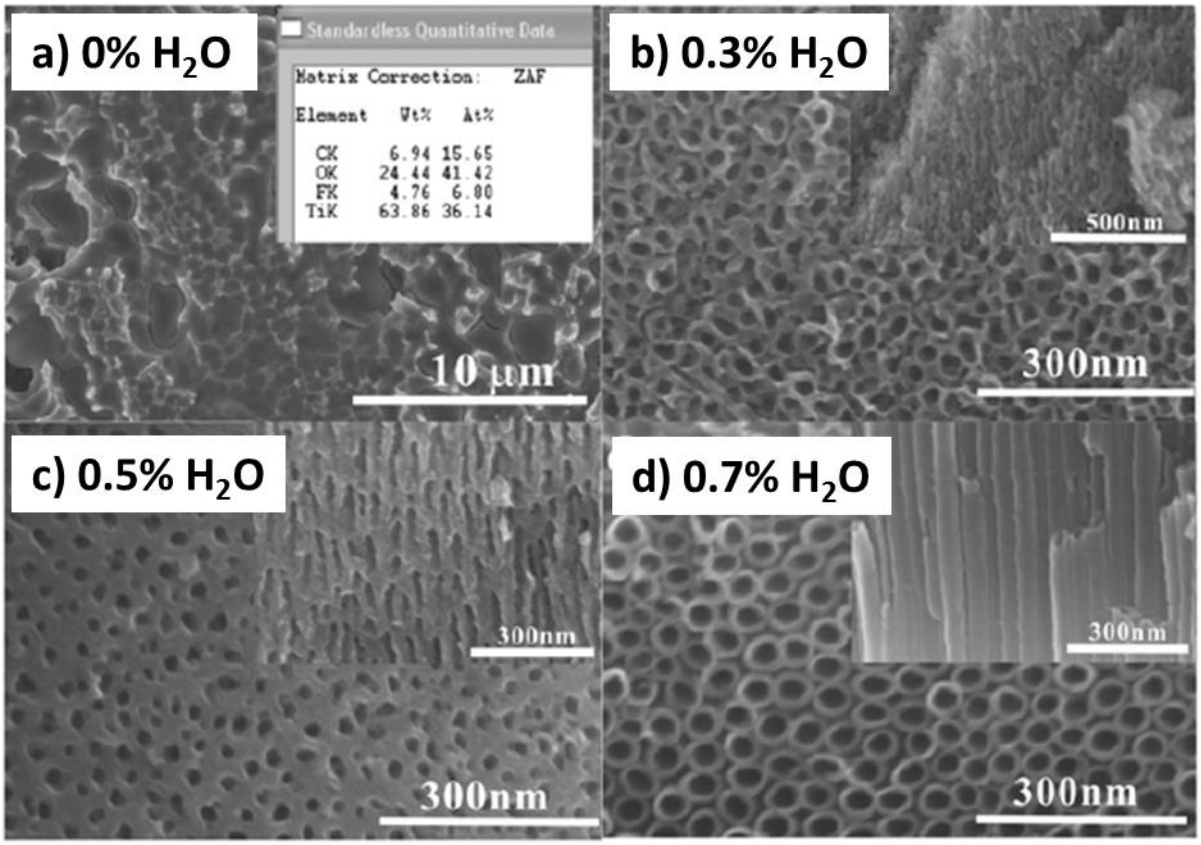

Figure 15. Effect of water content on the anodization of Ti in a fluoride containing ethylene glycol electrolyte. With no water **(a)** the formation of the oxide is patchy whereas for 0.3wt% **(b)** and 0.5wt% **(c)** porous irregular layers are obtained; ordered NTs are formed for water content ≥0.7wt% **(d)**. Reprinted from ref. [221] with permission from Elsevier

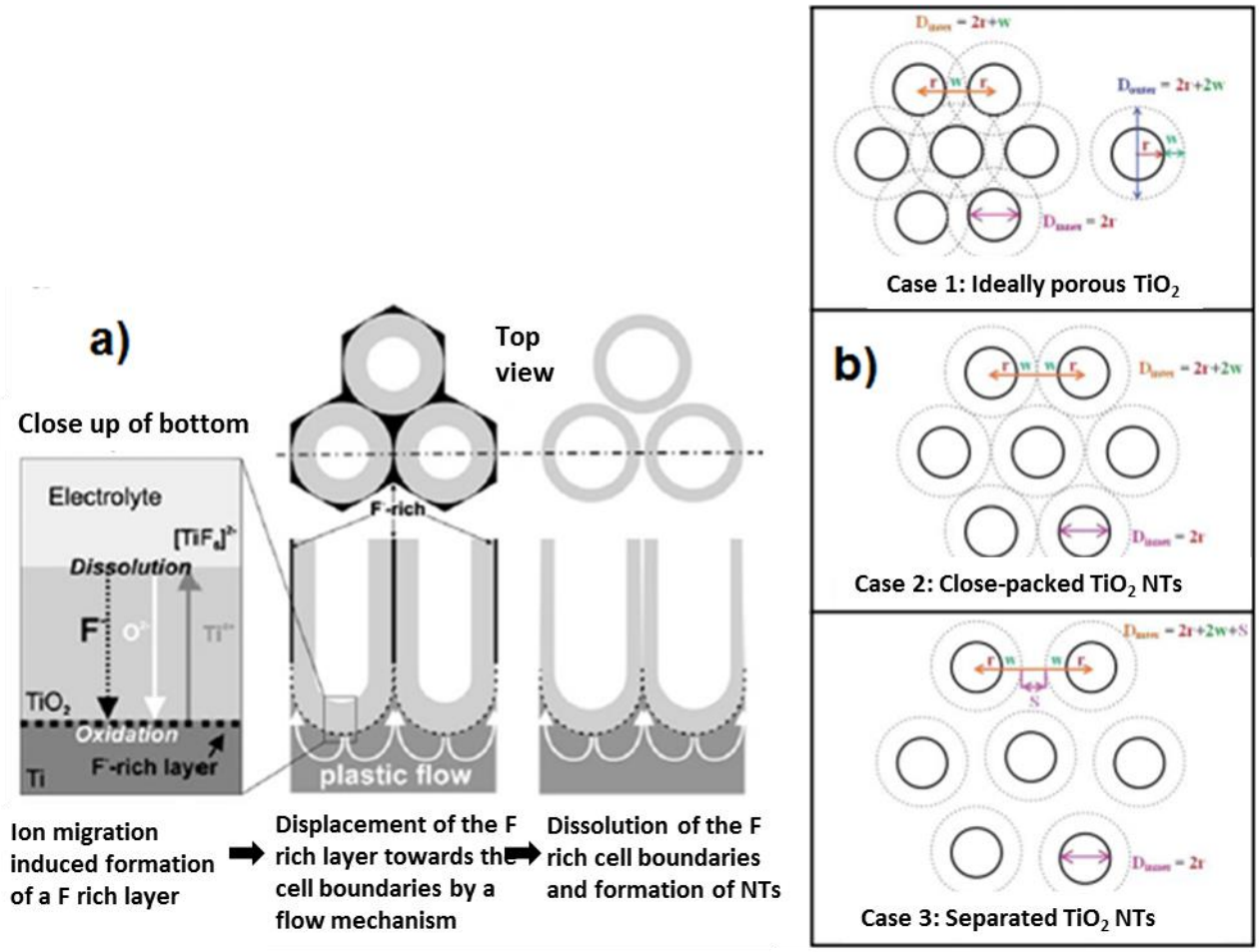

Figure 16. Transition from nanopores to NTs promoted by a fluoride rich layer on the outer wall of each single TiO_2 cell. Eventually the fluoride rich layer will lead to splitting of different cells into well-defined NTs **(a),** Reprinted and adapted from ref. [211] with permission from Elsevier. The electrical conductivity of the electrolyte is believed to play a role in determining the porosity and spacing between TiO_2 cells, ultimately determining whether nanopores or NTs are formed **(b),** reprinted and adapted from ref. [234] with permission from The Royal Society of Chemistry.

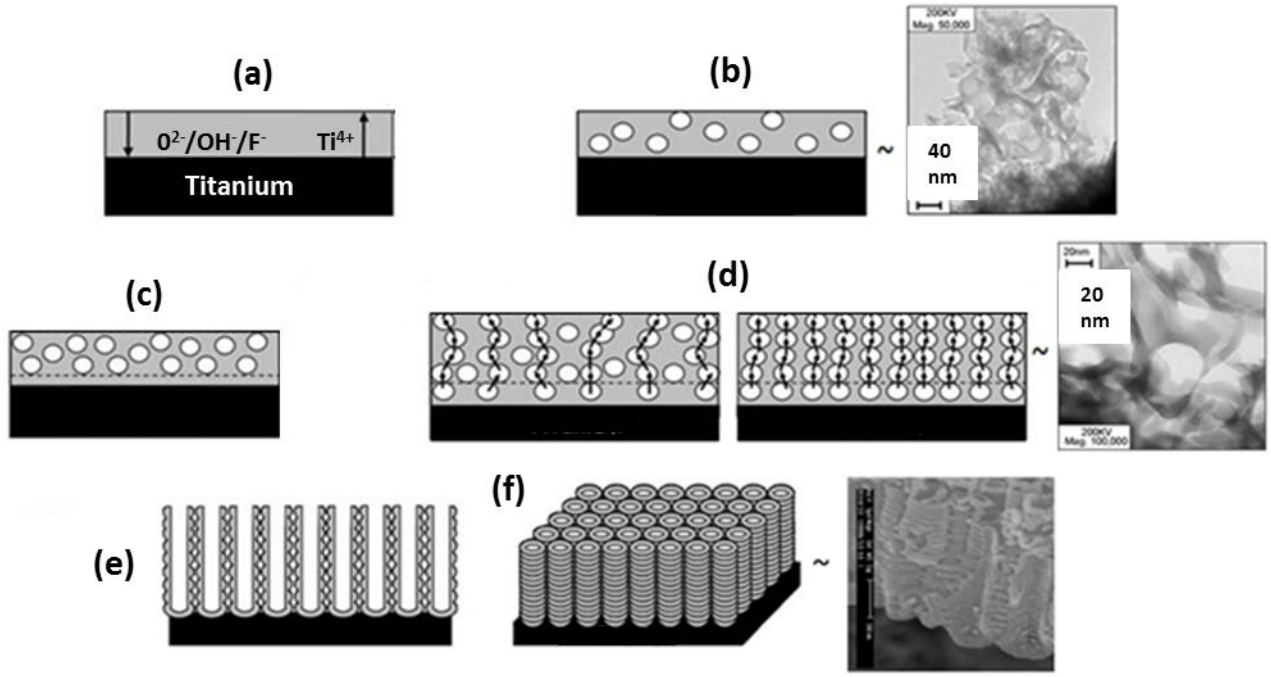

Figure 17. The movement of anions (O^{2-}, OH^{-}, F^{-}) toward the anode and Ti^{4+} toward the electrolyte under the action of the electric field, allowing for the growth of the oxide at the metal/oxide interface and the ejection of Ti ions at the beginning of the anodization **(a)**. Almost simultaneously (i.e. very early stages) cavities generate in the anodic layer because of the presence of fluoride ions **(b).** Oxide grow continues and the highly interconnected film move towards the alignment of cavities and the reshape of the structure **(c-d).** Longer channels generate in the anodic layer as the walls separating different cavities collapse **(e-f)** leading to the final structure, which consists of stacked oxide rings, developing normal to the metal substrate to form a nanotubular array, clearly visible from SEM micrograph **(g).** Reprinted and adapted from ref. [76] with permission from Springer.

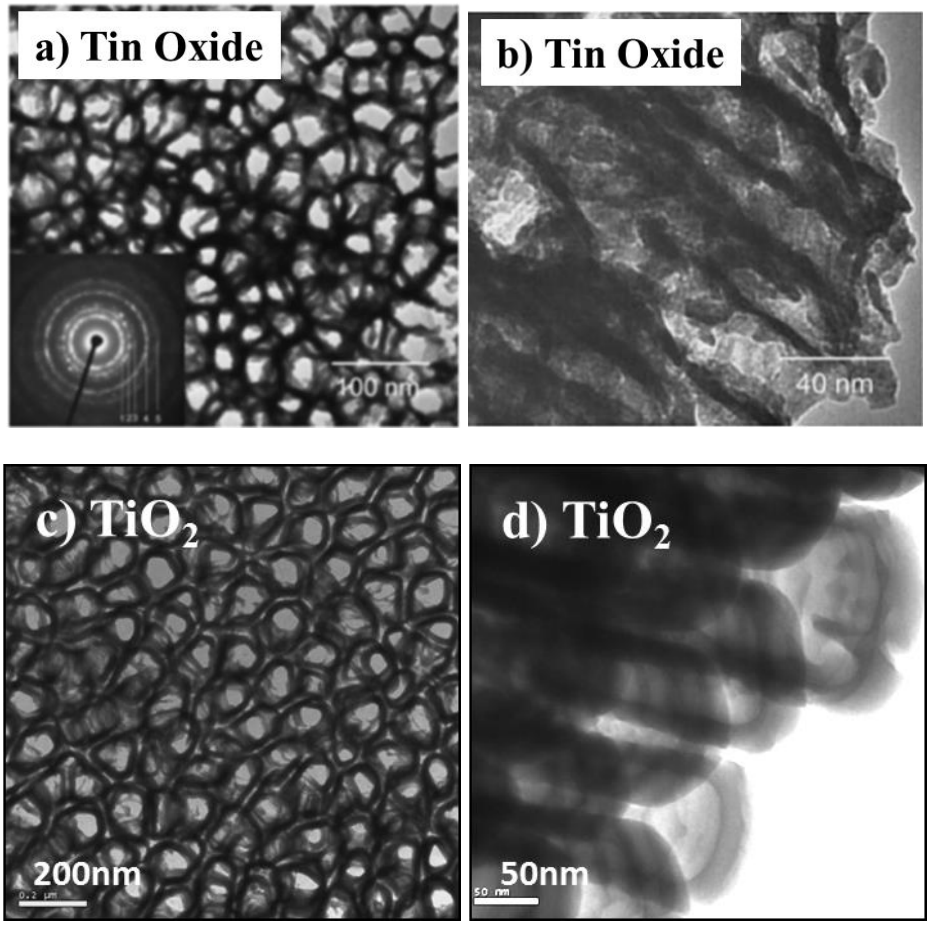

Figure 18. Similarities between tin oxide (**a, b**) [244] and titanium oxide (**c, d**) [114], both grown anodically and perturbed by the evolution of oxygen bubbles at the anode. Fig. 16a,b reprinted from ref. [244] with permission from Wiley; Fig. 16c,d reprinted from ref. [114] with permission from Materials Research Society.

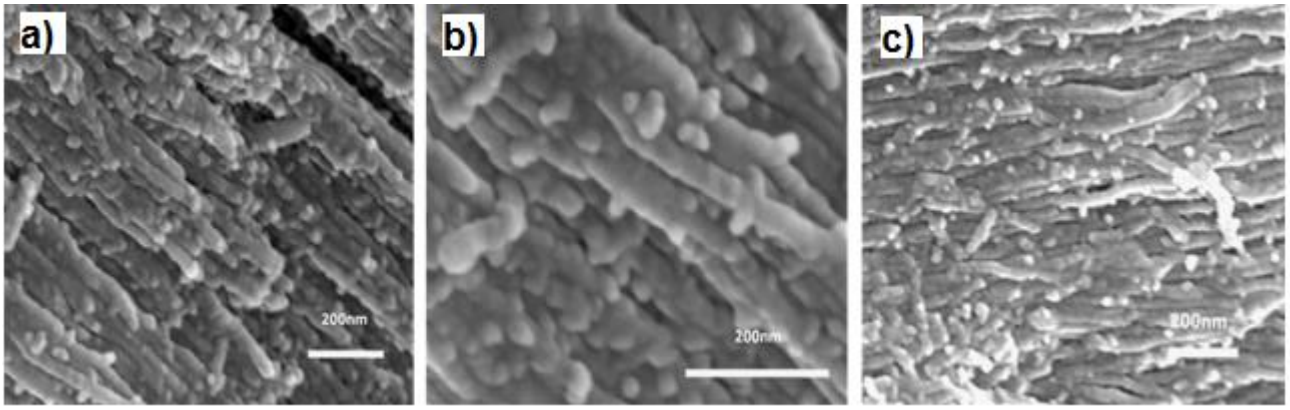

Figure 19. TiO_2 NTs grown by RBA in fluoride free solutions. The interconnection between the different nanoparticles is typical of fast processes whereby fewer than desired nucleation and growth points are available. Reprinted from ref. [48] with permission from Elsevier.

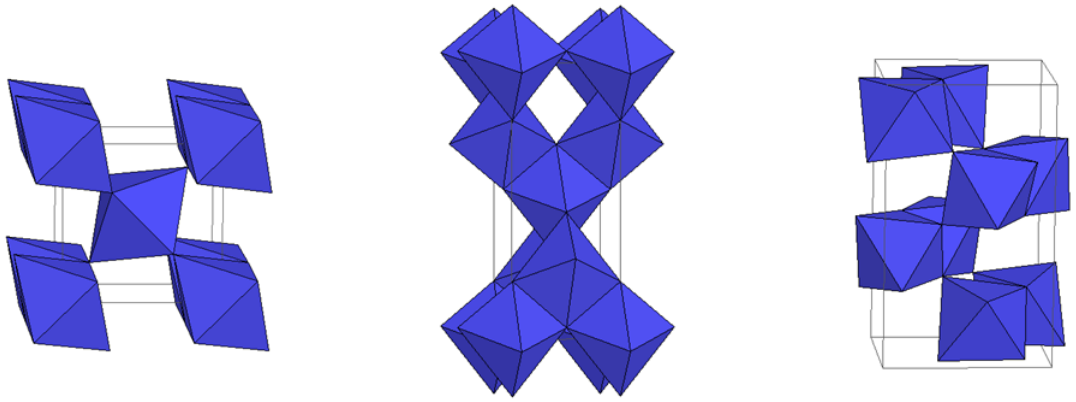

Figure 20. TiO_2 crystal structures: rutile **(a)**, anatase **(b)** and brookite **(c)**. Images courtesy of Joseph R. Smith, University of Colorado [260] . Ti^{4+} sits at the centre of the octahedron and O^{2-} at each corner.

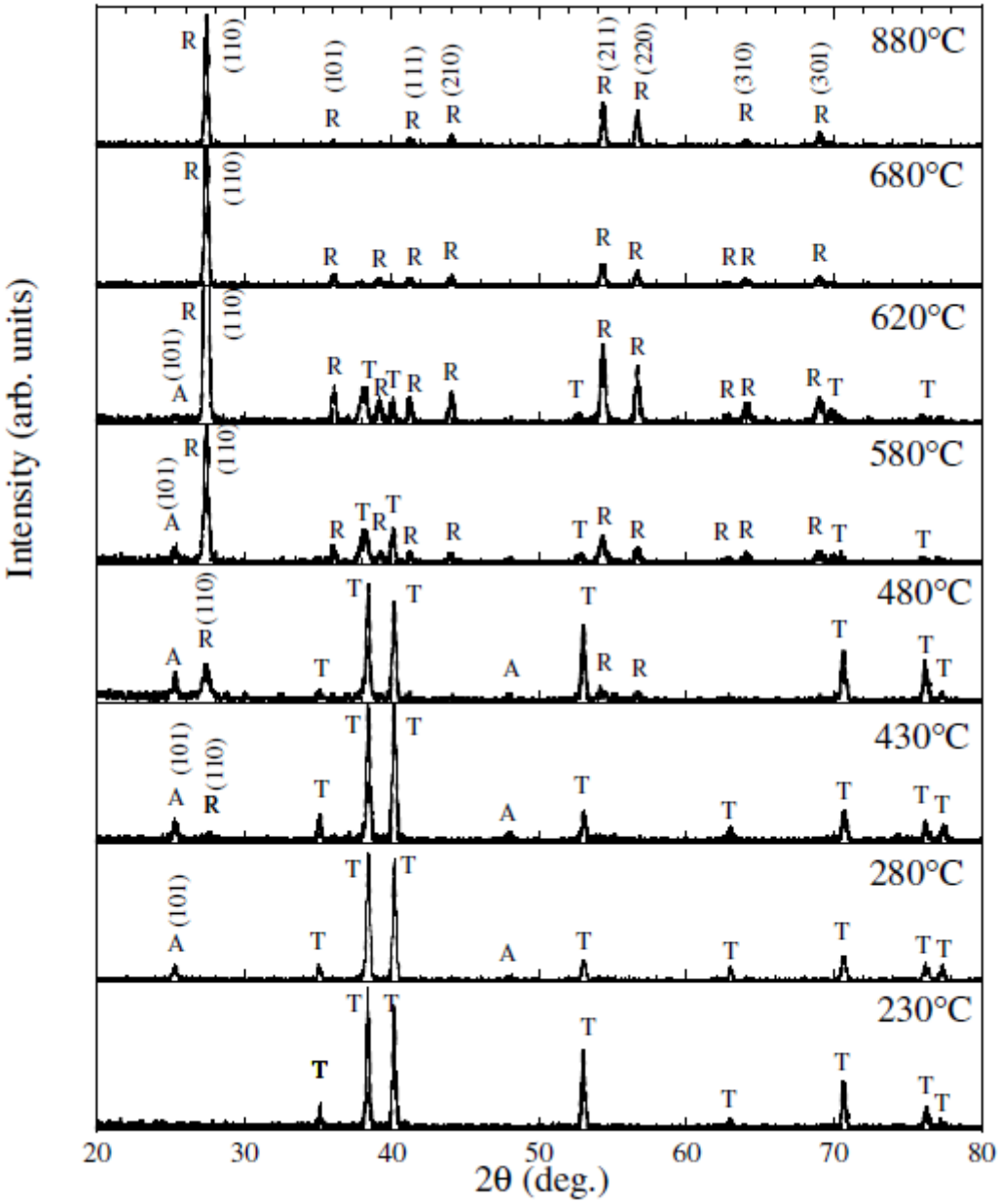

Figure 21. Glancing Angle X-Ray Diffraction (GAXRD) spectra of TiO_2 NTs annealed at temperatures ranging from 230 to 880°C in dry oxygen. A, R and T indicates anatase, rutile and titanium (substrate), respectively. Reprinted from ref. [34] with permission from Materials Research Society.

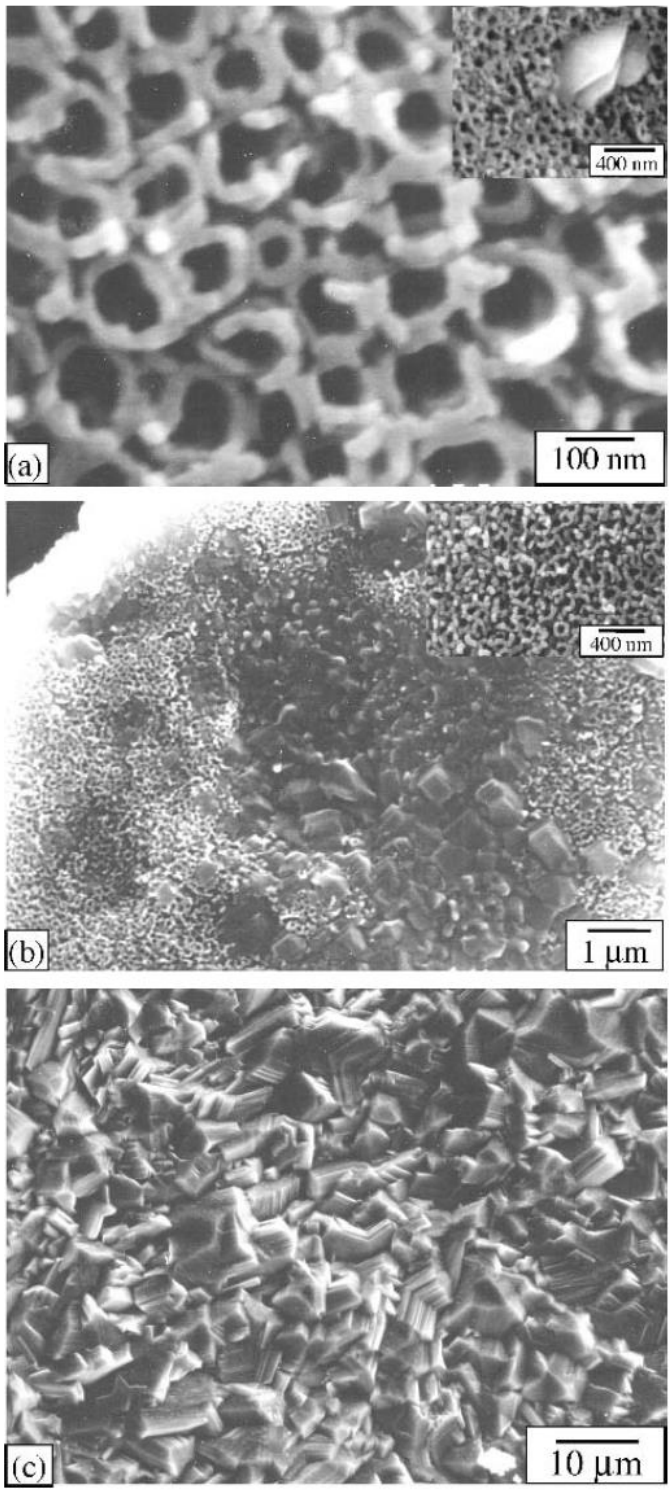

Figure 22. Rutile protrusions emerging from the titanium substrate and disrupting the NTs can be seen using SEM images for a specimen annealed at 580°C **(a)**; the protrusion eventually becomes dominant at 680°C **(b)** and there is no trace of the NTs at 880°C **(c)**. Reprinted from ref. [34] with permission from Materials Research Society.

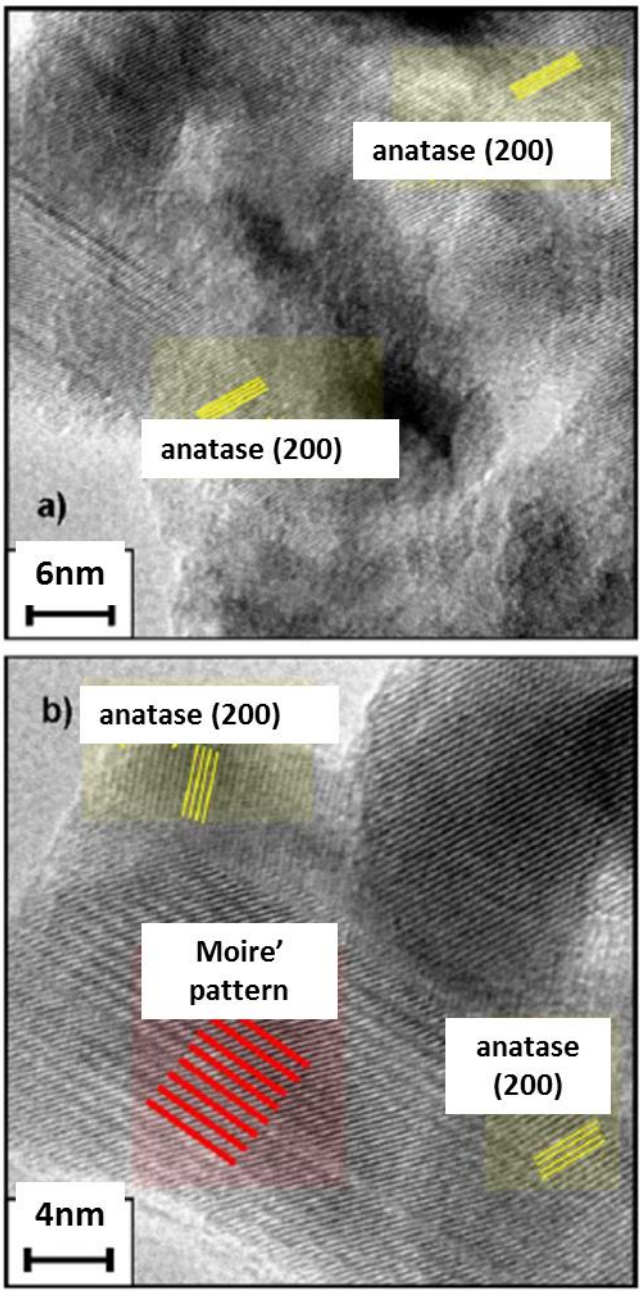

Figure 23. HRTEM details of the crystalline structure of TiO_2 NTs after calcination at 300°C showing the presence of anatase **(a, b)**. Reprinted and adapted from ref. [33] with permission from Elsevier.

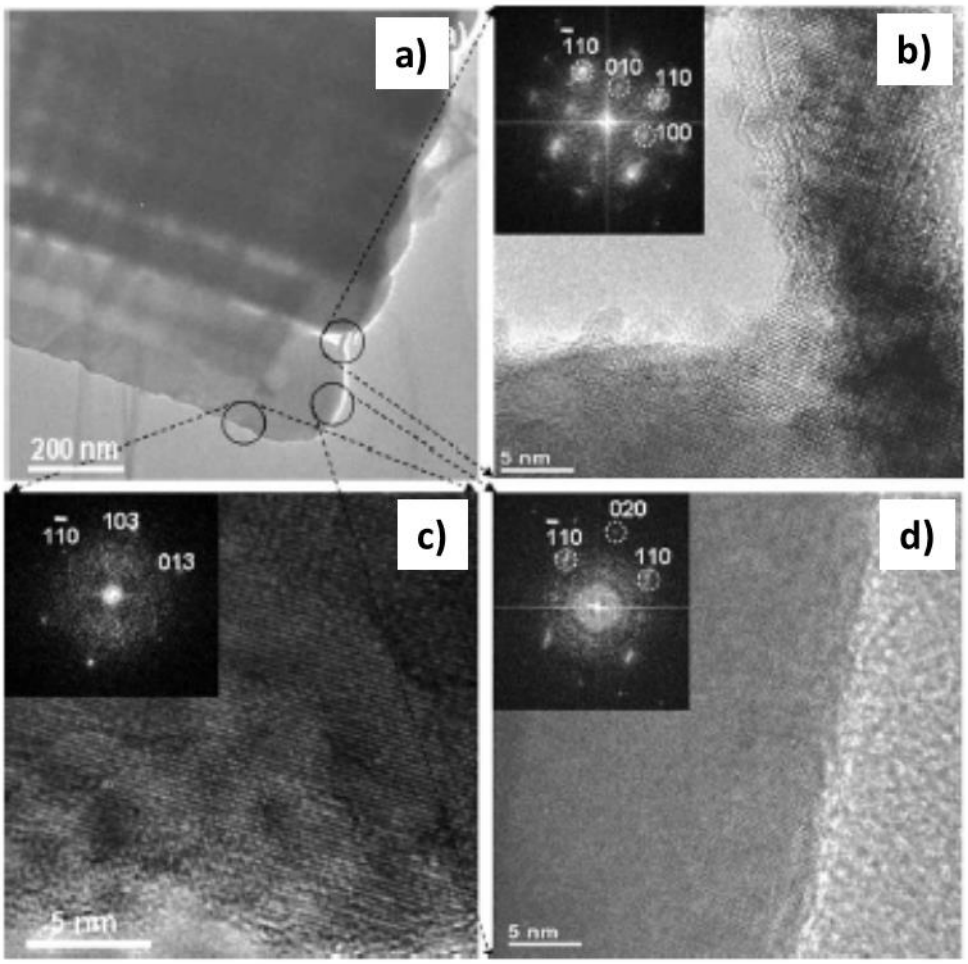

Figure 24. HRTEM details of the crystalline structure of TiO_2 NTs after calcination at 300°C **(a)**. In this case in addition to the presence of anatase **(c)**, rutile crystals can also be detected at the tube bottom **(b, d)**. Reprinted from ref. [305] with permission from The Royal Society of Chemistry.